

ESTIMATING THE EFFECT OF KRILL ON THE SOUTHERN OCEAN
ECOSYSTEM FUNCTIONING

A THESIS SUBMITTED TO
THE INSTITUTE OF MARINE SCIENCES
OF
MIDDLE EAST TECHNICAL UNIVERSITY

BY
ONUR KARAKUŞ

IN PARTIAL FULFILLMENT OF THE REQUIREMENTS
FOR
THE DEGREE OF MASTER OF SCIENCE
IN
OCEANOGRAPHY

OCTOBER 2018

Approval of the thesis:

ESTIMATING THE EFFECT OF KRILL ON THE SOUTHERN OCEAN
ECOSYSTEM FUNCTIONING

Submitted by ONUR KARAKUŞ in partial fulfillment of the requirements for the degree of **Master of Science in Department of Oceanography, Institute of Marine Sciences, Middle East Technical University** by,

Assoc. Prof. Dr. Barış Salihoğlu
Head of Institute, **Institute of Marine Sciences**

Prof. Dr. Süleyman Tuğrul
Head of Department, **Oceanography**

Assoc. Prof. Dr. Bettina Fach Salihoğlu
Supervisor, **Oceanography**

Assoc. Prof. Dr. Barış Salihoğlu
Co-Supervisor, **Oceanography**

Examining Committee Members:

Assoc Prof. Dr. Bettina Fach Salihoğlu
Oceanography Dept., METU

Assoc. Prof. Dr. Barış Salihoğlu
Oceanography Dept., METU

Assist. Prof. Dr. Koray Özhan
Oceanography Dept., METU

Dr. Judith Hauck
FB2 Biology and Chemistry., Uni Bremen

I hereby declare that all information in this document has been obtained and presented in accordance with academic rules and ethical conduct. I also declare that, as required by these rules and conduct, I have fully cited and referenced all material and results that are not original to this work.

Name, Last name : Onur Karakuş

Signature

ABSTRACT

ESTIMATING THE EFFECT OF KRILL ON THE SOUTHERN OCEAN ECOSYSTEM FUNCTIONING

Onur Karakuş

M.Sc., Department of Oceanography

Supervisor: Assoc. Prof. Dr. Bettina Fach Salihođlu

Co-Supervisor: Assoc. Prof. Dr. Barış Salihođlu

October 2018, 85 pages

In this study, a three dimensional, coupled ocean ecosystem model (FESOM-REcoM2) is used to investigate the impact of krill on the ecosystem dynamics of the Southern Ocean in modeling studies. A new, second zooplankton group defined to be Antarctic krill is added to an already existing and validated setup of the modelling system. This species was chosen because it is a key organisms in the Southern Ocean. The effect of grazing on net primary production and export production due to the addition of Antarctic krill was investigated. It was hypothesized that inclusion of macrozooplankton (Antarctic krill) as a second zooplankton group in the model would improve the capability of the model to better represent relevant biogeochemical processes.

After the implementation and parameterization of the new zooplankton group in the FESOM-RecoM2 model, two separate model runs over the duration of 25 years (with and without krill) were conducted, and the effect of Antarctic krill on nutrient distribution, total production, export production and the seasonal cycle of chlorophyll concentrations was analysed. Incorporating Antarctic krill in the model increased simulated nutrient concentrations (nitrate, silicate and iron) due to enhanced nutrient recycling. Also, the simulated spatial distribution and seasonal variation of primary production in the Southern Ocean were affected. The total net primary production did not show major differences between the simulations with and without the krill

parametrization. However, export production decreased slightly after the implementation of krill. The seasonal cycle of nanophytoplankton chlorophyll concentrations as well as its concentration increased. However, the diatom chlorophyll concentrations did not show the similar change. After the implementation of the second zooplankton group, total chlorophyll concentrations did not show major changes. The krill simulation produced more zooplankton in the Southern Ocean compared to a previous study using REcoM2 in the Southern Ocean, which is considered as a major model improvement.



Keywords: Antarctic krill; Ecosystem modeling; The Southern Ocean; Carbon cycle

ÖZ

Antarktik Krilinin Güney Okyanusu Ekosistemi Üzerine Olan Etkileri

Onur Karakuş

Yüksek Lisans, Oşinografi Bölümü

Tez Yöneticisi: Doç. Dr. Bettina Fach Salihoğlu

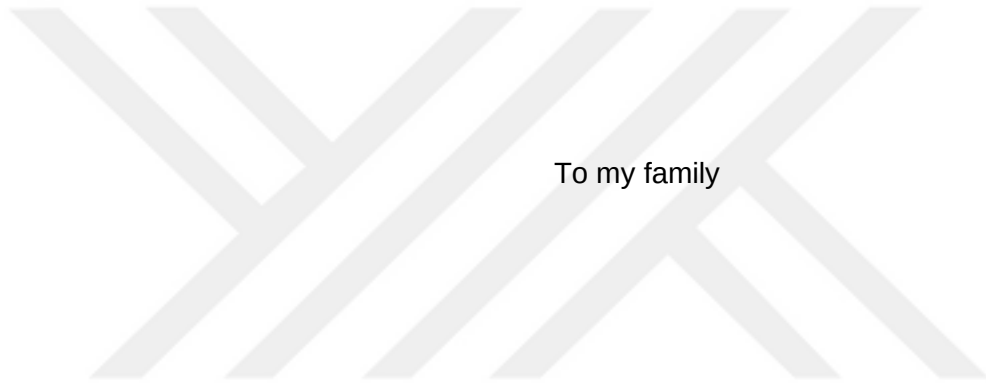
Ekim 2018, 85 sayfa

Bu çalışmada, üç boyutlu FESOM-REcoM2 okyanus ekosistemi modeli kullanılarak Güney Okyanusu ekosistemi anlaşılmasına çalışılmıştır. Hali hazırda kullanılan okyanus ekosistem modeline yeni bir zooplankton grubu eklenmiştir. Bu yeni grup Güney Okyanusu ekosisteminde önemli role sahip olan Antarktik krili olarak parametrize edilmiştir. Bu yapılan değişimin net birincil üretime ve karbon döngüsüne olan etkisi araştırılmıştır. Kril gibi Güney Okyanusu'nda kritik bir öneme sahip makrozooplankton türünün FESOM-REcoM2 okyanus ekosistem modelinde temsilinin modelin biyojeokimyasal özelliklerini etkilemesi beklenmiştir.

Yeni zooplankton grubu eklendikten sonra değişimi görmek amacıyla modelin orijinal hali ve yeni hali ile iki simulasyon yapılmış ve sonuçlar karşılaştırılmıştır. Antarktik krilinin toplam üretim, karbon transferi, mevsimsel klorofil değişimleri üstüne etkisi analiz edilmiştir. Aynı zamanda iki farklı zooplankton özellikleri araştırılmıştır.

Yeni zooplankton grubu eklendikten sonra Güney Okyanusu ortalama besin tuzu değerlerinde artış gözükmiştir. Bu aynı zamanda hem alansal hem de mevsimsel olarak birincil üretimi etkilemiştir. Net birincil üretimde değişim gözlenmemiş ancak derine transfer olan karbon miktarında azalış gözlemlenmiştir. Nanofitoplankton grubunda kış ve bahar ayları ortalama klorofil değişimlerinde azalma görülmüştür. Benzer değişim yeni zooplankton grubu eklenmesi ile diatom grubunda görülmemiştir.

Anahtar Kelimeler: Kril; Güney Okyanusu; Karbon döngüsü; Ekosistem modellemesi



To my family

ACKNOWLEDGMENTS

Foremost, I would like to express my sincerest gratitude to my advisors Assoc. Prof. Dr. Bettina Fach Salihođlu and Assoc. Prof. Dr. Barıř Salihođlu for their valuable and continuous guidance, advice, criticism, encouragements and insight throughout the research.

I would like to express my sincerest gratitude to Dr. Judith Hauck and Dr. Christoph Volker from Alfred Wegener Institute for their valuable guidance, advice and encouragements.

I would like to acknowledge to Assist. Prof. Dr. Koray zhan, member of my examining committee, and Dr. Sinan Hsrevođlu, second reader of my thesis. I am gratefully indebted to them for their very valuable criticism and comments on my thesis.

In this study, computational resources were made available by the Norddeutscher Verbund fr Hoch - und Hchstleistungsrechnen (HLRN).

I am gratefully thankful to academic and administrative people, R/V Bilim-2 crew, and all people from the institute for the invaluable supports.

I am sincerely thankful to all friends in Setst and in the Institute. Especially thanks to Ehsan Sadighrad, Batuhan Yapan, Berivan Temiz, İsmail Akçay for their special friendships.

I am sincerely thankful to my friends Mustafa evrim, Ece Yce, Nazmi Oyar.

I am deeply thankful to my family members, especially zer Karakuř, zge Mısırlı and zgr Mısırlı for their endless support.

Contents

ABSTRACT.....	IV
ÖZ.....	VI
DEDICATION.....	VII
ACKNOWLEDGMENTS.....	VIII
List of Tables.....	XI
List of Figures.....	XII
CHAPTER 1.....	1
INTRODUCTION.....	1
1.1 Southern Ocean.....	3
1.1.1 Oceanographic Setting of Southern Ocean.....	4
1.1.2 Southern Ocean Ecosystem and Its Role on Global Scale.....	5
1.1.3 Antarctic Krill as a Key Species.....	6
1.2 Biological Carbon Pump.....	8
1.3 The Role of Macrozooplankton in the Carbon Cycle.....	10
1.4 Study Objectives.....	11
CHAPTER 2.....	13
MATERIAL AND METHODS.....	13
2.1 Physical Model FESOM.....	13
2.2 Biogeochemical Model REcoM2.....	14
2.2.1 State Equations for Zooplankton Compartment.....	16
2.3 Implementation of Antarctic Krill as a Second Zooplankton Group to REcoM2.....	19
2.3.1 State Equations for the New Zooplankton Group Krill.....	20
2.3.2 Parameterization of the Second Zooplankton Group Krill.....	23
2.4 Model Experiments.....	27
2.5 Datasets for the Model Results Comparison.....	28
2.5.1 Krill Dataset.....	28
2.5.2 Satellite Chlorophyll Data.....	29
CHAPTER 3.....	30
RESULTS.....	30
3.1 Model Results of REcoM2 with one Zooplankton Group.....	30
3.1.1 Global Nutrient Fields.....	30
3.1.2 Global Primary Production Features.....	34
3.1.3 Southern Ocean Nutrient Fields.....	39
3.1.4 Southern Ocean Primary Producers Fields.....	40
3.2 Southern Ocean Analysis of Krill simulation.....	45

3.2.1 Changes in Southern Ocean Nutrient Fields in Krill Simulation.....	45
3.2.2 Changes in Southern Ocean Primary Producers Fields in Krill Simulation.....	49
3.2.3 Features of Different Zooplankton Groups in Krill Simulation.....	50
3.3.3 Changes in NPP and Seasonal Cycles of Chl in Krill Simulation.....	59
3.3 Model Simulations and Observation Comparisons.....	64
CHAPTER 4.....	66
DISCUSSION.....	66
4.1 Control FESOM-REcoM2 Simulation.....	66
4.2 Effect of Antarctic Krill on the Simulated Ecosystem.....	67
4.3 Particulate Organic Carbon production.....	71
4.4 Simulated Antarctic krill biomass and distribution.....	71
CHAPTER 5.....	74
CONCLUSION.....	74

List of Tables

Table 1. Model coefficients and their values for zooplankton groups 27

Table 2. Change in nutrients and primary producers fields after the implementation of the krill for the whole Southern Ocean, regions between 0°W – 140°E, 140°E-60°W and 0°W–60°W68



List of Figures

- Figure 1.** a) Map of Antarctica and Southern Ocean. b) Bathymetry and topography of Southern Ocean and Antarctica. Important gyres (such as Weddell gyre) and the locations of the fronts associated with the Antarctic Circumpolar Current (ACC) are shown (modified from Meredith and Brandon, 2017)..... 4
- Figure 2.** a) Map of the Southern Ocean showing the mean positions of SAF and PF. Green arrows indicate direction and strength of the currents at the surface (reproduced from Marshall and Speer, 2012). b) Temperature profiles of different regions on 150°W a-tropical, b-subtropical, c-subpolar, d-polar (reproduced from Tomczak and Godfrey, 2005). 5
- Figure 3.** a) Trophic transfer pathways in Southern Ocean food web (reproduced from Murphy et. al., 2012). b) Number of Krill densities per m² (reproduced from Atkinson,2004)8
- Figure 4.** a) Schematic representation of biological carbon pump (adopted from Passow and Carlson, 2012) b) Representation of nutrient cycling and biological carbon pump of Southern Ocean and Subtropical regions (adopted from Sigman and Hain, 2012). 10
- Figure 5.** Schematic representation of the role of zooplankton in the global carbon cycle (adapted from Steinberg and Landry, 2017 11
- Figure 6.** FESOM CORE2 mesh spatial resolution in the surface ocean. 14
- Figure 7.** Schematic description of REcoM-2. The 21 tracers can be grouped into primary producers diatoms (DiaN, DiaC, DiaSi, DiaChl) and non-diatoms (PhyN, PhyC, PhyCaCO₃, PhyChl), zooplankton (ZooC, ZooN), detritus (DetC, DetN, DetSi, DetCaCO₃), dissolved nutrient (DIC, DIN, DFe, DSi, ALK) and dissolved organic material (DOC, DON). There is exchange of CO₂ with the atmosphere and a source of Fe by atmospheric dust deposition. Detritus sinks to deeper layers with a prescribed sinking velocity. All sources and sinks are identified with the direction of the arrows. For example grazing is a source for zooplankton compartment but respiration, excretion and mortality are sinks for it.....15
- Figure 8.** Schematic description of REcoM-2 with second zooplankton compartment. The 21 tracers can be grouped into primary producers diatoms (DiaN, DiaC, DiaSi, DiaChl) and non-diatoms (PhyN, PhyC, PhyCaCO₃, PhyChl), zooplankton (ZooC, ZooN), second zooplankton (Zoo2C, Zoo2N), detritus (DetC, DetN, DetSi, DetCaCO₃), dissolved nutrients (DIC, DIN, DFe, DSi, ALK) and dissolved organic material (DOC, DON). There is exchange of CO₂ with the atmosphere and a source of Fe by atmospheric dust deposition. Detritus sinks to

deeper layers with a prescribed sinking velocity. Arrows are the same as in the previous figure of REcoM2	20
Figure 9. Implemented respiration functions for krill. Feeding activity and respiration activity terms.....	23
Figure 10. Implemented temperature function for the second zooplankton group krill	26
Figure 11. Spatial distribution of Krillbase data base	29
Figure 12. Three-year average of surface dissolved inorganic nitrogen (DIN) concentrations from model run with one zooplankton group (CTRL).....	31
Figure 13. a) Surface annual mean nitrate concentrations from WOA13 b) Residual plot of nitrate concentration: modelled values minus observed values.....	31
Figure 14. Three-year average surface DSi concentrations from CTRL simulation	32
Figure 15. a) Surface annual mean silicate concentrations from WOA13 b) Residual plot of silicate concentration: modelled values minus observed values.....	33
Figure 16. Three-year average surface iron concentration from CTRL.....	34
Figure 17. Three-year average chl concentrations from CTRL simulation	35
Figure 18. Three-year average of chl concentration of different groups of primary producers from CTRL simulation. a) Contribution of diatoms b) Contribution of nanophytoplankton	35
Figure 19. Three-year average of NPP from CTRL simulation.....	36
Figure 20. Three-year average of NPP from different groups of primary producers in CTRL. a) Contribution from diatom group b) Contribution from nano-phytoplankton group.	37
Figure 21. Time series of global total NPP and EP of the last 15 years of the model run with one zooplankton group. a) Global total NPP, b) Global total EP.	38
Figure 22. Three-year average of macronutrients in the Southern Ocean. a) DIN b) DSi	39
Figure 23. Three-year average of iron in the Southern Ocean in the CTRL simulation.	40

Figure 24. Three-year average of chl concentration in the Southern Ocean of model run with one zooplankton group	41
Figure 25. Three-year average of sea ice thickness in the Southern Ocean of model run with one zooplankton group	42
Figure 26. Three-year average of a) Diatom Chl and b) Nano-phytoplankton Chl concentrations of model run with one zooplankton group	42
Figure 27. Time series of annual average of chl (total chl-blue runs, diatom chl-red line, nanophytoplankton chl-green line) during the last 15 years of control run with one zooplankton group	43
Figure 28. Three-year average of NPP in the Southern Ocean of model run with one zooplankton group	44
Figure 29. Three-year average of a) NPP from diatoms and b) NPP from nano-phytoplankton in the Southern Ocean of model run with one zooplankton group	44
Figure 30. Total NPP in the Southern Ocean during the last 15 years of the control run	45
Figure 31. Residual plots (krill simulation - one zooplankton simulation) of three years average of macro-nutrients a) DIN and b) Dsi	46
Figure 32. Residual plots (krill simulation - one zooplankton simulation) of three years average of iron	47
Figure 33. Residual plots (model result - observation (WOA13)) three years average of DIN a) CTRL simulation b) Krill simulation.....	48
Figure 34. Residual plots (model result - observation (WOA13)) three years average of DSi a) CTRL simulation b) Krill simulation.	48
Figure 35. Residual plots (krill simulation - one zooplankton simulation) three years average of primary production fields a) chl concentrations and b) NPP	49
Figure 36. Three-year average surface spatial distribution at surface of a) First zooplankton group carbon pool b) Second zooplankton carbon pool in krill simulation.....	50
Figure 37. Spatial distribution of Antarctic Krill a) Data from krillbase b) Three-year average second zooplankton carbon pool with the data from krillbase overlaid.....	51
Figure 38. Three-year average percentage distribution of krill biomass in data (red bars) and in the model result (blue bars) for 3 regions a) Between 0°W and 140°E b) Between 140°E and 60°W and c) 60°W and 0°W	51

Figure 39. Three-year average total grazing patterns of each zooplankton group at surface a) Total grazing of first zooplankton b) Total grazing of second zooplankton group	53
Figure 40. Three-year average grazing on different phytoplankton groups of first zooplankton group at surface a) Grazing on nano-phytoplankton b) Grazing on diatoms.	53
Figure 41. Three-year average grazing on diatoms of second zooplankton group at surface (krill)	54
Figure 42. Three-year average grazing on different phytoplankton groups of second zooplankton group at surface a) Grazing on nano-phytoplankton b) Grazing on first zooplankton group	55
Figure 43. Three-year average DOC production of different zooplankton groups at surface a) DOC production of first zooplankton group b) DOC production of second zooplankton group	56
Figure 44. Three-year average respiration rates of different zooplankton groups at surface a) Respiration of first zooplankton group b) Respiration of second zooplankton group.....	56
Figure 45. Three-year average POC production of different zooplankton groups at surface a) POC production of first zooplankton b) POC production of second zooplankton	57
Figure 46. Three-year average seasonal cycle of zooplankton groups in the surface of the Southern Ocean	58
Figure 47. Time series of total NPP in the Southern Ocean during the last 5 years of the simulations.....	59
Figure 48. Time series of total EP in the Southern Ocean during the last 5 years of the simulations.....	60
Figure 49. Three-year average seasonal cycle of chl concentration at the surface of the Southern Ocean (black line and dots - model run with two zooplankton group, red line and dots - model run with one zooplankton group, green dots - Satellite data chl concentrations).....	61
Figure 50. Three-year average seasonal cycle of nano-phytoplankton chl concentration at the surface of the Southern Ocean	62
Figure 51. Three-year average seasonal cycle of diatom chl concentration at the surface of the Southern Ocean (black line and dots - model run with two zooplankton group, red line and dots - model run with one zooplankton group)	62

Figure 52. Three-year average seasonal cycle of the first zooplankton carbon pool at the surface of the Southern Ocean (black line and dots- model run with two zooplankton group, red line and dots - model run with one zooplankton group).....63

Figure 53. Three-year average residual plots (krill simulation - one zooplankton simulation) of surface first zooplankton group carbon pool concentration..... 64

Figure 54. Taylor diagrams for three-year means of simulated DIN, DSi and chl. Black dot and K stands for krill simulation, red dot and S stands for control simulation and magenta dot and Obs. stands for observation. Black circle lines: standard deviation, green circle lines: RMSE, blue lines: correlation..65

Figure 55. Diagrammatic representation of the ecosystem structure and the particle formation mechanisms in the Southern Ocean a) control simulation, b) krill simulation. The green boxes show diatom (Dia) and nanophytoplankton (Nano). Yellow boxes show the first zooplankton group (Zoo1) and the second zooplankton group (Zoo2). The numbers in the boxes are the percentage of the related compartment to all living compartments in the Southern Ocean. The pink box shows particulate organic carbon (POC). The black arrows show the contribution of each living compartment to the POC production (percentage of total POC production). The red arrows show the grazing of the zooplankton groups on diatom and nanophytoplankton groups (percentage of total grazing on all groups). 69

CHAPTER 1

INTRODUCTION

The Southern Ocean, which is the southernmost waters of the World Ocean, plays a major role in global biogeochemical cycles and the ocean circulation system (Frölicher et al., 2015, Khatiwala et al., 2009, Sarmiento et al., 2004, Langlais et al., 2017). Sea ice dynamics, endemic species within its ecosystem and the related hydrodynamics make the Southern Ocean one of the most unique of the global oceanic systems (Turner et al., 2009).

Numerical ocean biogeochemical models coupled to ocean circulation models are powerful tools to estimate future changes in marine ecosystems. With such models the current status of ecosystems as well as their response to future scenarios can be explored. However, some of the current models disclude important processes that are needed to capture main ecosystem features to make robust projections. Therefore, the choice of how many and which species or functional types should be in the ocean ecosystem models has great importance. The effect of implementing a macro-zooplankton group in a global model was investigated by Moriarty (2009) and improvement in the representations of other functional groups was seen. Processes such as grazing and aggregation should be well defined in the ecosystem model. Since grazing has a direct impact on primary production and carbon export, it is important to describe zooplankton groups in the models well. For example, comparisons of different ocean biogeochemistry models with respect to net primary production and export production showed that their outputs may differ due to the representation of zooplankton groups and phytodetritus (Laufkötter et al., 2016).

A range of numerical ocean-ecosystem models with varying complexities have been developed to better understand the Southern Ocean ecosystem.

Hense et al. (2003) studied phytoplankton dynamics in the Antarctic Circumpolar Current (ACC) with a three dimensional coupled ocean-ecosystem model. A regional model was set up for the Ross Sea nutrient and plankton dynamics (Arrigo et al., 2003). Moreover, ecosystem dynamics of the Atlantic sector of Southern Ocean have been modelled by Lancelot et al. (2000). These models focus on biogeochemical and microbial components of the ecosystem and they do not include larger zooplankton groups. Other global biogeochemistry and ecosystem models were used to study the Southern Ocean biogeochemistry (Lovenduski et al., 2007, Lenton et al., 2007, Hauck et al., 2015, Leung et al., 2015). The biogeochemical model used in this study, RecoM2, was previously used for studies of the Southern Ocean iron and carbon cycles by Schourup-Kristensen et al. (2014), Hauck et al. (2013, 2015) and Hauck and Völker (2015). REcoM2 is used to forecast future changes of global marine export production (Laufkötter et al., 2016). The analyses showed that REcoM2 produces a much lower flux from grazing to particulate organic carbon in the Southern Ocean than the simulated flux by other models. However, observations to validate these rates are sparse. Additionally, the role of zooplankton dynamics in the Southern Ocean has been studied with dynamic green ocean models with different plankton functional types (Le Quere et al., 2016).

One of the key organisms in the Southern Ocean is Antarctic krill which is known to be highly abundant in the Southern Ocean (Atkinson, 2008). Krill occurs in large swarms and plays an important role for nutrient dynamics, primary production and global net export (Hamner et al., 1983). Because of this, a better understanding of the Southern Ocean ecosystem dynamics requires a better representation of the Antarctic krill in ocean ecosystem models. Transport and distribution models have been developed to understand advection of krill by the ocean currents (Webb et al., 1991, Hoffmann et al., 1998, Fach et al., 2002). It was found that open ocean concentrations of phytoplankton are unlikely to provide sufficient food for the krill to travel from the Antarctic Peninsula to South Georgia. Modelling studies

showed that sea ice algae could provide an additional important food source for krill (Fach et al., 2002). Therefore, a new zooplankton group representing Antarctic krill was implemented into the RecoM2 model and the effects of this representation on the biogeochemistry and lower trophic dynamics of the Southern Ocean was explored.

1.1 Southern Ocean

The Southern Ocean is the region south of 60°S, defined as the southern portions of the Pacific, Atlantic, and Indian oceans (IHO, 2000). The Southern Ocean is the fourth largest ocean in the world with a total area of about 20,327 million km² (IHO, 2000). The Antarctic continent forms the southern boundary of the Southern Ocean. However, the northern boundary varies between 30°S and 60°S. The definition varies with some oceanographic features such as the Subtropical Front (SF) and the Antarctic Circumpolar Current (ACC; Talley et al., 2011). For example, with the variations in the location of the SF, the effective area of the Southern Ocean can exceed 77 million km² (Tomczak, 2005). The Southern Ocean encircles the extreme and isolated continent Antarctica entirely. The Amundsen Sea, Bellingshausen Sea, part of the Drake Passage, Ross Sea, a small part of the Scotia Sea, Weddell Sea, and other tributary water bodies are the regional seas in the Southern Ocean (Figure 1a).

The Antarctic continental shelf is very steep and deeper than most continental shelf areas, with an average depth of 100 m (Meredith, 2017). The depth range is between 0-6000 m in the Southern Ocean (Figure 1b). There are 3 major basins: (i) the Pacific-Antarctic basin that includes the Amundsen, Bellingshausen and Ross Seas; (ii) the Australian-Antarctic basin located in the Indian Sector bounded in the west by the Kerguelen Plateau; and (iii) the Atlantic-Antarctic basin which includes the Enderby Abyssal Plain and the Weddell Gyre.

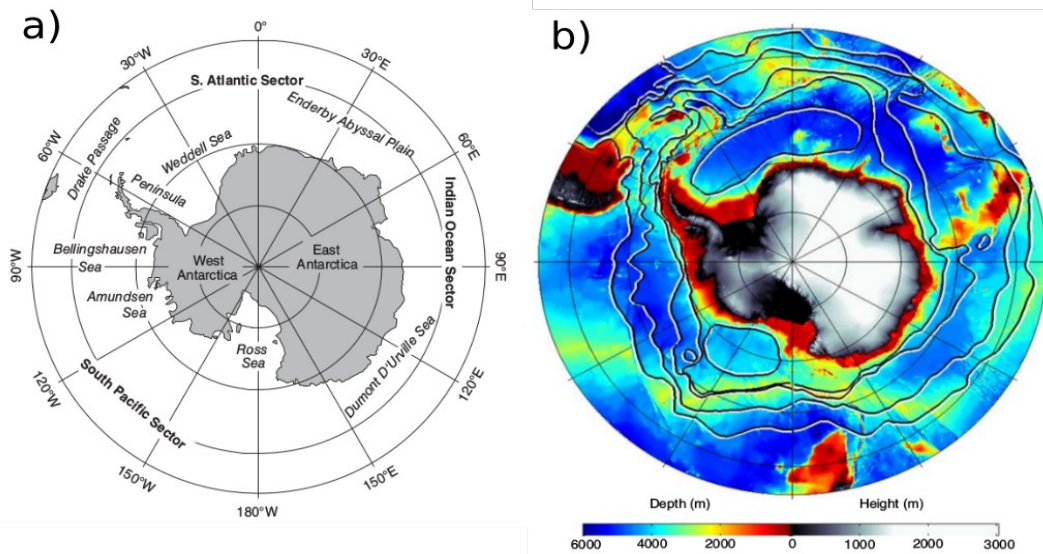


Figure 1. a) Map of Antarctica and the Southern Ocean. b) Bathymetry and topography of the Southern Ocean and Antarctica. Important gyres (Weddell and Ross gyres) and the locations of fronts associated with the ACC are shown (modified from Meredith and Brandon, 2017).

1.1.1 Oceanographic Setting of Southern Ocean

The Southern Ocean plays an important role in the global climate and water exchange among major ocean basins. The ACC is the strongest current in the world ocean and connects these major basins, transferring salt, heat and other dissolved and particulate quantities such as nutrients (Turner et al., 2009). Moreover, the ACC has an important role in the global ocean conveyor belt, transporting water masses all around the planet (Tomczak, 2005).

With unrestricted circumpolar circulation, the ACC is conceptually similar to atmospheric circulation in the Southern Hemisphere. The eastward flowing ACC is mainly driven by the Westerlies, the wind system located between 45°S and 55°S (Trenberth, 1990). This wind pattern allows the ACC an annual mean water flux of about 130 Sv at the Drake Passage (Cunningham et. al., 2003). Three main frontal features are considered in the Southern Ocean: Subantarctic Front (SAF), the Antarctic Polar Front (PF) and the Southern ACC front (SACCF; Orsi et. al., 1995). Of these three fronts, the PF

and the SAF feature the highest speed jets and also the steepest temperature and density gradients. The SACCF is only observed in the Drake Passage (Figure 2a).

In the Southern Ocean, another important feature is the deep mixed layer. In polar regions, differences of seawater temperature between the surface and deeper parts of the ocean are relatively small (Figure 2b, blue line). Since the density variations with depth are relatively small, currents can easily penetrate the deeper parts of the ocean. For example, observations in Drake Passage showed that at 2500 m depth, the mean current speed is 10-30% of the current at 500 m depth (Tomczak and Godfrey, 2001).

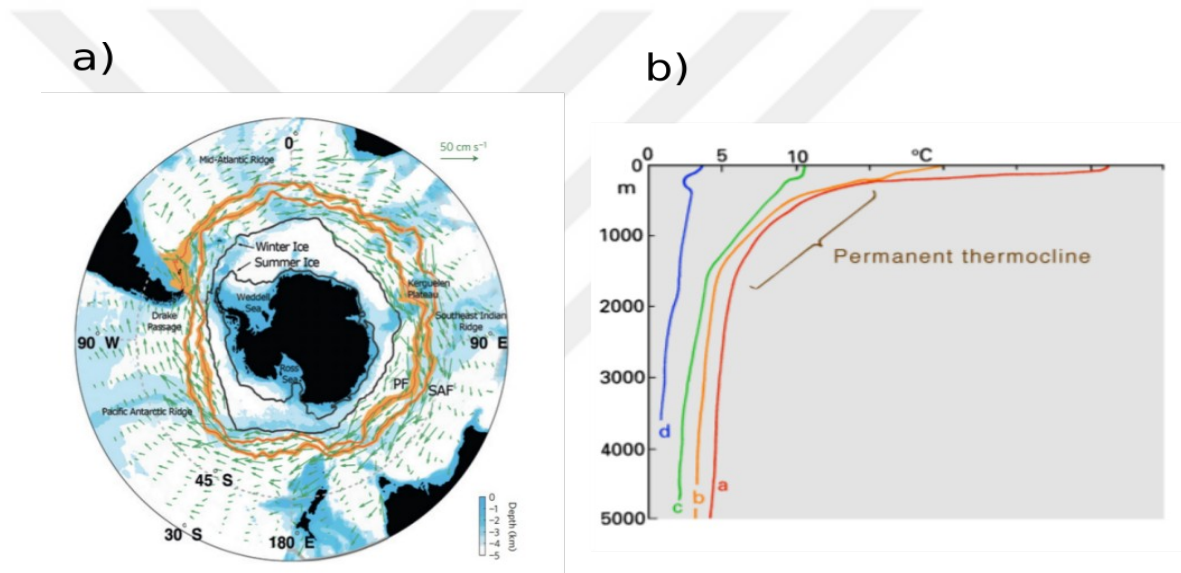


Figure 2. a) Map of the Southern Ocean showing the mean positions of SAF and PF. Green arrows indicate direction and speed of the currents at the surface (reproduced from Marshall and Speer, 2012). b) Temperature profiles of different regions on 150°W a-tropical, b-subtropical, c-subpolar, d-polar (reproduced from Tomczak and Godfrey, 2005).

1.1.2 Southern Ocean Ecosystem and Its Role on Global Scale

With its dynamical features and isolated location, the Southern Ocean hosts a unique ecosystem. There are many species endemic to the Southern Ocean with high biomass (Clarke and Johnston, 2003). There is a large

consumption of some zooplankton species (such as the Antarctic krill) and finfish commercially (Clarke and Johnston, 2003).

In general, it can be said that the Southern Ocean has high concentrations of nutrients such as nitrate and silicate and low concentrations of iron (Pollard et al., 2009). Zooplankton species such as krill play an important role as a link between the lower and higher trophic levels (Murphy et al., 2012). Many special and unique mammals and birds are also part of this unique ecosystem (Constable et al., 2014).

As the Southern Ocean is important for the global ocean circulation, it is also important for the global biogeochemical cycles of nutrients and carbon (Arrigo et al., 2008). It can affect the distribution of nutrients on a global scale (Pollard et al., 2009). Moreover, it is important also for carbon sequestration (Le Quéré et al., 2007; Khatiwala et al., 2009; Gruber et al., 2009). It takes up 25% of the atmospheric CO₂ even though its surface area is only 10% of that of the global ocean (Takahashi et al., 2002). Besides physical factors affecting CO₂ uptake, biological activity is an important factor (Arrigo et al., 2008).

Even though there is a high concentration of macro-nutrients due to upwelling in the Southern Ocean (Pollard et al., 2006), these nutrients cannot be fully utilized by primary producers because of iron limitation (Martin et al., 1990; Smetacek, 2012). The Southern Ocean is therefore one of the High Nutrient Low Chlorophyll (HNLC) areas, like the north Pacific. Other hypothesis about why the Southern Ocean is an HNLC include the high grazing rates and light limitation (Morel et al., 1991; Sunda and Huntsman, 1997).

1.1.3 Antarctic Krill as a Key Species

The Euphausiid crustacean Antarctic krill reaches a maximum size of 65 mm and has a lifespan of 5-7 years (Siegel, 2016). Many of the vertebrate and invertebrate predators graze on krill, especially mammals. The krill in turn,

grazes on autotrophs (Everson, 1977; Laws, 1984). Because of this, Antarctic krill has a key role in the Southern Ocean ecosystem enabling a short pathway of trophic transfer, meaning primary production is transferred to the higher trophic levels efficiently (Figure 3a). With this role, krill shapes the structure of the marine ecosystem in the Southern Ocean (Meyer, 2011).

Spatial biomass distribution of krill depends on food availability, sea ice cover and circulation (Meyer, 2011). In the Atlantic-Antarctic basin, especially around the Antarctic Peninsula, a high number of krill is observed (Atkinson, 2004; Figure 3b). Previous studies showed that 58-71% of the krill biomass is located in the southwest Atlantic (Siegel 2016; Atkinson et. al. 2004). In contrast, in the Indian-Antarctic and the Pacific-Antarctic basins krill density is relatively small.

Krill feeds on different food types such as zooplankton, phytoplankton, sea ice algae and detritus (Meyer, 2011). It feeds on phytoplankton by filter feeding and it generally prefers diatoms over other phytoplankton (Atkinson, 2016). Also, it feeds on zooplankton such as copepods. There are two ways of feeding on copepods: small copepods are grazed by filter feeding, whereas larger ones are grazed via complex detection and attack strategies (Schmidt and Atkinson, 2016). Another food source for krill is the benthos. After they dive and resuspend a small volume of sediment, krill feeds on phyto-detritus and other food sources via filter feeding (Clarke and Tyler, 2008). This behaviour can be observed in the 500-3500 m depth range. Furthermore, another important food source for krill is sea ice algae. Feeding on sea ice algae is reported to be an important source of food especially in spring (Meyer, 2011).

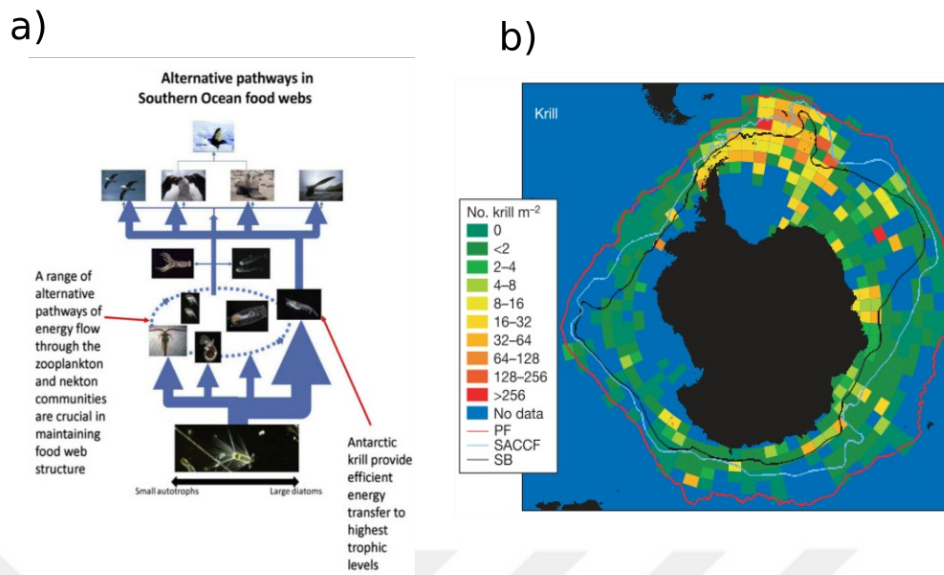


Figure 3. a) Trophic transfer pathways in Southern Ocean food web (from Murphy et. al., 2012). b) Number of Krill per m² (from Atkinson, 2004)

Overwintering strategies of krill are important in the extreme conditions of the Southern Ocean. Use of food sources other than phytoplankton, shrinkage of the body, presence of sea ice and surviving inside the rafting ice refuges are some of these strategies (Fach et al., 2008; Meyer, 2011). Krill feeds on various sources of food as mentioned above due to lack of phytoplankton in mid-winter. Body shrinkage is observed in winter when conditions are unfavourable in terms of low chl A concentrations (Atkinson, 2006). Moreover, the presence of sea ice drives aggregation of small zooplankton under sea ice in winter and production of sea ice algae in spring. Because of this, sea ice provides additional food sources which are important for krill survival (Kohlbach et al., 2017).

1.2 Biological Carbon Pump

Atmospheric CO₂ concentration increased from 277 ppm in 1750 (Joos and Spahni, 2008) to 409.56 ppm in July 2018 (Keeling et al., 2001). Over the last 6 decades, an almost 30% increase in CO₂ concentrations in the atmosphere

due to anthropogenic activities has been recorded (Keeling et al., 2001). This increase and the accompanying global warming does not only affect the atmosphere but also the oceans. Sea level rise, increased seawater temperature and ocean acidification are some of the observed effects (IPCC, 2013).

The oceans play an important role in the global carbon cycle. Uptake of atmospheric CO₂ by the ocean is estimated to be 2.9 ± 0.5 Gt C per year (Le Quéré et al, 2015). It is almost 30% of the total emissions originating from fossil fuels and industry. Due to the increase in atmospheric CO₂ concentration, the uptake rate of the ocean increased from 1.1 ± 0.5 Gt C per year (during the 1960s) to 2.6 ± 0.5 Gt C per year (during 2005-2014) (Le Quéré et al., 2015). Storage of carbon in the deep ocean occurs via physical processes (carbon solubility pump) and the biological carbon pump (BCP). Both of the pathways are vehicles to transfer the surface ocean carbon content to the deep ocean reservoir. The physical process occurs because of the high solubility of the gases in cold high latitudes waters (Zeebe and Wolf-Gladrow, 2001). Sinking intermediate and deep water formed at the surface carries carbon to the deep ocean reservoir (Khatiwala et al., 2009).

The BCP is driven by the living organisms in the ocean (Volk and Hoffert, 1985). It is important for the transfer of carbon to deep waters and sediments and for converting the carbon species to new carbon compounds. In the oceans, some of the dissolved inorganic carbon is converted to organic matter via photosynthesis. Although primary production happens in the surface oceans where the sunlight can reach, remineralization processes occur in the whole water column. Particulate organic matter (POM) is exported via sinking, vertical mixing, advection, and vertical migration of zooplankton to deeper layers (Figure 4a). In the deeper layers of the ocean it accumulates or is respired by other biological activities.

The biological carbon pump in the Southern Ocean is not very efficient because of the limitation of primary production due to a lack of micro-

nutrients such as iron (Fe; Boyd et al.,1999). However as it is mentioned in previous studies (e.g. Smith and Nelson 1985; Smetacek 1985; Beaulieu 2002), under some conditions such as mass-sinking events of diatoms, the effect of marginal ice zones or enhanced iron supply, high export rates and high productive times can be observed. Therefore, it can be said that BCP also plays a significant role in the Southern Ocean (Figure 4b).

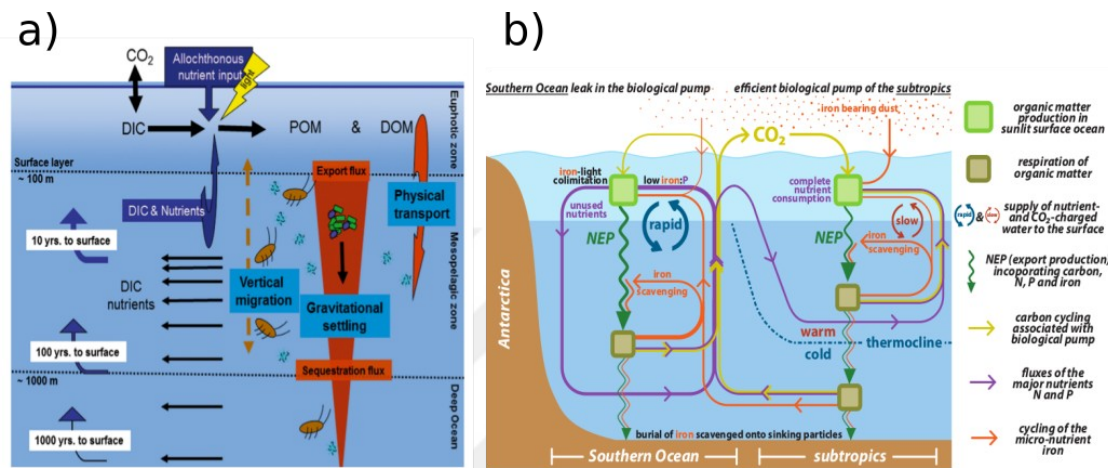


Figure 4. a) Schematic representation of biological carbon pump (adopted from Passow and Carlson, 2012) b) Representation of nutrient cycling and biological carbon pump of Southern Ocean and subtropical regions (adopted from Sigman and Hain, 2012)

1.3 The Role of Macrozooplankton in the Carbon Cycle

Plankton are autotrophic or heterotrophic organisms which drift and are transported by ocean currents. Heterotrophic components of the plankton community are zooplankton. According to their size fractions zooplankton classify as nano (2-20 μm), micro (20-200 μm), meso (0.2-20 mm), macro (2-20 cm) and mega (20-200 cm) zooplankton after Sieburth et al. (1987).

Zooplankton play an important role in the global carbon cycle. Their key place between the lower trophic and the higher trophic levels, such as fish, is important for the carbon transfer between trophic levels. Also, they transfer carbon to the deep ocean reservoir via fecal pellet production and export of dead tissue. Carbon which is not assimilated is egested as fecal pellets and these fecal pellets transform to dissolved organic carbon (Steinberg and

Landry, 2017). Since zooplankton grazes on many different food sources such as autotrophic, heterotrophic and detritus, they repackage this carbon source in the ocean. The carbon taken by grazing is transferred to the higher trophic level by predation (Figure 5).

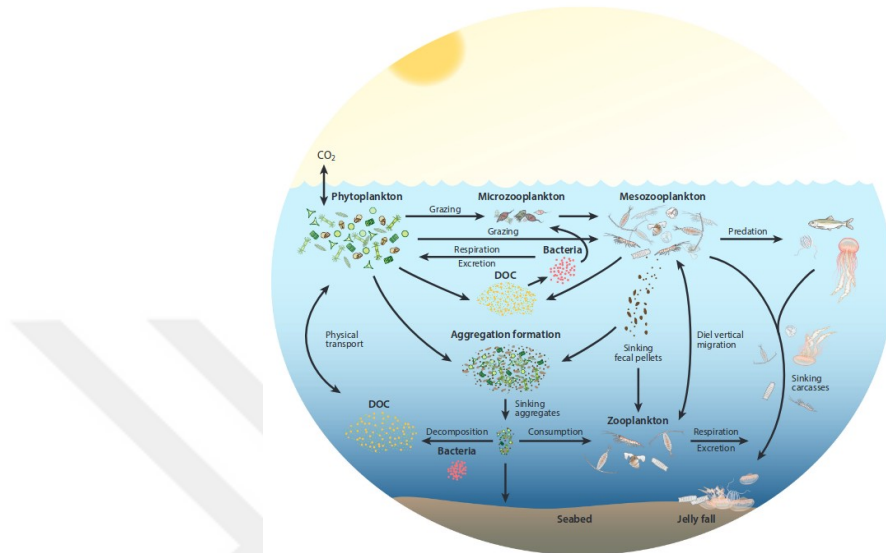


Figure 5. Schematic representation of the role of zooplankton in the global carbon cycle (adapted from Steinberg and Landry, 2017)

Macro-zooplankton differ among zooplankton classes in terms of fecal pellet production and their sinking rate to the deep ocean (Moriarty, 2009). Fecal pellet production by macro-zooplankton is higher than by smaller zooplankton types and the sinking rate of them is higher, even faster than marine snow (Turner, 2002). This fast sinking rate of fecal pellets prevent microbial degradation in the euphotic zone and leads to direct sinking to the deep ocean (Turner, 2002).

1.4 Study Objectives

The principal objectives of this study were:

- To include krill in a validated Southern Ocean ecosystem model and investigate the effect of this new group on the ecosystem of the Southern Ocean.

Modelling of krill biomass in the Southern Ocean was done via implementation of the new zooplankton group to ecosystem model REcoM2 and parametrization of the new group as Antarctic krill.

Within the scope of these broad objectives, the following aims were identified for particular attention:

- To compare two different model runs and to estimate the effect of the new group on simulated nutrient fields.
- To calculate the effect of krill on primary producer fields for different regions.
- To identify the grazing fluxes from different phytoplankton groups to zooplankton groups.
- To estimate particulate organic carbon (POC) production of zooplankton and phytoplankton groups.

CHAPTER 2

MATERIAL AND METHODS

In this chapter, the three dimensional ocean circulation model FESOM (Finite Element Sea Ice Ocean Model) coupled with the ocean ecosystem model REcoM2 (Regulated Ecosystem Model) used in this study are described. The details of the implementation of the new zooplankton group into REcoM2 are provided. Also, the datasets which were used for the comparison of model results with observations are introduced.

2.1 Physical Model FESOM

Ocean general circulation models differ from each other in terms of numerical techniques which are used for solving primitive equations. Some of the ocean models use finite difference methods while others use finite element or finite volume methods. In this study, FESOM (Wang et al., 2008) was used as the physical component of the coupled ocean-ecosystem model. FESOM uses the finite element method for solving the primitive equations, with an unstructured mesh which allows calculations with higher resolutions in more dynamical areas and coarser resolution in others. FESOM was developed by a team at the Alfred Wegener Institute, Helmholtz Centre for Polar and Marine Research. Further information is provided at the website <http://www.fesom.de>. In this study, the CORE2 mesh was used (Figure 6). In the CORE2 mesh, there are 126859 2D nodes. The time step is 15 minutes. Output of the model was saved monthly.

As it can be seen in the map of spatial resolution (Figure 6), the resolution is higher in the equatorial and the polar regions than in the subtropical areas. It increases the capability of the model to simulate the processes more realistically in the ocean in higher latitudes and equatorial regions. This study focuses on the Southern Ocean south of 50°S.

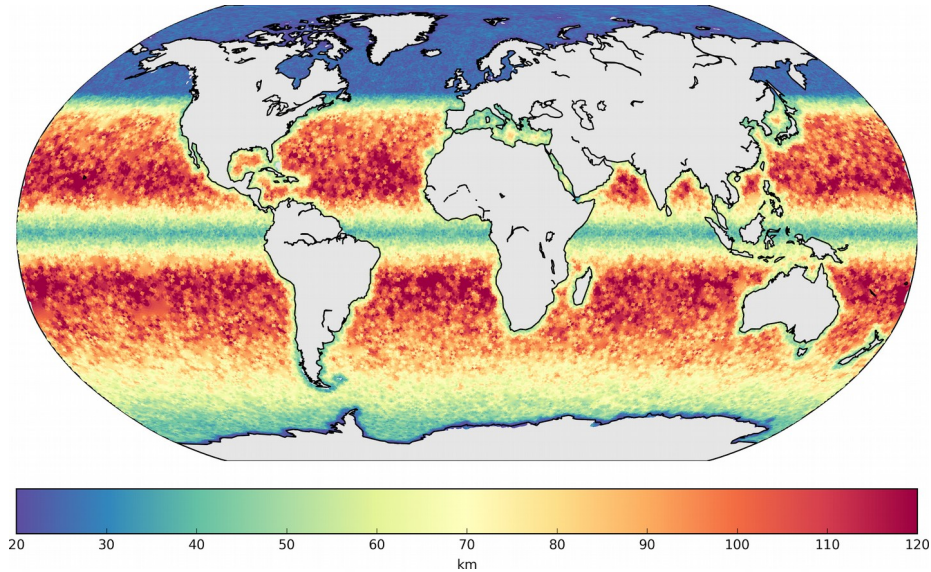


Figure 6: FESOM CORE2 mesh spatial resolution in the surface ocean

2.2 Biogeochemical Model REcoM2

The aim of REcoM2 (Hauck et al., 2013; 2016; Schourup-Kristensen et al., 2014) is describing the ocean ecosystem and biogeochemistry with a model. In the model there are 5 different compartments: dissolved inorganic nutrients, dissolved organic nutrients, detritus, zooplankton and phytoplankton (Figure 7). There are 21 tracers in total. The phytoplankton compartment has 2 functional types which are parameterized as nanophytoplankton and diatoms. In the model, phytoplankton stoichiometry is allowed to vary with environmental conditions (variable N:C:Chl:Si for diatoms and N:C:Chl for nanophytoplankton).

The model solves the following mass balance equation to calculate volumetric concentration of each tracer:

$$\frac{\partial A}{\partial t} = -(U+w)\nabla A + \nabla(k\nabla A) + S(A) \quad (1)$$

A is the volumetric concentration of a tracer (Equation 1). U is the three-dimensional advection velocity and k is the diffusivity. U and k are supplied by the physical circulation model FESOM. The term w is the sinking velocity of particles which is positive downwards. $S(A)$ refers to the source and sinks of the tracer in the biogeochemical model.

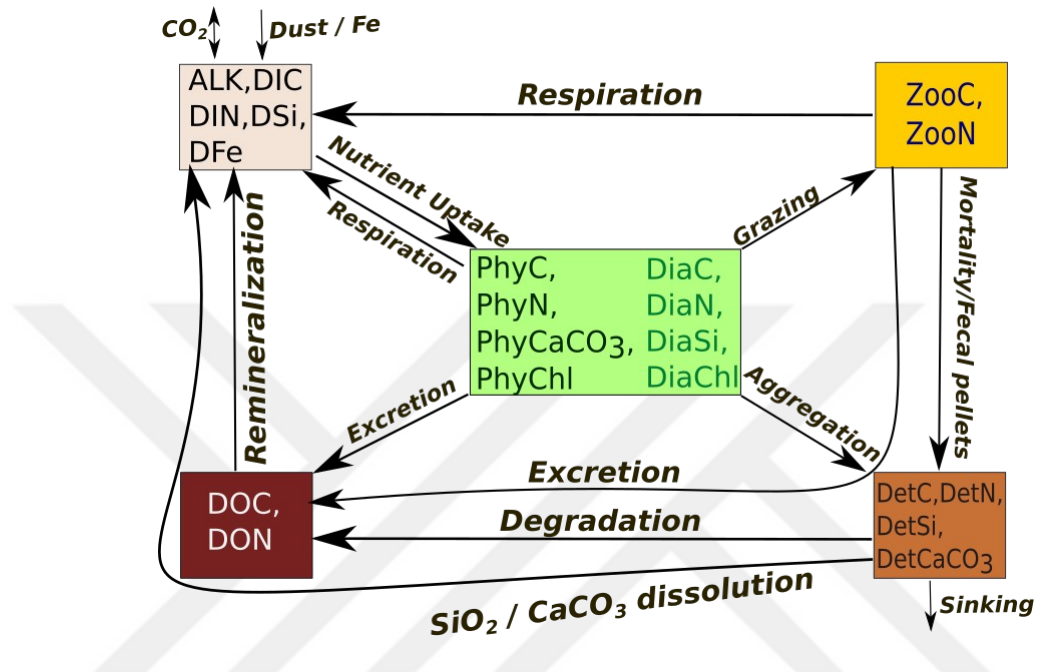


Figure 7: Schematic description of REcoM-2. The 21 tracers can be grouped into primary producers diatoms (DiaN, DiaC, DiaSi, DiaChl) and non-diatoms (PhyN, PhyC, PhyCaCO₃, PhyChl), zooplankton (ZooC, ZooN), detritus (DetC, DetN, DetSi, DetCaCO₃), dissolved nutrient (DIC, DIN, DFe, DSi, ALK) and dissolved organic material (DOC, DON). There is exchange of CO₂ with the atmosphere and a source of Fe by atmospheric dust deposition. Detritus sinks to deeper layers with a prescribed sinking velocity. All sources and sinks are identified with the direction of the arrows. For example grazing is a source for zooplankton compartment but respiration, excretion and mortality are sinks for it.

The relationships between the compartments are indicated in Figure 7 with arrows. The arrows which go out from a compartment indicate a sink for this compartment. Respiration, mortality, excretion, remineralization, degradation, nutrient uptake, grazing and aggregation are the main processes which describe relations among compartments.

Phytoplankton compartment: For this compartment, the main source is the nutrient uptake. There is a growth due to photosynthesis. Grazing, excretion, respiration and aggregation are the reasons for loss in this compartment.

Zooplankton compartment: For the zooplankton compartment, grazing on diatoms and nano-phytoplankton groups is the main source. Loss is due to the mortality, excretion and respiration processes.

Detritus compartment: For this compartment, sources are aggregation of the phytoplankton and mortality/fecal pellet production by zooplankton. The loss from this compartment is due to the degradation and SiO_2 / CaCO_3 dissolution. Also sinking through the sediment is another reason for the loss.

Dissolved organic nutrient compartment: The excretion and degradation are the main sources for this compartment. This flow comes from zooplankton and phytoplankton compartments. The loss occurs because of the remineralization.

Dissolved inorganic nutrient compartment: The reason for loss of this compartment is nutrient uptake by primary producers. Respiration in the living compartments (phytoplankton and zooplankton) is a source for DIC. Moreover, remineralization of the dissolved organic nutrients and SiO_2 / CaCO_3 dissolution are other sources. In the dissolved inorganic nutrient compartment of the model, carbonate chemistry is also defined. CO_2 exchange between atmosphere and ocean surface was taken into account. Fe-input through dust deposition is also a source for the compartment.

2.2.1 State Equations for Zooplankton Compartment

One of the main focus of this study is to understand the effect of grazing in the Southern Ocean. How the zooplankton group is represented in the original model is described here. The zooplankton group in the model has two pools, nitrogen and carbon pools, respectively. The main processes such

as grazing, respiration, mortality, and excretion are described with the following equations (Hauck et al., 2013; Schourup-Kristensen et al., 2014).

Nitrogen pool: The main source for the nitrogen pool of the first zooplankton group is grazing. Excretion and mortality are the loss terms. These relation can be followed in Equation 2.

$$S(N_{zoo1}) = G_{zoo1} \cdot \gamma_1 - m_{zoo1} \cdot N_{zoo1}^2 - \epsilon^N_{zoo1} \cdot N_{zoo1} \quad (2)$$

Mortality is defined with a quadratic term ($m_{zoo1} \cdot N_{zoo1}^2$) and a daily mortality rate (m_{zoo1}) is used. How much of the grazing will become biomass of the nitrogen pool is defined by the grazing efficiency (γ_1) term. The grazing efficiency term is also used for the sloppy feeding. Transfer of first zooplankton nitrogen pool to DON pool is calculated by multiplication of excretion rate and first zooplankton nitrogen pool ($\epsilon^N_{zoo1} \cdot N_{zoo1}$).

Total grazing of the first zooplankton group (G_{zoo1}) is represented as:

$$G_{zoo1} = \varepsilon \cdot \frac{(N'_{phy} + N'_{dia})^2}{\varphi + (N'_{phy} + N'_{dia})^2} \cdot f_T \cdot N_{zoo1} \quad (3)$$

In the Equation 3, ε is the maximum grazing rate, φ is half saturation constant and f_T (Equation 10) is the temperature function. The total grazing rate is calculated as the constant grazing rate multiplied with the nutritional intake. N'_{dia} and N'_{phy} are the preference terms for the grazing on diatoms and nano-phytoplankton. The equation for these terms can be found below.

$$N'_{dia} = \tau_1 \cdot \frac{N_{dia}^2}{\varphi_1 + N'_{dia}} \cdot N_{dia} \quad (4)$$

$$N'_{phy} = \tau_1 \cdot \frac{N_{phy}^2}{\varphi_2 + N'_{phy}} \cdot N_{phy} \quad (5)$$

In the Equation 4, φ_1 is the half saturation constant for grazing on diatoms. The term τ_1 is food preference on diatom. The grazing preference varies with the diatom biomass. However, if φ_1 is set to 0, it means there is a constant preference. This is the same for the nano-phytoplankton and it is shown in Equation 5.

In the model, the relative contributions of grazing on each functional phytoplankton group ($G_{zoo1phy}$, $G_{zoo1dia}$) is calculated by the following equations.

$$G_{zoo1phy} = G_{zoo1} \cdot \frac{N'_{phy}}{N'_{phy} + N'_{dia}} \quad (6)$$

$$G_{zoo1dia} = G_{zoo1} \cdot \frac{N'_{dia}}{N'_{phy} + N'_{dia}} \quad (7)$$

In Equations 6 and 7, the total grazing of the first zooplankton group (G_{zoo1}) is multiplied with nano-phytoplankton or diatom food source (N'_{phy} , N'_{dia}) and divided by the total food source ($N'_{phy} + N'_{dia}$) to identify grazing flux from each food source.

Carbon pool: Mortality, carbon excretion and respiration are the loss terms for the carbon pool of the zooplankton group. Grazing is the source term. In Equation 8, the description of these processes in the model can be found.

$$S(C_{zoo1}) = \left(\frac{1}{q_{phy}} \cdot G_{zoo1phy} + \frac{1}{q_{dia}} \cdot G_{zoo1dia} \right) \cdot \gamma_1 - \frac{1}{q_{zoo1}} \cdot m_{zoo1} \cdot N_{zoo1}^2 - \epsilon_{zoo1}^C \cdot C_{zoo1} - r_{zoo1} \cdot C_{zoo1} \quad (8)$$

As mentioned before, the grazing flux is calculated in the nitrogen pool. For the carbon pool the same grazing flux is used. The only difference is the multiplication of the grazing flux by the respective intercellular N:C ratios

$(\frac{1}{q_{phy}}, \frac{1}{q_{dia}}, \frac{1}{q_{zoo1}})$. The reason for this multiplication is the conversion of nitrogen biomass to carbon biomass. Respiration for the zooplankton group is defined to drive the nitrogen and carbon pools back towards the Redfield ratio. When the C:N ratio exceeds the Redfield ratio, respiration (r_{het}) drives this ratio to the Redfield ratio with a time scale K_{het} :

$$r_{het} = \begin{cases} f_T \cdot (q_{het}^{C:N} - q_{Redfield}^{C:N}) / \kappa_{het} & \text{if } q_{het}^{C:N} > q_{Redfield}^{C:N} \\ 0 & \text{if } q_{het}^{C:N} \leq q_{Redfield}^{C:N} \end{cases} \quad (9)$$

Growth as most metabolic processes is faster at higher temperatures. This is parameterized with multiplication of maximum grazing rate by the Arrhenius function, f_T (Equation 10) with reference temperature $T_{ref} = 288.15$ K, for the first zooplankton group.

$$f_T = \exp\left(-4500\left(\frac{1}{T} - \frac{1}{T_{ref}}\right)\right) \quad (10)$$

2.3 Implementation of Antarctic Krill as a Second Zooplankton Group to REcoM2

The aim of this study is to investigate the effect of one of the macrozooplankton species, Antarctic Krill, on the Southern Ocean ecosystem functioning and carbon export. For this reason, a new zooplankton group is implemented in REcoM2 and it is parameterized as Antarctic Krill.

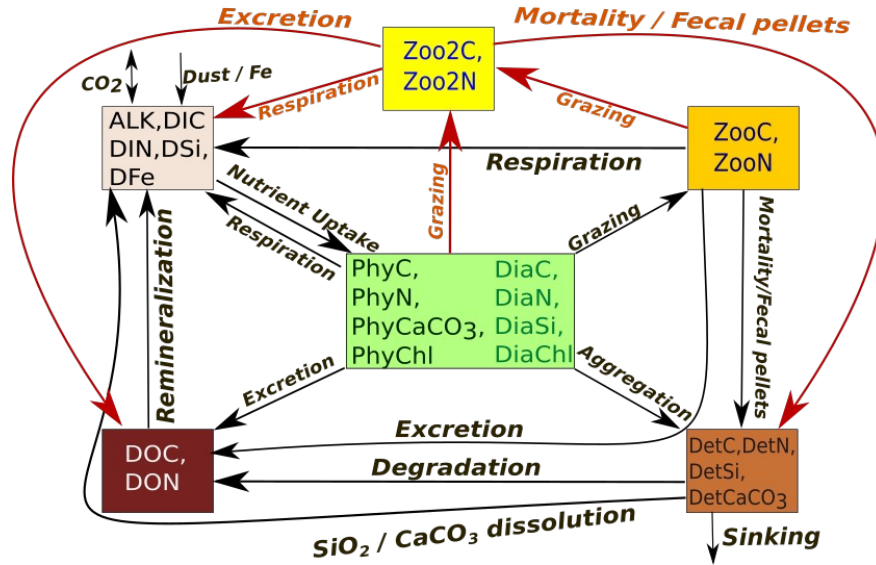


Figure 8: Schematic description of REcoM-2 with second zooplankton compartment. The 21 tracers can be grouped into primary producers diatoms (DiaN, DiaC, DiaSi, DiaChl) and non-diatoms (PhyN, PhyC, PhyCaCO₃, PhyChl), zooplankton (ZooC, ZooN), second zooplankton (Zoo2C, Zoo2N), detritus (DetC, DetN, DetSi, DetCaCO₃), dissolved nutrients (DIC, DIN, DFe, DSi, ALK) and dissolved organic material (DOC, DON). There is exchange of CO₂ with the atmosphere and a source of Fe by atmospheric dust deposition. Detritus sinks to deeper layers with a prescribed sinking velocity. Arrows are the same as in the previous figure of REcoM2.

2.3.1 State Equations for the New Zooplankton Group Krill

Nitrogen Pool: The source and sink processes for the nitrogen pool of the second zooplankton group are described in Equation 11. Quadratic mortality ($m_{zoo2} \cdot N_{zoo2}^2$) and excretion ($\epsilon_{zoo2}^N \cdot N_{zoo2}$) is a sink and grazing ($G_{zoo2} \cdot \gamma_2$) is a source term. It is similar to the first zooplankton group.

$$S(N_{zoo2}) = G_{zoo2} \cdot \gamma_2 - m_{zoo2} \cdot N_{zoo2}^2 - \epsilon_{zoo2}^N \cdot N_{zoo2} \quad (11)$$

Grazing is defined with the same method. However, for each type of food sources (diatoms, nano-phytoplankton and first zooplankton group) grazing preference options were implemented. The total grazing flux of the second zooplankton group is presented in Equation 12. Equations 13, 14 and 15 are

used for food preferences. The temperature function, which is used in Equation 12, for krill, can be found in Equation 23.

$$G_{zoo2} = \varepsilon_2 \cdot \frac{(N'_{phy} + N'_{dia} + N'_{zoo1})^2}{\varphi_3 + (N'_{phy} + N'_{dia} + N'_{zoo1})^2} \cdot f_{T_{krill}} \cdot N_{zoo2} \quad (12)$$

$$N'_{dia} = \tau_3 \cdot \frac{N_{dia}^2}{\varphi_4 + N'_{dia}} \cdot N_{dia} \quad (13)$$

$$N'_{phy} = \tau_4 \cdot \frac{N_{phy}^2}{\varphi_5 + N'_{phy}} \cdot N_{phy} \quad (14)$$

$$N'_{zoo1} = \tau_5 \cdot \frac{N_{zoo1}^2}{\varphi_6 + N'_{zoo1}} \cdot N_{zoo1} \quad (15)$$

The relative contributions of each group ($G_{zoo2phy}$, $G_{zoo2dia}$, $G_{zoo2zoo1}$) to the grazing are calculated similarly to the first zooplankton group.

$$G_{zoo2phy} = G_{zoo2} \cdot \frac{N'_{phy}}{N'_{phy} + N'_{dia} + N'_{zoo1}} \quad (16)$$

$$G_{zoo2dia} = G_{zoo2} \cdot \frac{N'_{dia}}{N'_{phy} + N'_{dia} + N'_{zoo1}} \quad (17)$$

$$G_{zoo2zoo1} = G_{zoo2} \cdot \frac{N'_{zoo1}}{N'_{phy} + N'_{dia} + N'_{zoo1}} \quad (18)$$

Carbon pool: The source and sink equation of the carbon pool of the second zooplankton is in Equation 19. Grazing is a source term. On the other hand mortality, excretion and respiration are the loss terms.

$$S(C_{zoo2}) = \left(\frac{1}{q_{phy}} \cdot G_{zoo2phy} + \frac{1}{q_{dia}} \cdot G_{zoo2dia} + \frac{1}{q_{zoo1}} \cdot G_{zoo2zoo1} \right) \cdot \gamma_2 - \frac{1}{q_{zoo2}} \cdot m_{zoo2} \cdot N_{zoo2}^2 - \epsilon_{zoo2}^C \cdot C_{zoo2} - r_{zoo2} \cdot C_{zoo2} \quad (19)$$

The important difference between the second zooplankton group and the first zooplankton group is how the respiration is defined. In this study, respiration is implemented into the model from one previous study (Hoffman and Lascara, 2000). Respiration of krill has three components; standard respiration (R_s), respiration activity factor (R_a) and feeding activity term (R_f). It is defined in Equation 20.

$$R = R_s(1 + R_f + R_a) \quad (\text{Hoffmann and Lascara, 2000}) \quad (20)$$

R_a is the function of Julian days and it is used for calculating the respiration activity. R_a has a seasonal dependence. R_a is set to -0.5 from Julian Day 150 through 250 (winter) based on reduced winter respiration rates of krill (Ikeda and Dixon, 1982, Hofmann and Lascara, 2000). The total metabolism is reduced by 50% in winter. In transition periods between winter and summer, a linear decrease and increase is defined for R_a (Hofmann and Lascara, 2000). R_f is the function of the daily ration ingested by krill. It is used for including metabolic cost of feeding activity of krill (Ikeda and Dixon, 1984). R_f increases linearly from 0 to 1 up to a daily ration of 10% of the body weight and remains constant for higher daily rations (Hofmann and Lascara, 2000). The R_f and R_a implementation to the model is illustrated in Figure 9. R_s is the standard respiration rate and the combination of these 3 terms as in Equation 20 is the total respiration of krill in our model.

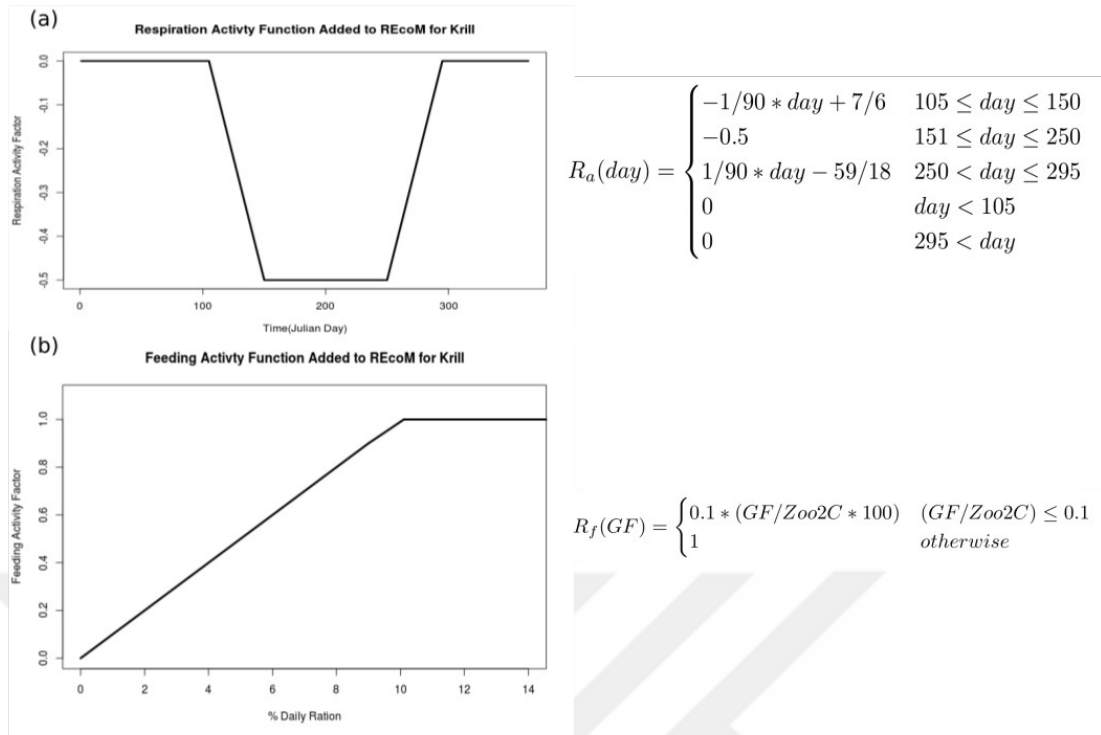


Figure 9: Implemented respiration functions for krill, a) Feeding activity and b) respiration activity terms.

2.3.2 Parameterization of the Second Zooplankton Group Krill

After implementation of the second zooplankton group, it was needed to find parameters from the literature for this group of zooplankton. For this purpose, previous studies were examined and parameters were found with additional calculations.

Maximum grazing rate and half saturation constant: The maximum grazing rate for the krill was chosen as 0.1 (Hofmann and Lascara, 2000). The half saturation constant for Antarctic krill (0.16 $\mu\text{g Chl/L}$) was taken from Meyer (2009) and was converted to $(\text{mmol N m}^{-3})^2$. After conversions of Chl to C and C to N, the half saturation constant was calculated to be 0.01 $(\text{mmol N m}^{-3})^2$. Conversion factors of C:Chl, C:N, μmol to mmol and liter to m^{-3} are 60, 106, 10^{-3} and 10^{-3} , respectively.

Grazing Efficiency: Assimilation efficiency values from the literature were used to determine grazing efficiency. Assimilation efficiency varies in a range between 72% - 94% (Hoffman and Lascara, 2000). Here it is set to 80% and is used for grazing efficiency. The same value is also used in previous bioenergetic modelling of krill studies (Fach et al., 2002).

Standard respiration rate: Equation 21 (Hofmann and Lascara, 2000) was used to calculate the standard respiration rate R_s . In this study, it is assumed that dry weight (DW) of krill is 200 mg.

$$R_s = 0.847 * DW^{0.850} \mu l h^{-1} \quad (21)$$

Finally, Equation 22 (ICES Zooplankton Methodology Manual) was used to convert O_2 respiration to carbon units per day.

$$ml O_2 (\text{individual h})^{-1} * 0.97 * 12 / 22.4 = mg C (\text{individual h})^{-1} \quad (22)$$

Lastly, conversion from μl to ml and from h^{-1} to d^{-1} was done and R_s was calculated to be $0.01 d^{-1}$.

N and C excretion rates: C and N excretion rates are set to the same values. Literature values vary between 0.1% and 6% (Atkinson, 2000). For this study, it was chosen as 2% (Atkinson, 2000).

Grazing preference for different foods: There is no quantified information about grazing preference for the different food sources. However, it is known that diatoms are their staple food (Atkinson, 2016). In this study, the grazing preference is taken as 1, 0.5 and 0.8 for diatoms, small phytoplankton and heterotrophs, respectively.

Mortality rate: The mortality rate was chosen from literature as 0.3% (Fach et al., 2002).

Half saturation constants for different types of foods: Half saturation constants for different types of food were not considered. Therefore, they were set to 0 in this step of the research.

Temperature function for krill: It is needed to define an exponential temperature function for the second zooplankton group krill. Information on temperature dependence of daily growth rate (mm d^{-1}) of krill is used for the formulation of the new temperature function (Atkinson et al., 2006). As it is mentioned in the study, maximum growth of krill occurs at 0.5°C . Below 1°C , temperature function varies between 0.6 and 1. However, above 1°C the temperature function decreases to zero. The new temperature function is derived from Butzin and Pörtner (2016) and rearranged for krill group in the model. The Equation 23 gives the temperature function.

$$f_{T_{krill}} = \frac{\exp\left(\frac{Q_a}{T_r} - \frac{Q_a}{T}\right)}{1 + \exp\left(\frac{Q_h}{T_h} - \frac{Q_h}{T}\right)} \quad (23)$$

In the Equation 23, the optimum temperature $T_r = 272.5$ K, inhibitive processes starting temperature $T_h = 274.15$ K, Arrhenius temperatures for uninhibited and inhibited reaction kinetics $Q_a = 28145$ K and $Q_h = 105234$ K were chosen. The plot of the new temperature function can be found in Figure 10.

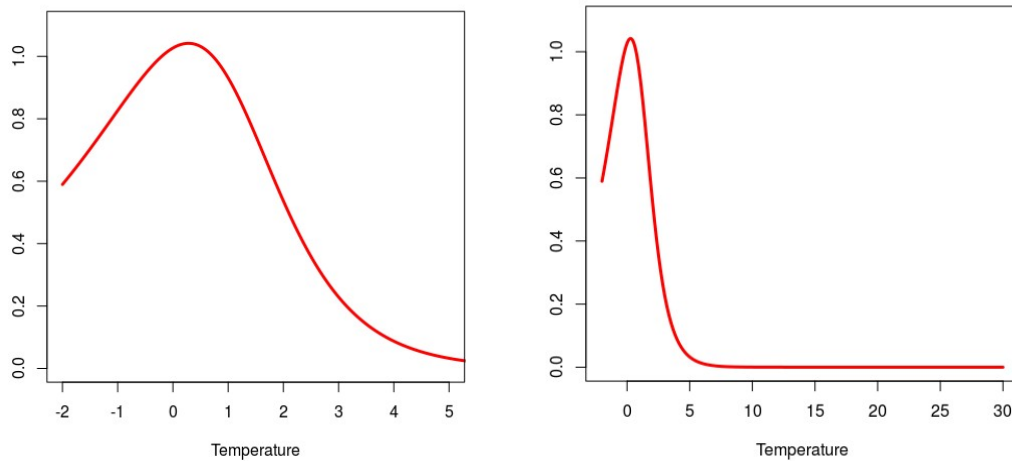


Figure 10: Implemented temperature function for the second zooplankton group krill

This temperature function (Figure 10), gives a similar growth pattern as in the description of the growth rate derived from body length of krill from literature (Atkinson, 2006).

REcoM2 was already used with one zooplankton group in several studies. Therefore we have already a set of parameters for the first zooplankton group. The list of parameters of first zooplankton group (copepod) and second zooplankton group (krill) can be found in Table 1.

Table 1. Model coefficients and their values for zooplankton groups

	Copepod		Krill		Unit
	Model Code	Value	Model Code	Value	
Max. grazing rate	graz_max	2.4	graz_max2	0.1	d ⁻¹
Grazing efficiency	grazEff	0.4	grazEff2	0.8	d ⁻¹
Respiration rate	res_het	0.01	res_zoo2	0.01	d ⁻¹
Mortality rate	loss_het	0.05	loss_zoo2	0.003	d ⁻¹
N excretion rate	lossN_z	0.15	lossN_z2	0.02	d ⁻¹
C excretion rate	lossC_z	0.15	lossC_z2	0.02	d ⁻¹
Half saturation constant	epsilon	0.35	epsilon2	0.01	(mmol N m ⁻³) ²
Half sat. cons. for diatoms	sdiaNsq	0	sdiaNsq2	0	(mmol N m ⁻³) ²
Half sat. cons. for small phy.	sphyNsq	0	sphyNsq2	0	(mmol N m ⁻³) ²
Half sat. cons. for het.	-	-	sHetNsq	0	(mmol N m ⁻³) ²
Max. preference on diatoms	pzDia	0.7	pzDia2	1.0	dimensionless
Max. preference on small phy.	pzPhy	1.0	pzPhy2	0.5	dimensionless
Max. preference on heterotroph	-	-	pzHet	0.8	dimensionless

The main differences between two zooplankton groups are grazing efficiency and maximum grazing rate. The maximum grazing rate of krill is set to 0.1 which is lower than in the copepod group. Also the grazing efficiency of krill is higher than in the copepod group. It is also consistent with the parameterization in other modelling studies that mention grazing rate of macro zooplankton is lower than that of microzooplankton groups (Moriarty, 2009). The mortality rate of krill is lower than for copepods. Excretion rates and respiration rates of the two groups are the same. Moreover, one of the biggest differences is in the food preference term. The food preference term of krill for diatoms is higher than for nano-phytoplankton. However, copepod prefers to graze on nano-phytoplankton rather than on diatoms (Table1).

2.4 Model Experiments

Two experiments were done with the FESOM-REcoM2 biogeochemical-ocean general circulation model. In the first experiment (CTRL), REcoM2 with one zooplankton group was used. The second experiment was done after the implementation of the second zooplankton group (krill). The tracers

for DIN and DSi were initialized with the values from the World Ocean Atlas climatology of 2013 (Garcia, 2014). Dissolved inorganic carbon (DIC) and total alkalinity (TA) tracers were initialized with values from Global Ocean Data Analysis Project (GLODAP) data set (Olsen et al., 2016 and Key et al., 2015). The DFe field was initialized with an output from the Pelagic Interaction Scheme for Carbon and Ecosystem Studies (PISCES) model, which has been modified with observed profiles from Tagliabue (2012). All other tracers were initialized with arbitrary values. The FESOM sea ice-ocean model was forced with the interannually varying (CORE-II) atmospheric states (Large and Yeager, 2004, 2009). Years between 1950 and 1975 were analysed. The first ten years of the runs were considered as a spin-up and the last three years of the runs were analysed.

The changes in the nutrient and primary producers fields with the implementation of the new group were analysed. Differences in the export production and net primary production between two simulations were investigated. Effects of the implementation of the new zooplankton group on the seasonal cycle of the first zooplankton group are shown.

2.5 Datasets for the Model Results Comparison

2.5.1 Krill Dataset

The global macrozooplankton dataset that was used for comparison with model results was “Global distributions of epipelagic macrozooplankton abundance and biomass - Gridded data product - Contribution to the MAREDAT World Ocean Atlas of Plankton Functional Types” (Moriarty, 2012). The data was downloaded from the AWI PANGAEA dataset repository (doi:10.1594/PANGAEA.777398). In the dataset global carbon biomass and abundance of macrozooplankton is available. The whole dataset is a collection of four different datasets. Over 387700 macro zooplankton abundance and 1330 carbon biomass data form this dataset. In Figure 11, the spatial distribution of krill data can be found. Most of the observations

were done around the Antarctic Peninsula. Available data can be reached from <https://doi.pangaea.de/10.1594/PANGAEA.777398>.

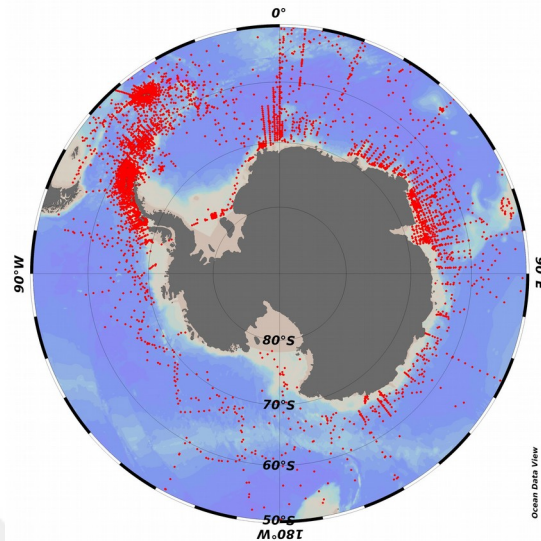


Figure 11: Spatial distribution of Krillbase data base

2.5.2 Satellite Chlorophyll Data

Data from ESA OC-CCI (Ocean Colour Climate Change Initiative dataset, Version [3.1]) was used. The data was downloaded for the years 2012-2015. The dataset is a composition of monthly means of chl a (mg m^{-3}). The data has a 4 km spatial resolution. Monthly data is used to create a climatology of the 3 years.

CHAPTER 3

RESULTS

In this chapter, results of two different model runs and comparisons of simulations are presented. Each model simulation was run for 25 years. The last 3 years of the runs (years 23-25) are used to analyse the results. The first 10 years thought as a spin-up. The results of the standard model with one zooplankton group (CTRL) are shown for the global and Southern Ocean. Afterwards, the results of the model run with the implementation of krill are presented for the Southern Ocean.

3.1 Model Results of REcoM2 with one Zooplankton Group

In this section, the simulated global fields of nutrients, net primary production (NPP), total chlorophyll concentration and zooplankton distribution are examined. Additionally, since the aim of the thesis is to see the effect of krill on the Southern Ocean ecosystem, the spatial distribution of nutrients and primary producers in the Southern Ocean are analyzed in more detail.

3.1.1 Global Nutrient Fields

Macro-nutrients in the biogeochemical model REcoM2 are DIN (dissolved inorganic nitrogen) and DSi (dissolved inorganic silicate). Simulated DIN concentrations vary between 0 to 30 mmol N m⁻³ (Figure 12). High concentrations of DIN are found in the Southern Ocean. Also in the Arctic Ocean DIN presence can be seen. However, concentrations in the subtropical gyres are lower. Chile- Peru and Namibia upwelling systems act as a nutrient supply to the surface that can be seen also in the model result (Figure 12). The spatial distribution compares well to the expected distribution from the World Ocean Atlas 2013 (Garcia et al., 2014, Figure 13a). There is a distinct difference in the equatorial Pacific, that has too low DIN concentration in the model.

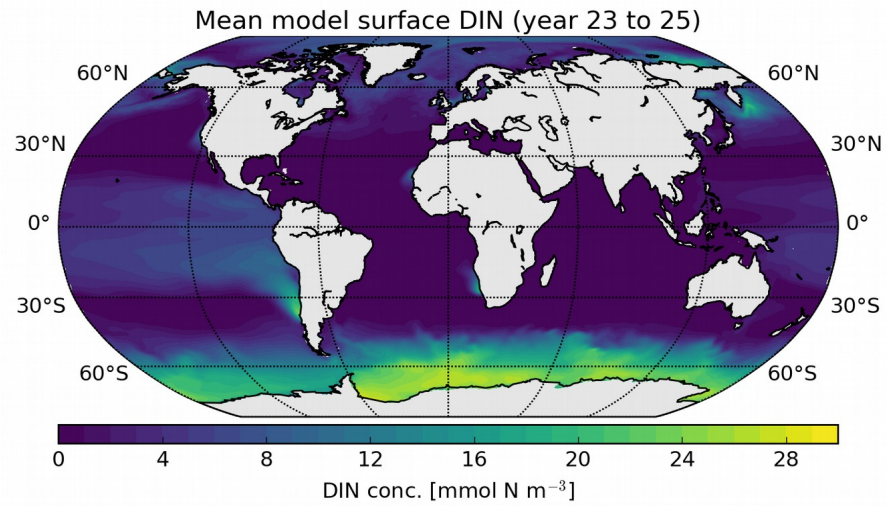


Figure 12: Three-year average of surface dissolved inorganic nitrogen (DIN) concentrations from the model run with one zooplankton group (CTRL)

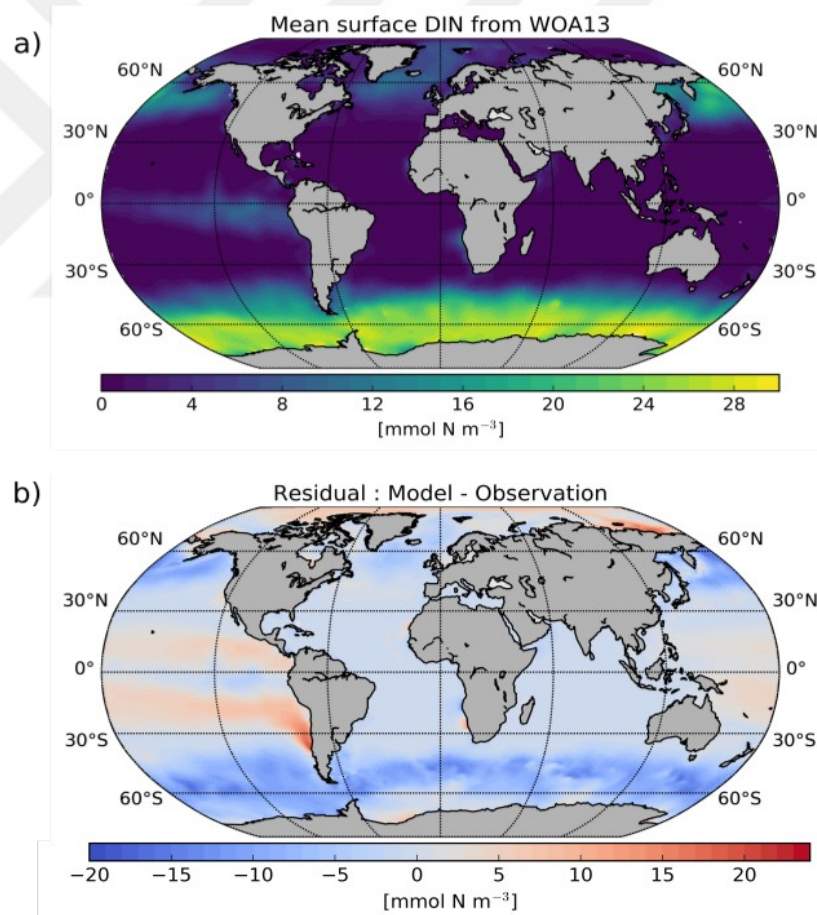


Figure13: a) Surface annual mean nitrate concentrations from WOA13 b) Residual plot of nitrate concentration: modelled values minus observed values.

The difference plot between modelled DIN and data shows that modeled DIN concentrations have a negative bias in the Southern Ocean (Figure 13b), while modeled DIN concentrations have a positive bias in the Arctic Ocean and Chile-Peru upwelling region. Moreover, a negative bias can be seen in the Equatorial Pacific when the spatial distributions of DIN in model and data are compared. These negative biases can be the result of either too weak upwelling or too strong productivity in the Southern Ocean.

DSi is another important macro-nutrient in the oceans. Modelled DSi concentrations are higher in the Southern Ocean than in other parts of the oceans (Figure 14). Concentrations vary between 0 and 60 mmol m^{-3} . However, global DSi concentrations from World Ocean Atlas 2013 (Garcia et al., 2014, Figure 15a) vary between 0 and 90 mmol m^{-3} . The spatial distribution compares well to the expected distribution from the World Ocean Atlas 2013 silicate concentrations (Garcia et al., 2014, Figure 13a). There is a difference in the polar regions and Equatorial Pacific.

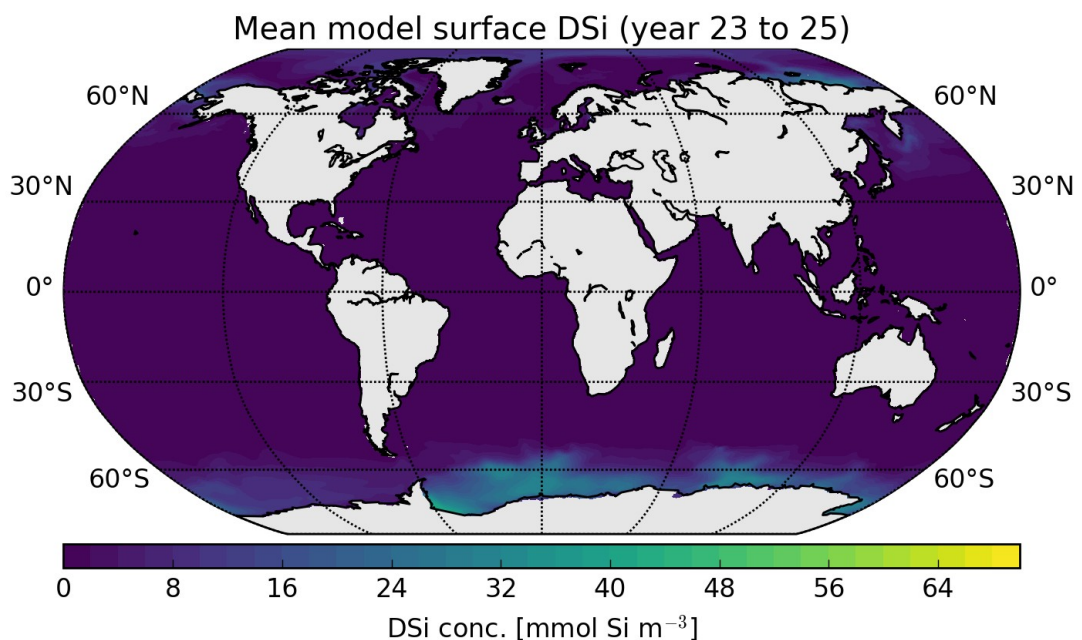


Figure 14. Three-year average surface DSi concentrations from CTRL simulation.

When modeled and observed values are compared, it can be seen that there is a negative bias in the Southern Ocean DSi concentration. The similar kind of negative bias is present in the Equatorial Pacific and in the North Pacific (Figure 15b). However, the model results showed a positive bias in the Southern Ocean in a previous study using this model in a different resolution (Schourup-Kristensen et al., 2014). This discrepancy between model simulations may be the result of different parameterizations of variables in the model. In this study an updated version of FESOM was used. Moreover, the runs were done for the different years.

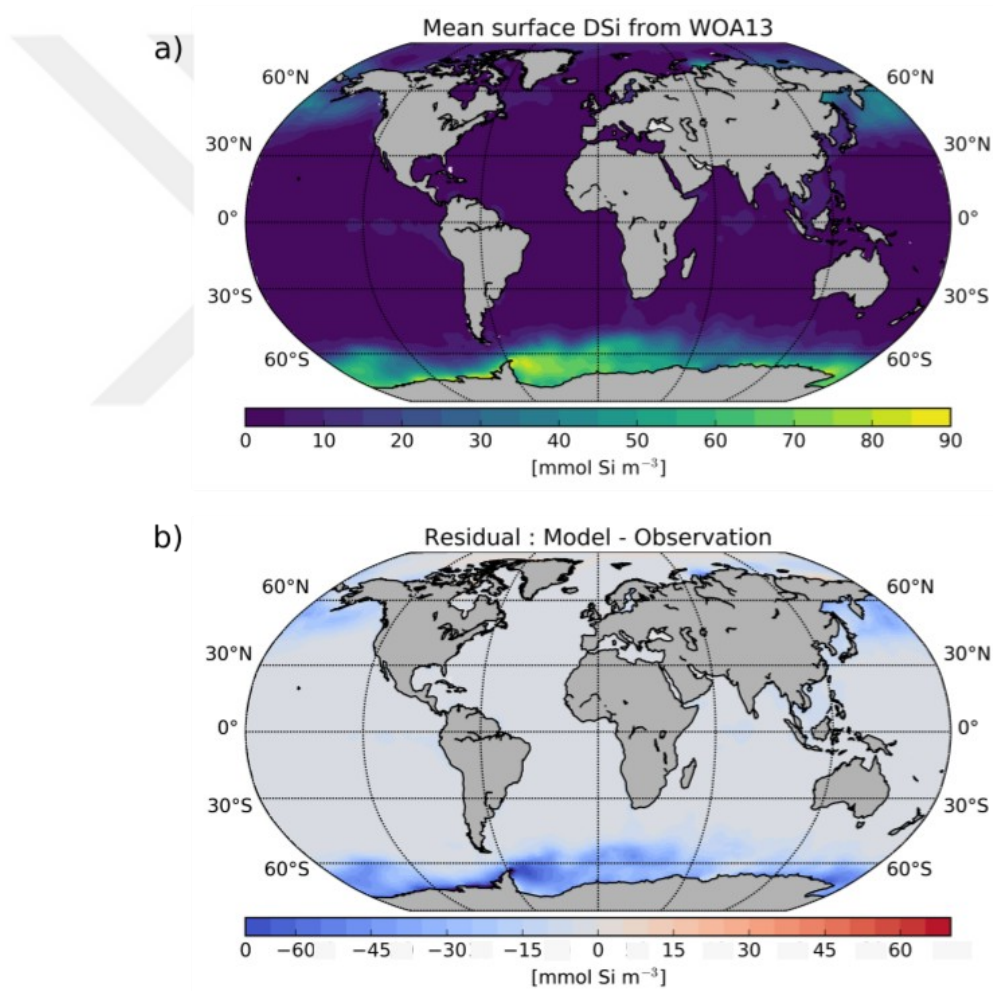


Figure 15. a) Surface annual mean silicate concentrations from WOA13 b) Residual plot of silicate concentration: modelled values minus observed values.

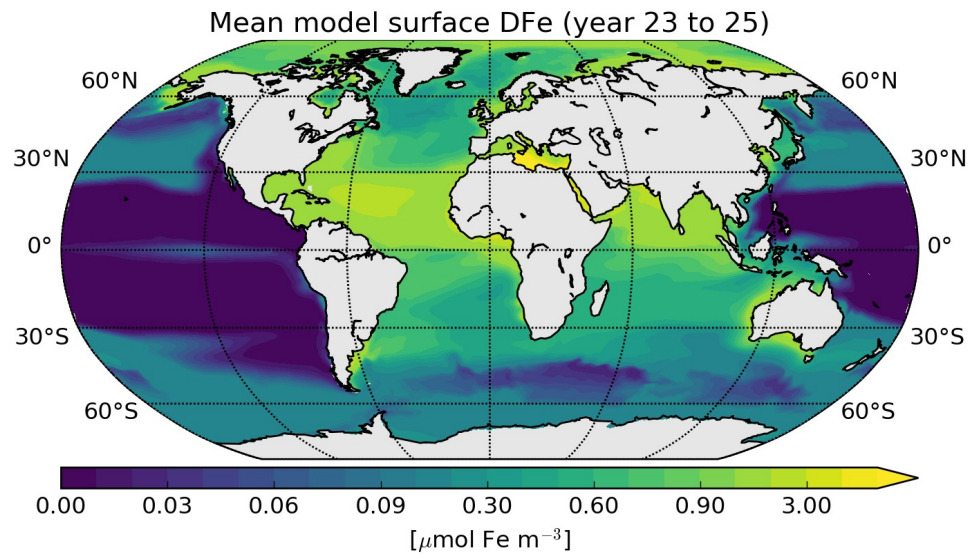


Figure 16. Three-year average surface iron concentration from CTRL.

Micro-nutrients such as iron play an important role for primary production. The model simulates high iron concentrations in the North Atlantic and in the Arctic Ocean. In contrast, it simulates low iron concentrations in the Southern Ocean and equatorial Pacific. The iron concentration varies between 0 - 3 $\mu\text{mol m}^{-3}$ (Figure 16). When the results from the model are compared with the observed values from the literature, overestimated iron concentrations can be seen in the Tropical Atlantic (Tagliabue et al., 2014).

3.1.2 Global Primary Production Features

Primary production varies greatly over different parts of the oceans. It is highly related to available nutrient concentrations and physical parameters. In this part of the results section, mean chlorophyll concentrations and net primary production (NPP) values of the last three years of the model run are presented. The contribution of the two different phytoplankton groups to the mean chl concentration and mean NPP is also shown.

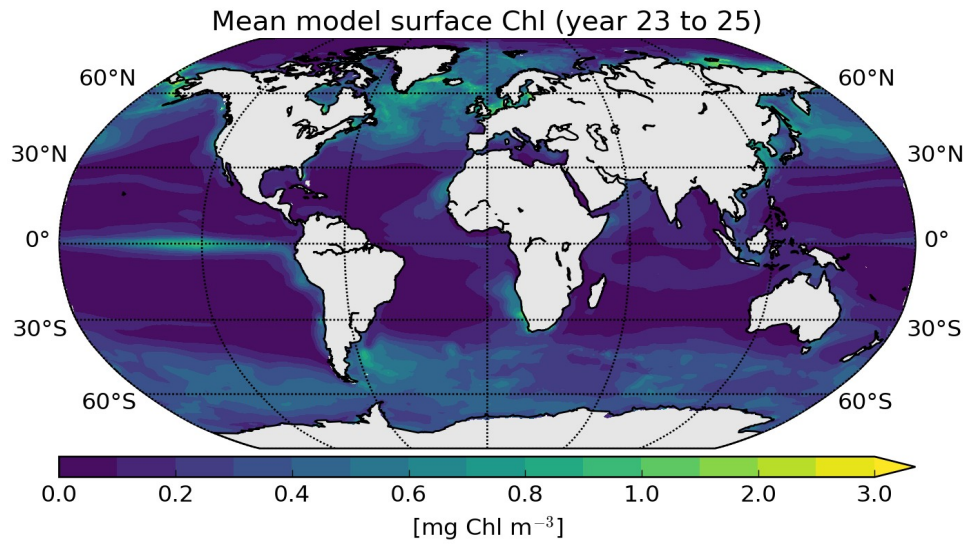


Figure 17. Three-year average chl concentrations from CTRL simulation.

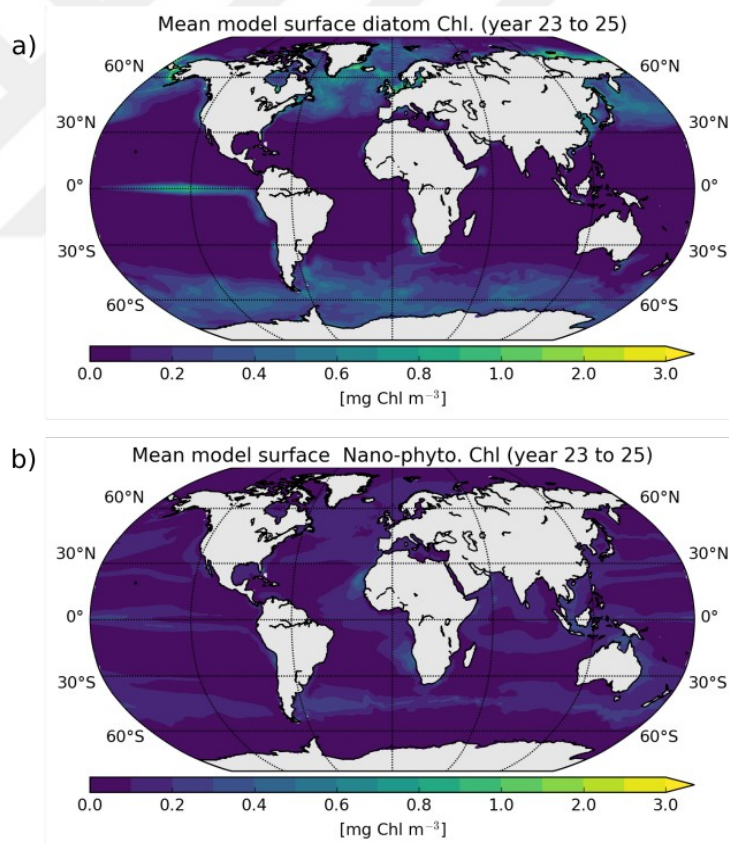


Figure 18. Three-year average of chl concentration of different groups of primary producers from CTRL simulation. a) Contribution of diatoms b) Contribution of nanophytoplankton.

The modeled mean chl concentrations in the global ocean vary between 0 and 3 mg chl m⁻³. While the subtropical gyres have low concentrations of chl, high concentrations can be seen in the most productive areas of the global oceans, such as upwelling areas and the high latitudes. This result is similar to the previous study which was done with REcoM2 (Schourup-Kristensen et al., 2014).

When the simulated contribution of different phytoplankton groups to the chl concentration is examined, the dominance of diatoms can be seen in high latitudes and equatorial regions. In contrast, the contribution of nanophytoplankton is seen in other places such as upwelling regions and around subtropical gyres with low concentrations (Figure 18 a,b).

The simulated net primary production distribution is similar to the spatial map of chl concentrations (Figure 19). Low net primary production is simulated in the center of the subtropical gyres. In contrast, there is high production in upwelling regions and intermediate production in the high latitudes. The mean NPP varies between 0 to 1000 mg C m⁻² per day (Figure 19). NPP shows similar large scale patterns as the observations and previous model results (Schourup-Kristensen, 2014).

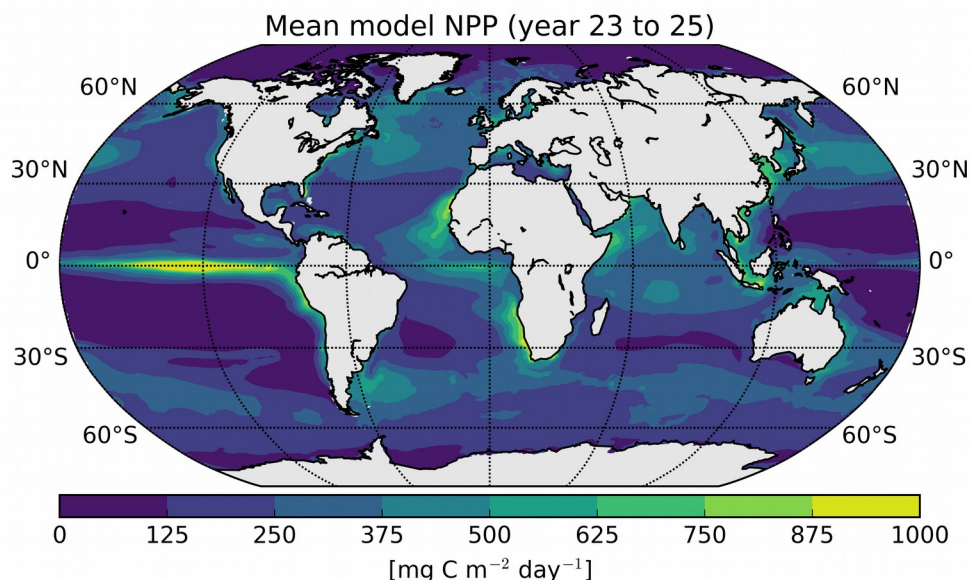


Figure 19. Three-year average of NPP from CTRL simulation.

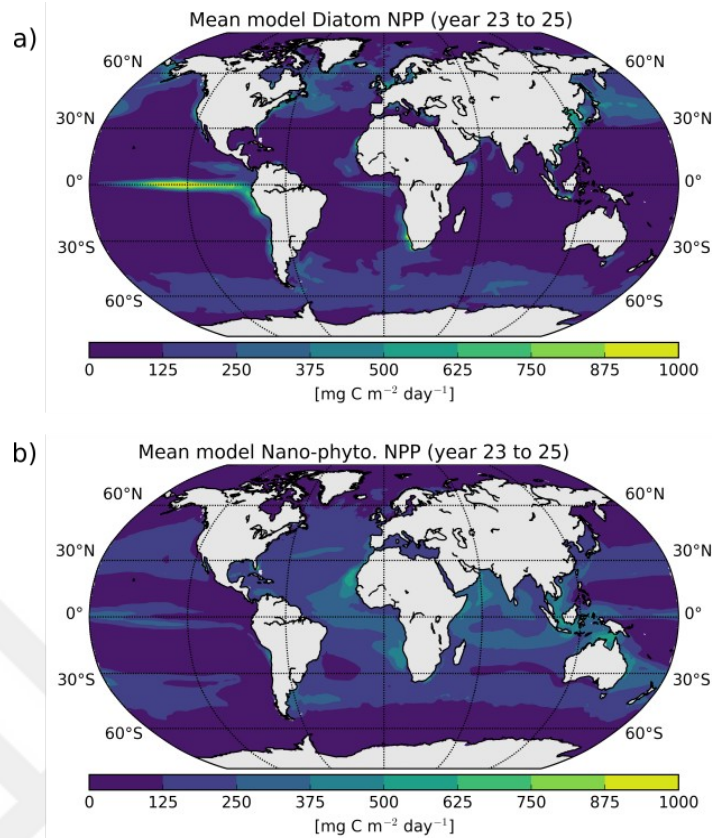
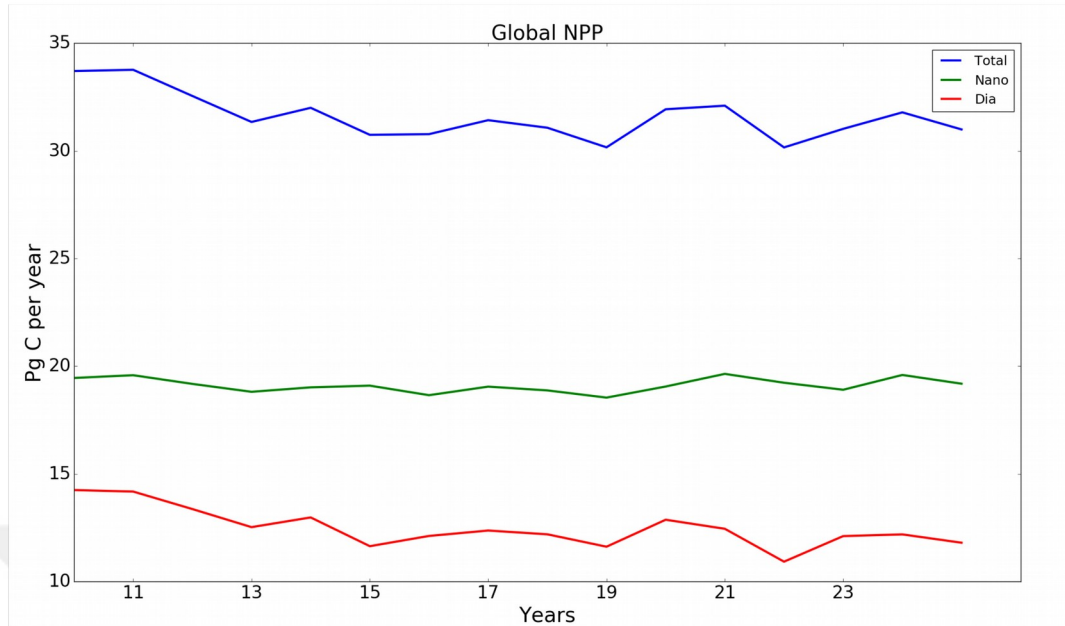


Figure 20. Three-year average of NPP from different groups of primary producers in CTRL. a) The contribution from diatom group b) The contribution from nano-phytoplankton group.

Diatom based production dominates in the high latitudes and the equatorial upwelling. In the other regions, mainly nano-phytoplankton are dominant or both groups co-occur (Figure 20 a,b).

In addition, the total global net primary production and global export production (EP) were calculated for each year of the model run. Global NPP and EP of the 25 years long model run with one zooplankton group are shown in Figure 21. The mean global total NPP and EP of the last three years of the run is 31.2 Pg C per year and 6.6 Pg C per year, respectively. The mean of last three years contribution of the diatom group to the total NPP is 19.2 Pg C per year. Contribution of the nanophytoplankton group is 12 Pg C per year.

a)



b)

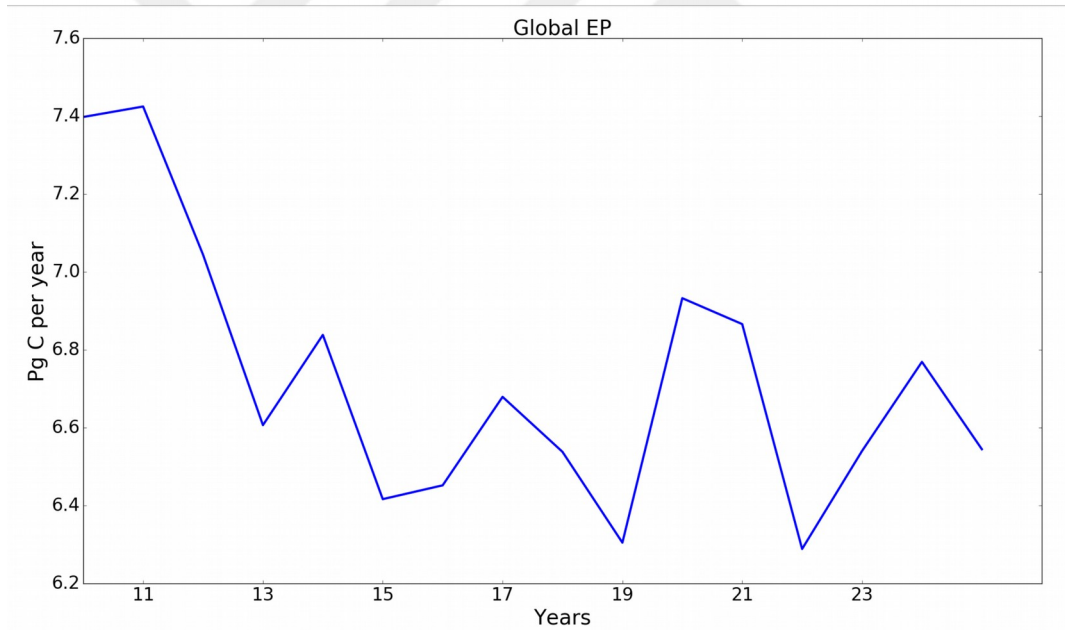


Figure 21: Time series of global total NPP and EP of the last 15 years of the model run with one zooplankton group. a) Global total NPP, b) Global total EP.

3.1.3 Southern Ocean Nutrient Fields

The simulated macro nutrients DIN and DSi concentrations can be seen in Figure 22. In the model results, there are higher nutrient concentrations in the Atlantic and Indian sectors of the Southern Ocean rather than in the Pacific sector of the Southern Ocean. The concentration range of the simulated macro-nutrients in the Southern Ocean is similar to the range in the global distribution of these nutrients.

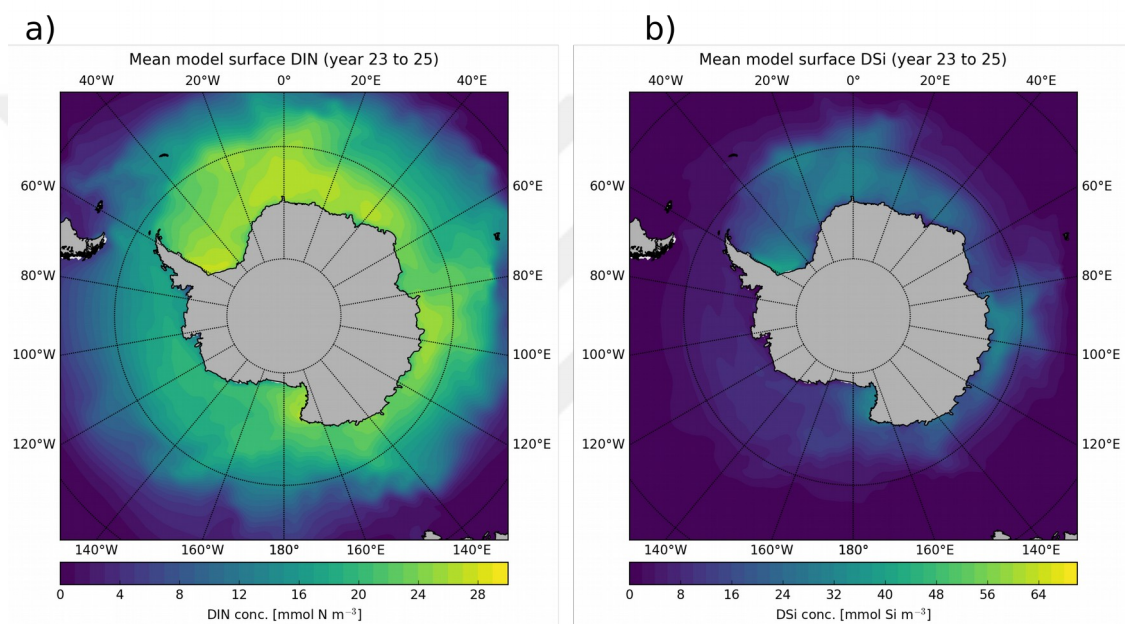


Figure 22. Three-year average of macronutrients in the Southern Ocean. a) DIN b) DSi

In contrast, low simulated iron concentrations can be seen in Figure 23. They vary between 0-0.6 $\mu\text{mol m}^{-3}$. The values are relatively low when compared to other parts of the oceans such as the North Atlantic and Arctic Ocean. In these parts of the ocean, iron concentrations reach up to 3 $\mu\text{mol m}^{-3}$. Simulated iron concentrations in the Southern Ocean are in the range of observations by Tagliabue et al. (2012). The mean concentrations calculated by Tagliabue et al. (2012) are 0.39, 0.33 and 0.15 $\mu\text{mol m}^{-3}$ for the Atlantic, Indian and Pacific sectors, respectively.

The simulated spatial distribution of nutrient concentrations shows that the model reproduces the HNLC conditions that are observed in the Southern Ocean (Falkowski et al., 1998).

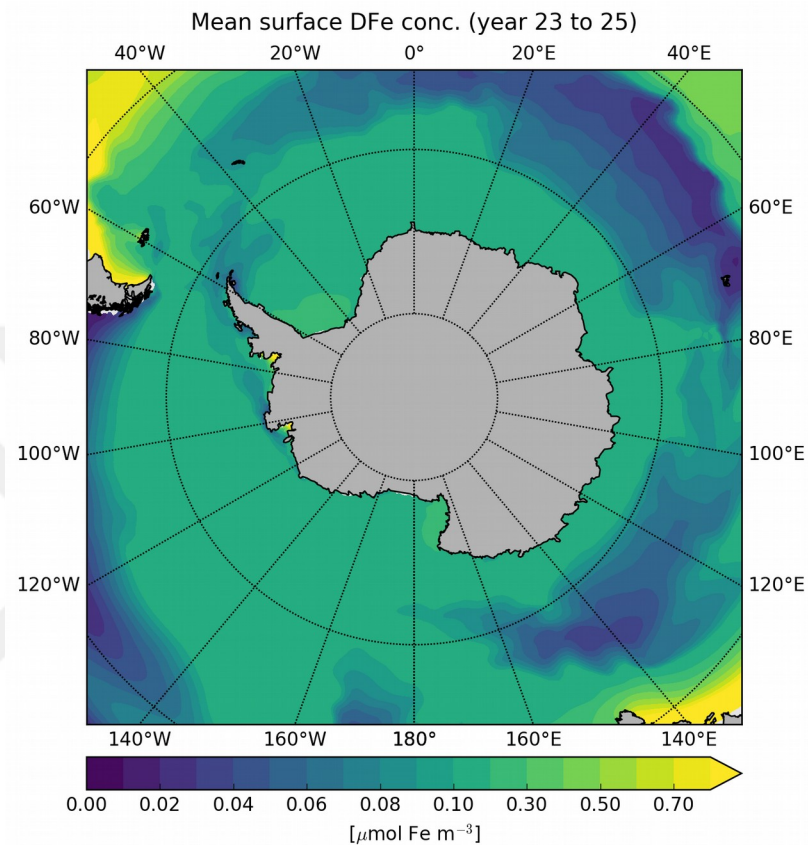


Figure 23. Three-year average of iron in the Southern Ocean in the CTRL simulation.

3.1.4 Southern Ocean Primary Producers Fields

In this section, the spatial distribution of chl and NPP are analysed. The surface mean distribution of chl concentration shows a similar pattern as the iron concentrations. It varies between high concentrations of 2 mg chl m^{-3} and low concentrations $0.02 \text{ mg chl m}^{-3}$. The tip of the South America has highest chl concentrations (Figure 24). Moreover, the mean chl concentrations are lower south of 70°S , since there is sea ice coverage in

this part of the Southern Ocean (Figure 25). The three years average of sea ice thickness varies between 0.1 to 4 meters. Sea ice can extend to north of 60°S in the Atlantic sector of the Southern Ocean (Figure 25).

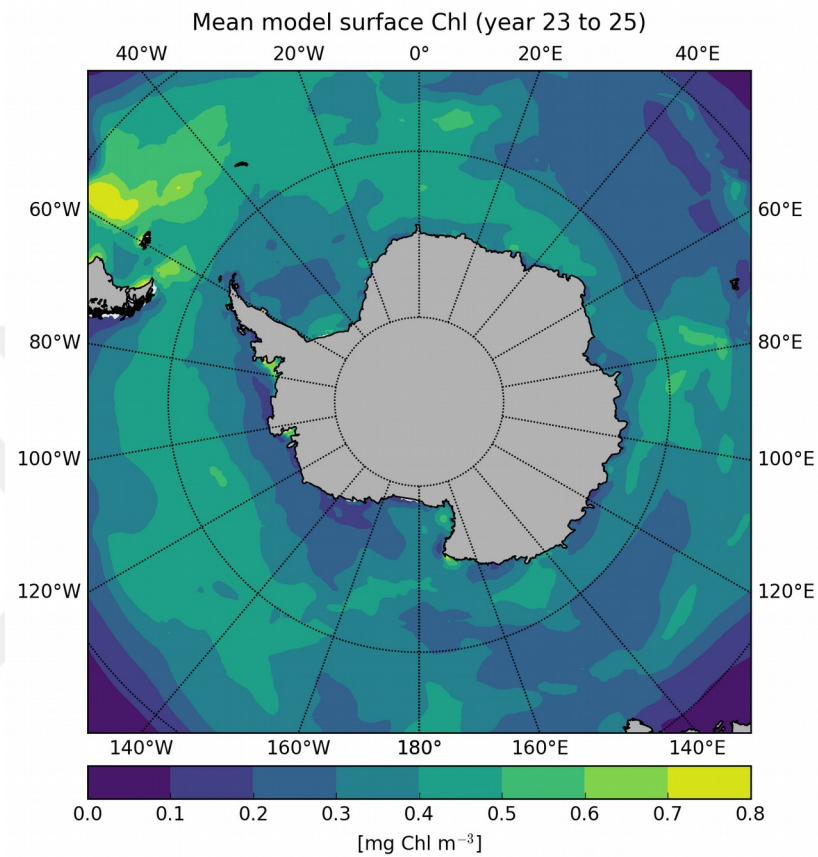


Figure 24. Three-year average of chl concentration in the Southern Ocean of model run with one zooplankton group.

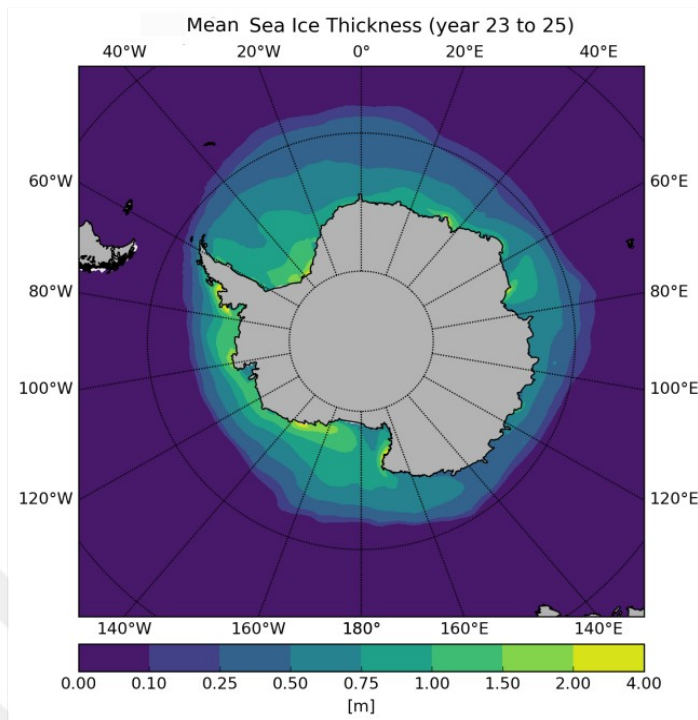


Figure 25. Three-year average of sea ice thickness in the Southern Ocean of model run with one zooplankton group

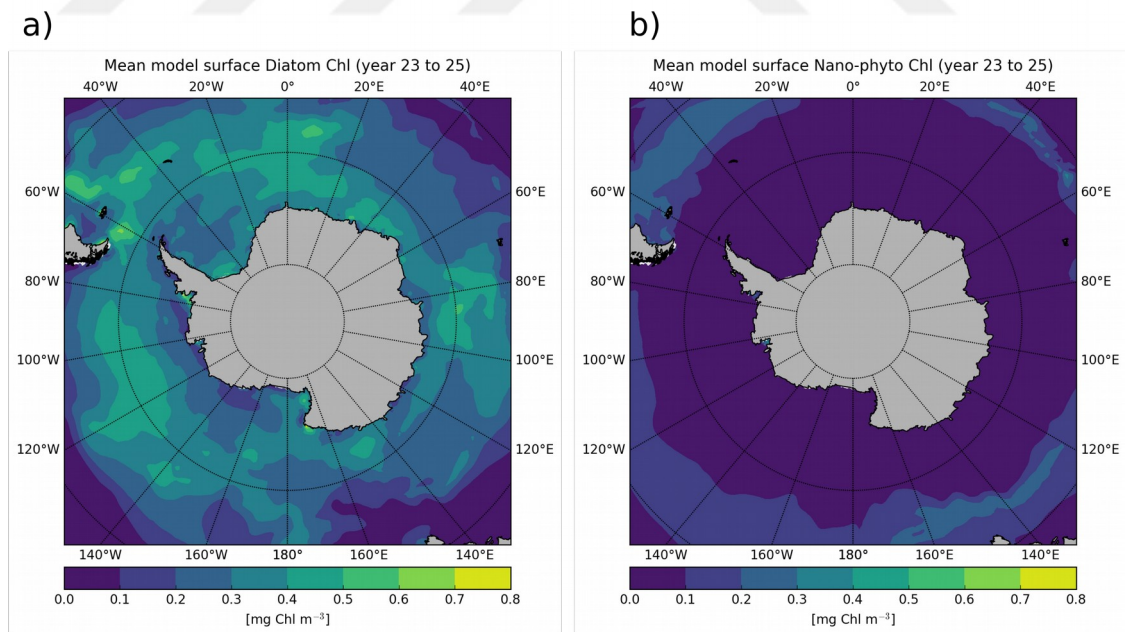


Figure 26. Three-year average of a) Diatom chl and b) Nano-phytoplankton chl concentrations of model run with one zooplankton group.

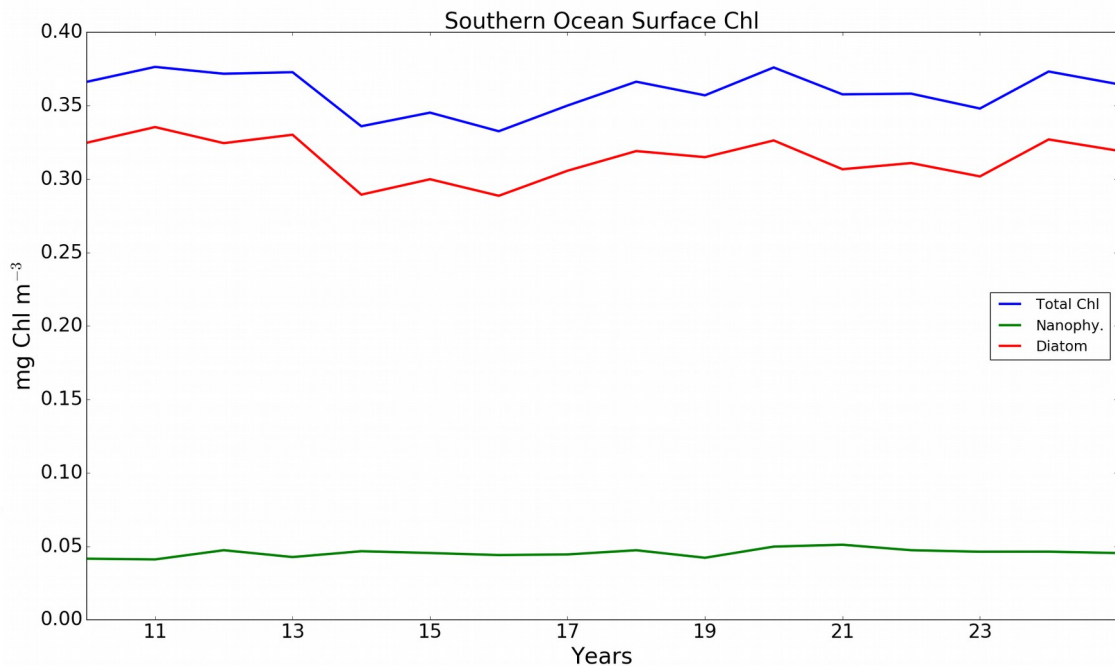


Figure 27: Time series of annual average of surface chl (total chl-blue runs, diatom chl-red line, nanophytoplankton chl-green line) during the last 15 years of control run with one zooplankton group.

Diatoms are dominant in the modelled Southern Ocean. Contribution of nano-phytoplankton group to the chl concentration is lower (Figure 26 a,b). The mean surface chl concentration of the last three years of nanophytoplankton and diatom groups are 0.05 and 0.36 mg chl m⁻³ in the whole Southern Ocean, respectively (Figure 27). However, nano-phytoplankton mainly contribute to total chl north of 70° S.

Also the NPP spatial distribution shows a similar pattern as chl. Diatoms clearly dominate over nanophytoplankton (Figure 29). The three years mean of NPP from diatoms is 170 mg C m⁻² in the whole Southern Ocean. In contrast, mean of the NPP from nanophytoplankton is 32.5 mg C m⁻² in the whole Southern Ocean. The mean total NPP for Southern Ocean is 3.3 Pg C per year. The contribution of diatoms to this NPP is 2.8 Pg C per year which is almost 80% of total NPP (Figure 30).

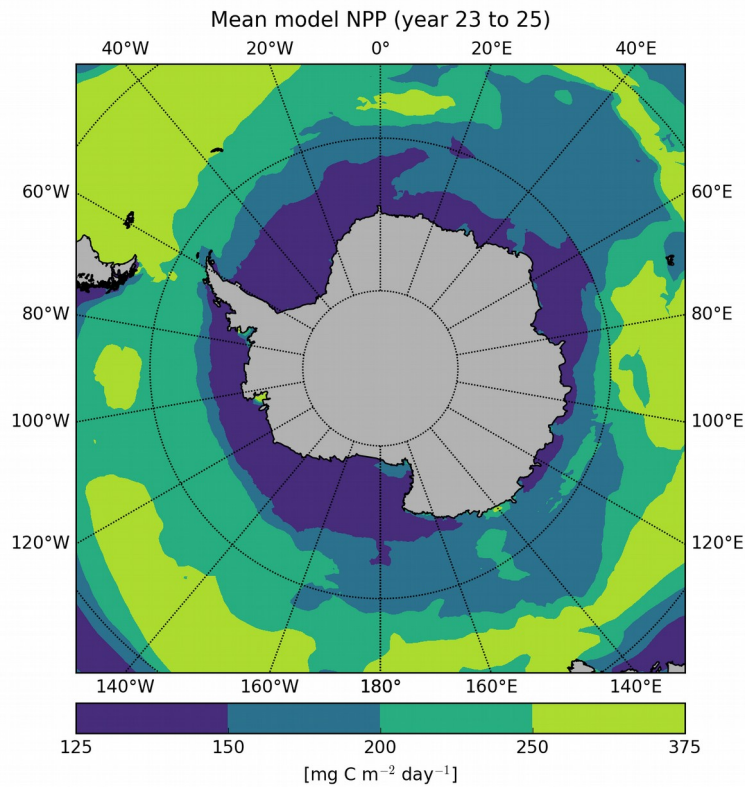


Figure 28. Three-year average of NPP in the Southern Ocean of model run with one zooplankton group.

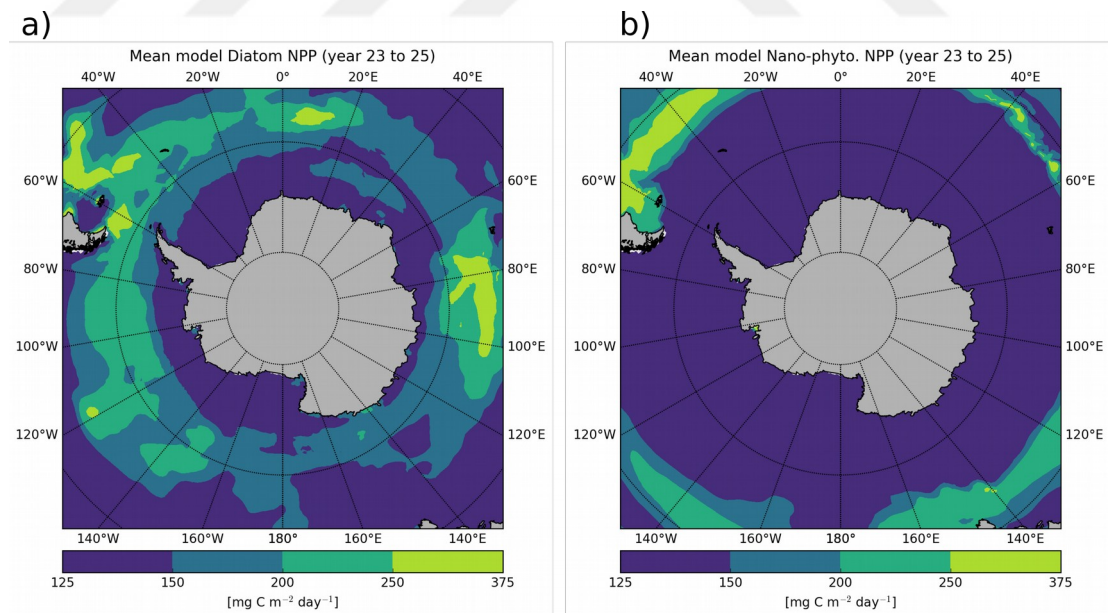


Figure 29. Three-year average of a) NPP from diatoms and b) NPP from nano-phytoplankton in the Southern Ocean of model run with one zooplankton group.

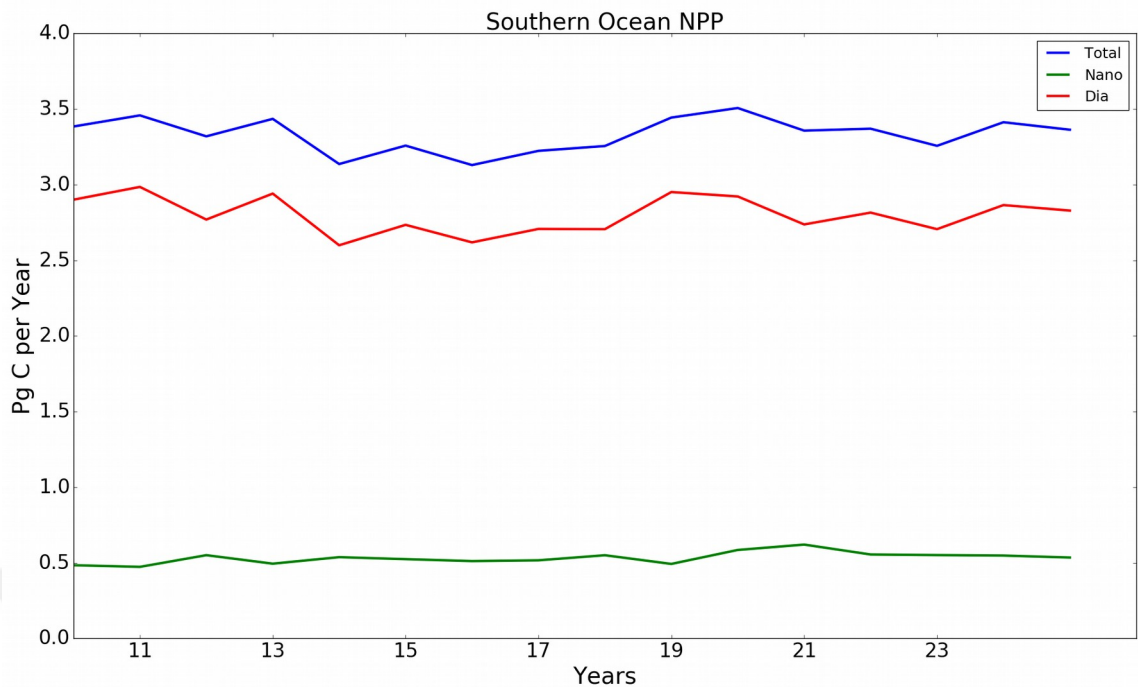


Figure 30. Total NPP in the Southern Ocean during the last 15 years of the control run

3.2 Southern Ocean Analysis of Krill simulation

In this section, changes in the simulated Southern Ocean with the implementation of krill in the biogeochemical model REcoM2 are presented. Residual plots of nutrient fields and primary producers are shown to visualize the changes in the krill simulation. The spatial distribution of zooplankton groups are shown. Moreover, dissolved organic carbon (DOC) and particulate organic carbon (POC) production by different groups, as well as respiration and grazing features of zooplankton groups are presented. Also, changes on the seasonal cycle of chl concentration in the Southern Ocean are investigated.

3.2.1 Changes in Southern Ocean Nutrient Fields in Krill Simulation

The general spatial pattern of nutrients did not change in the krill simulation. The simulated concentrations of nutrients DIN, DSi and DFe increased. The maximum increase and decrease in nutrient concentrations are around 7% of

the nutrient concentrations in the one zooplankton simulation nutrient concentrations.

Surface DIN concentrations increase almost throughout the whole Southern Ocean with the new zooplankton implementation, but especially in the Atlantic and Indian sectors. The three years mean of the surface DIN concentrations increased by 2.6% after the implementation of krill while surface DIN concentrations decreased in the northern part of the Pacific sector of the Southern Ocean (Figure 31a).

Southern Ocean surface DSi concentrations in surface of the whole Southern Ocean increased by 10.6% in the krill simulation. The highest increase in surface DSi occurs in the Indian sector of the Southern Ocean. In contrast, mean DSi concentrations decrease in the Weddell Sea (Figure 31b).

The micro-nutrient iron shows a 10.6% increase in the whole Southern Ocean in the krill simulation. The highest increase showed up in the Pacific sector of the Southern Ocean (Figure 32). The mean iron concentration increased by 0.11 to 0.13 $\mu\text{mol m}^{-3}$ in the Southern Ocean.

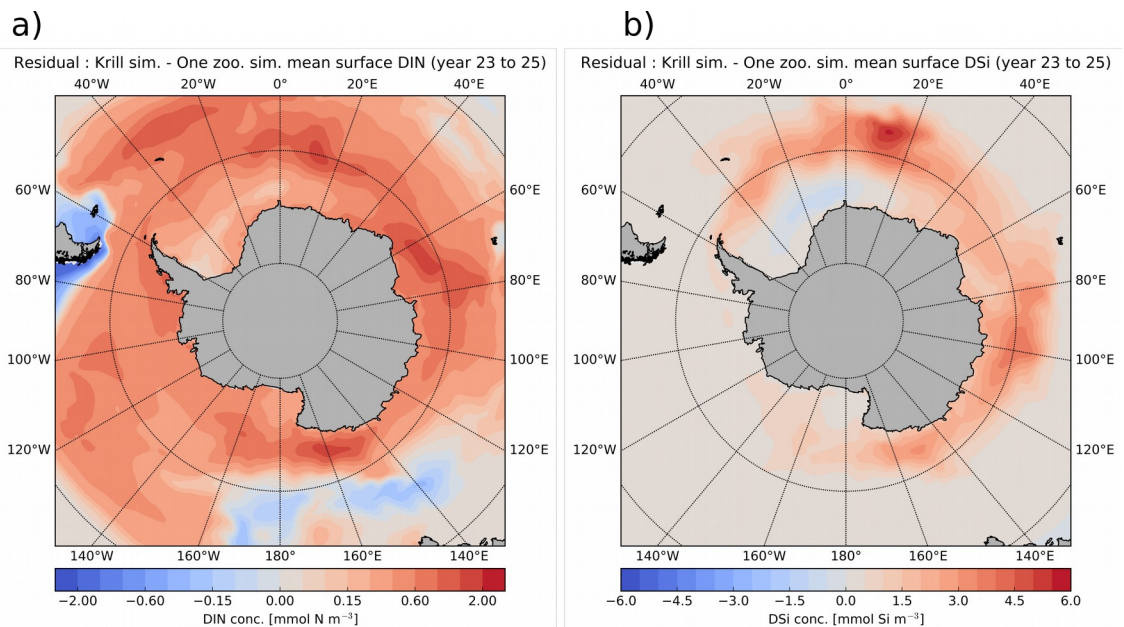


Figure 31. Residual plots (krill simulation - one zooplankton simulation) of three years average of macro-nutrients a) DIN and b) DSi.

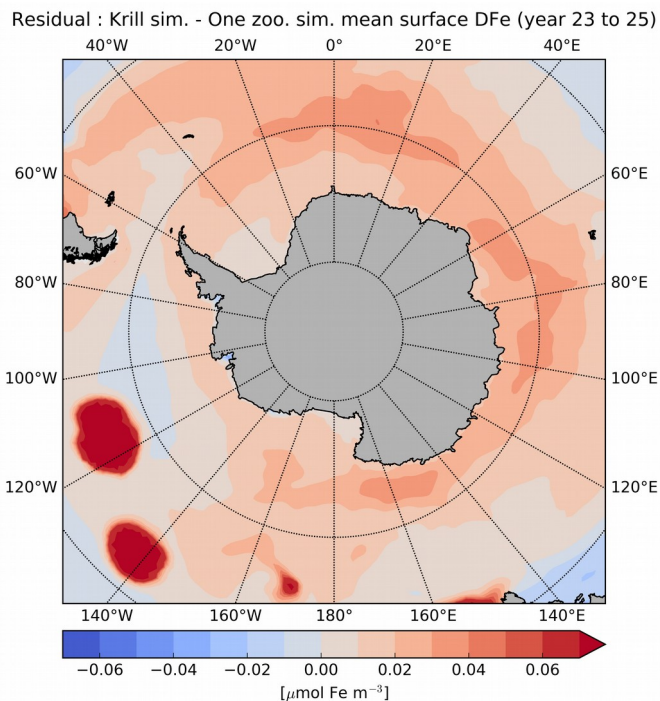


Figure 32. Residual plots (krill simulation - one zooplankton simulation) of three years average of iron

In both simulations, DIN concentrations are underestimated south of 40°S and partly overestimated south of 60°S (Figure 33a, b). When compared to the difference plots of simulations for DIN (Figure 31a), the krill simulation gives DIN concentrations closer to the observations south of 60°S and in the whole Pacific sector of the Southern Ocean. DIN concentrations get closer to the observational concentrations by about 2 mmol DIN m⁻³ (Figure 31a). In contrast, the model underestimated results in the Indian sector of the Southern Ocean, especially north of 60°S. This underestimation is centered in areas with 2 mmol DIN m⁻³ (Figure 31a).

Also, simulated DSi concentrations are lower than observed concentrations in both simulations (Figure 34a, b). The simulated DSi concentrations in the krill simulation is closer to the observational values. The underestimation increases slightly only in the Weddell Sea by around 1 mmol DSi m⁻³ (Figure 31b).

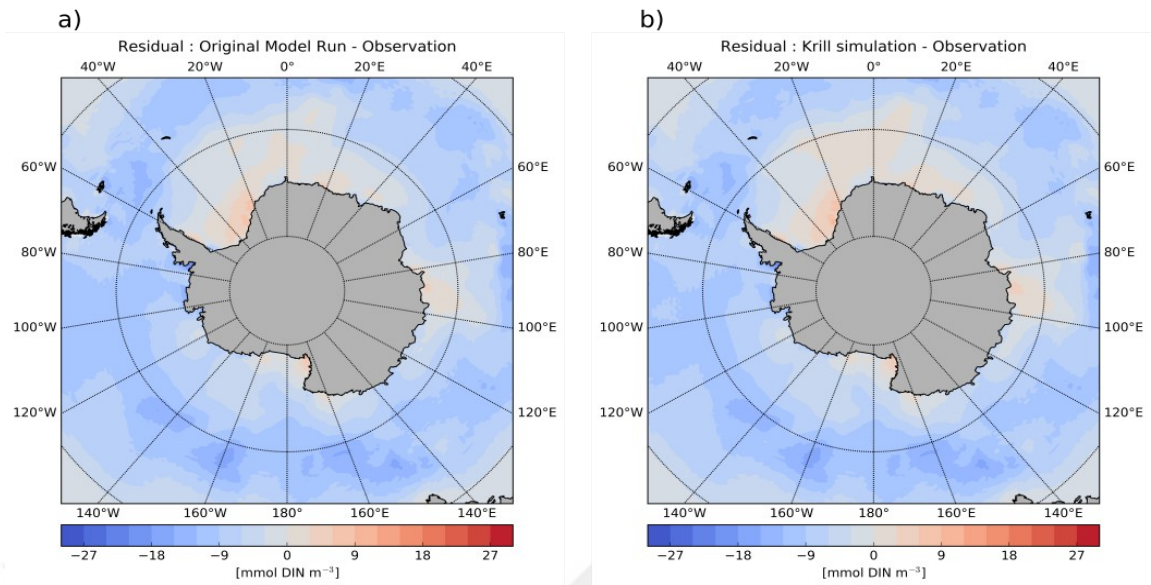


Figure 33. Residual plots (model result - observation (WOA13)) three years average of DIN a) CTRL simulation b) Krill simulation.

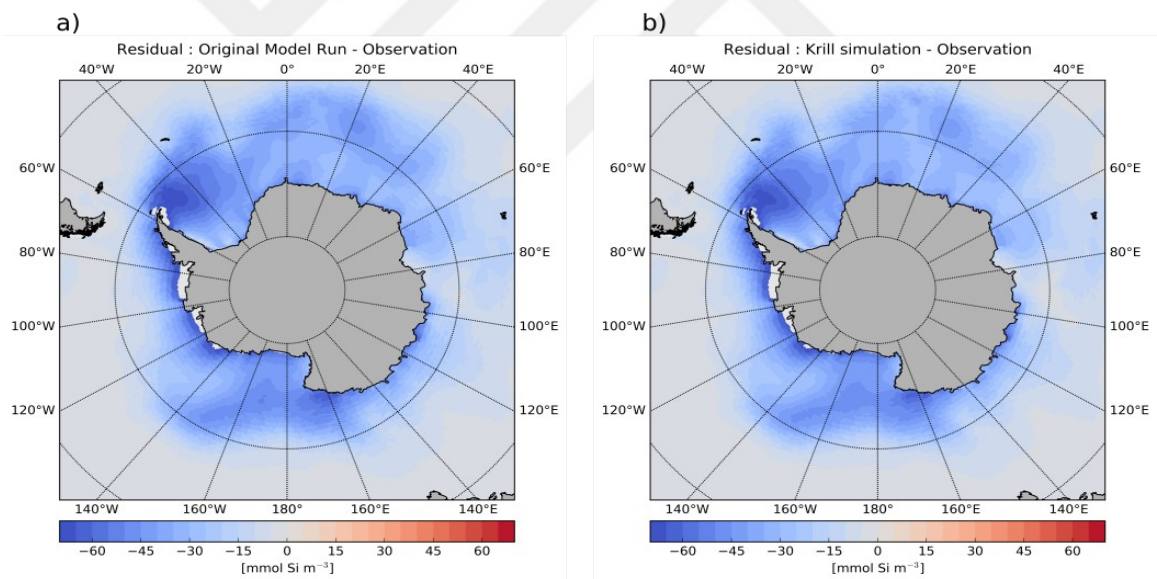


Figure 34. Residual plots (model result - observation (WOA13)) three years average of DSi a) CTRL simulation b) Krill simulation.

3.2.2 Changes in Southern Ocean Primary Producers Fields in Krill Simulation

The implementation of the new zooplankton group krill did not affect the general spatial distribution of the primary producers considerably. Even though the food preference term for the second zooplankton group is set to the highest value for diatoms, diatoms are still the dominant contributors to the simulated chl concentrations and NPP. Also, the range of simulated NPP concentrations did not show major changes in the spatial distribution.

Chl concentrations and NPP decreased between 20°W and 60°W. The average NPP increase was $7 \text{ mg C m}^{-2} \text{ day}^{-1}$. The highest increase in chl and NPP was seen in the Indian sector of the Southern Ocean. It is about 7 mg C m^{-2} per day and $0.02 \text{ mg chl m}^{-3}$ (Figure 35 a, b).

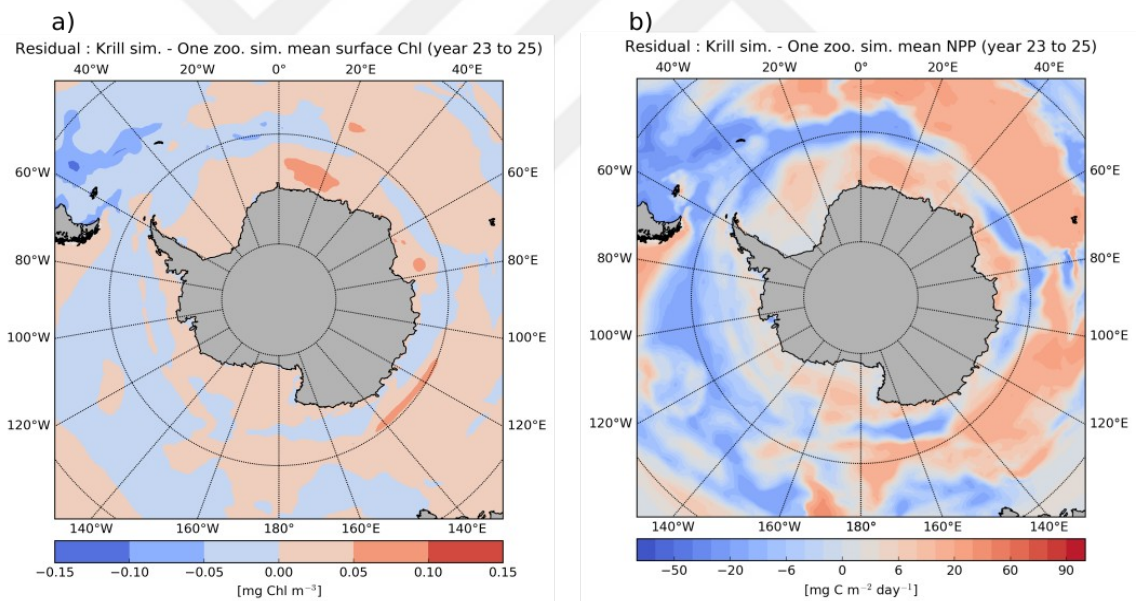


Figure 35. Residual plots (krill simulation - one zooplankton simulation) three years average of primary production fields a) Chl concentrations and b) NPP.

3.2.3 Features of Different Zooplankton Groups in Krill Simulation

In this section, the spatial distribution of zooplankton groups and their grazing, respiration, POC and DOC production rates in the Southern Ocean is shown.

3.2.3.1 Spatial Distribution and Grazing Patterns of Zooplankton Groups

The first zooplankton is mainly distributed in north of 60°S. The highest carbon concentrations of the first zooplankton group appears close to the tip of South America. However, the second zooplankton group is mainly distributed between 50°S-60°S. The second zooplankton concentrations are higher in the Atlantic and Indian sectors of the Southern Ocean. The second zooplankton group can grow further north in these two sectors as opposed to the Pacific sector of the Southern Ocean (Figure 36).

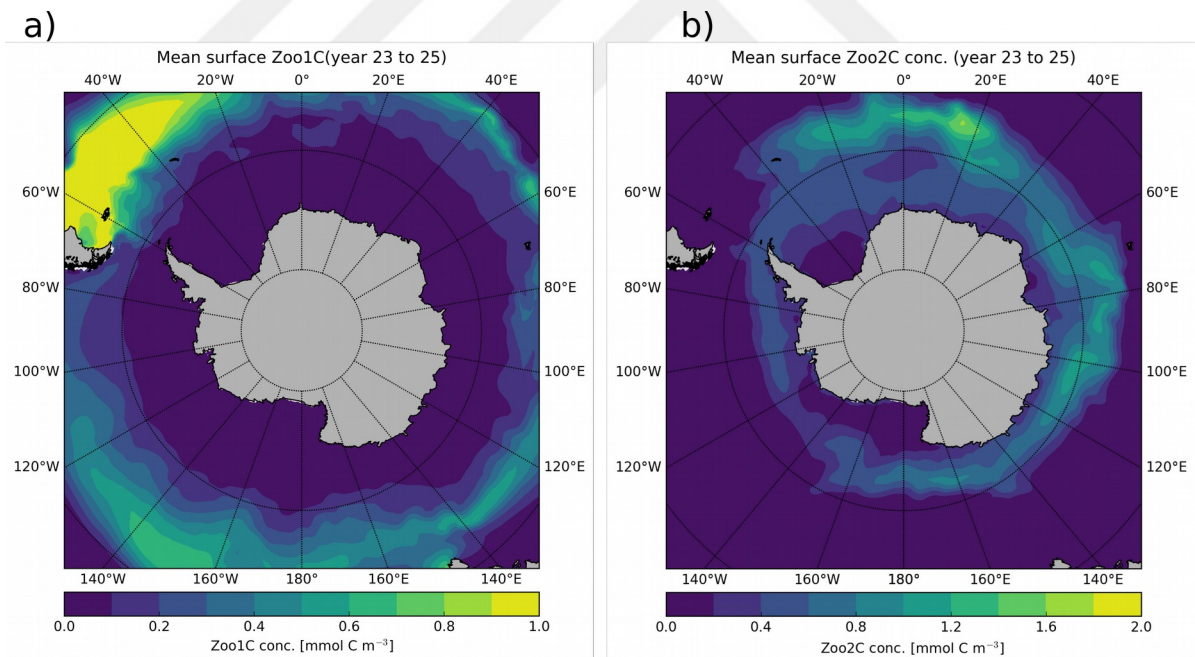


Figure 36. Three-year average surface spatial distribution of a) First zooplankton group carbon pool b) Second zooplankton carbon pool in krill simulation.

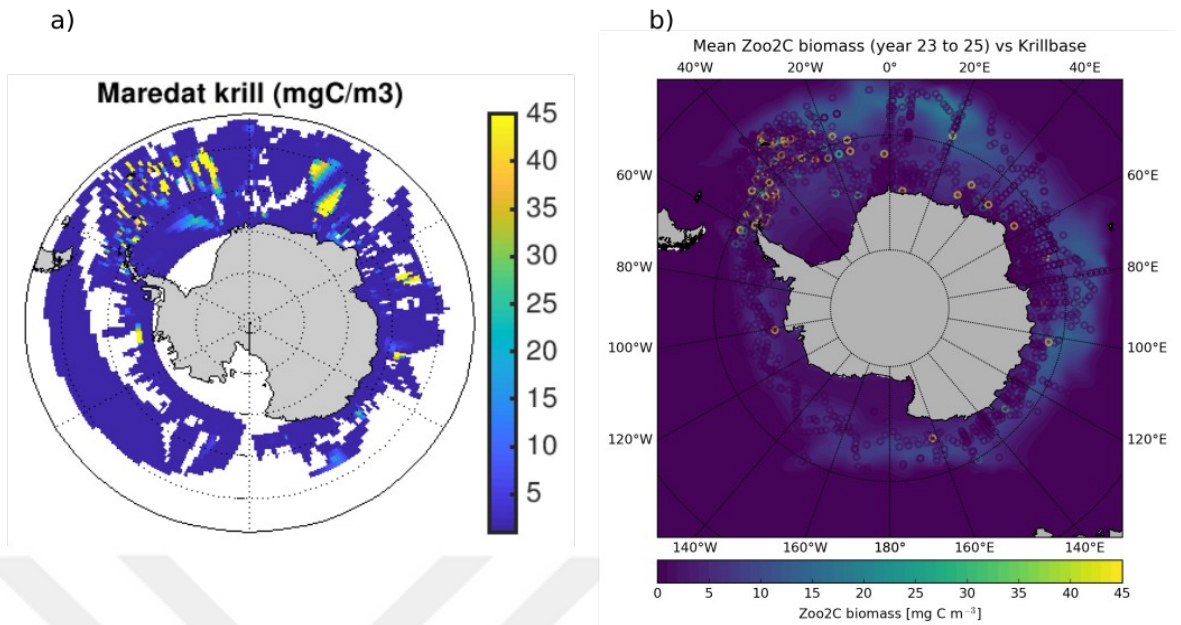


Figure 37. Spatial distribution of Antarctic Krill: a) Data from krillbase b) Three-year average second zooplankton carbon pool with the data from krillbase overlaid.

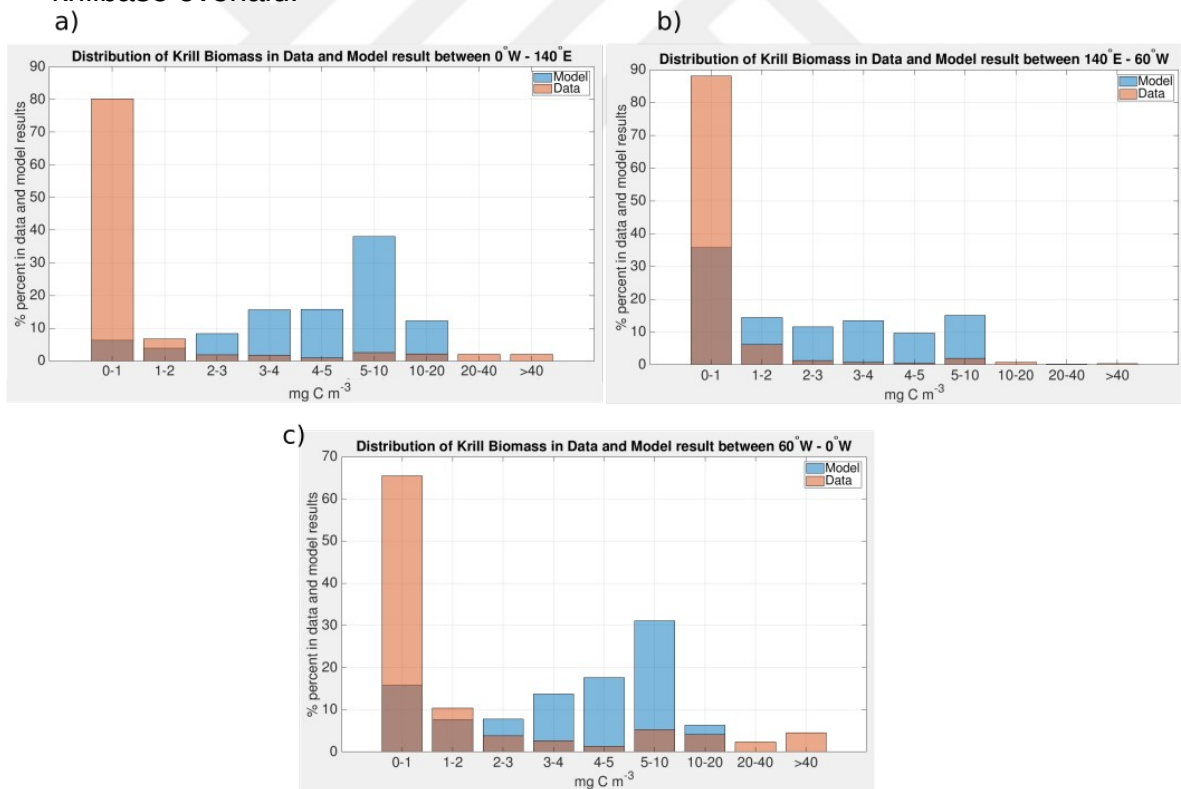


Figure 38. Three-year average percentage distribution of krill biomass in data (red bars) and in the model result (blue bars) for 3 regions a) Between 0°W and 140°E b) Between 140°E and 60°W and c) 60°W and 0°W

Simulated krill biomass is between 0-1 mg m⁻³ in almost 80% of the data points for each region (Figure 38a, b, c). In all regions, data points between 20-40 mg m⁻³ and higher than 40 mg m⁻³ can be seen. Especially in the regions between 0°W-140°E and 0°W-60°W, these high concentrations consist of 4% and 6.9% of data points, respectively (Figure 38a, b). In the region between 140°E and 60°W, these high concentrations are 0.6% of data points (Figure 38c). In contrast, model results of krill biomass range mostly between 2-20 mg C m⁻³ in all three regions (Figure 38 a, b, c). Modelled krill biomass which are in the 2-20 mg C m⁻³ range contribute more than 70% of the modelled biomass for the regions 0°W-140°E and 0°W-60°W. More than 50% of modelled krill biomass is in the range 2-20 mg m⁻³ between 140°E and 60°W. Modelled krill biomass does not reach the high concentrations seen in the data.

High krill biomass is observed around the Antarctic Peninsula (Figure 37a). In the Pacific sector of the Southern Ocean there is only a small amount of data available, which shows that krill biomass is lower in this area than in other areas of the Southern Ocean (Figure 37a). When observations and model results are plotted on top of each other, it can be seen that the spatial distribution pattern is similar, especially in the latitudinal distribution (Figure 36b; Figure 37a, b). There is a good agreement between model and data in the Pacific sector of the Southern Ocean. However, the simulated biomass of krill is relatively low compared to the observational data (Figure 37b). Modelled krill biomass is lower than observed especially around the Antarctic Peninsula. In this region, the observed biomass reaches 40 mg C m⁻³. In contrast, in the same region, the maximum modeled biomass is 19 mg C m⁻³.

Also, simulated grazing patterns of the zooplankton groups differ from each other. The first zooplankton group mainly grazes in the northern parts of the Southern Ocean. As it is expected from the spatial distribution of this group, the highest grazing activity is at the tip of South America (Figure 39a). However, the second zooplankton group grazes mainly between 50-70°S.

The grazing activity of this group is higher in the Atlantic and Indian sectors of the Southern Ocean (Figure 39b).

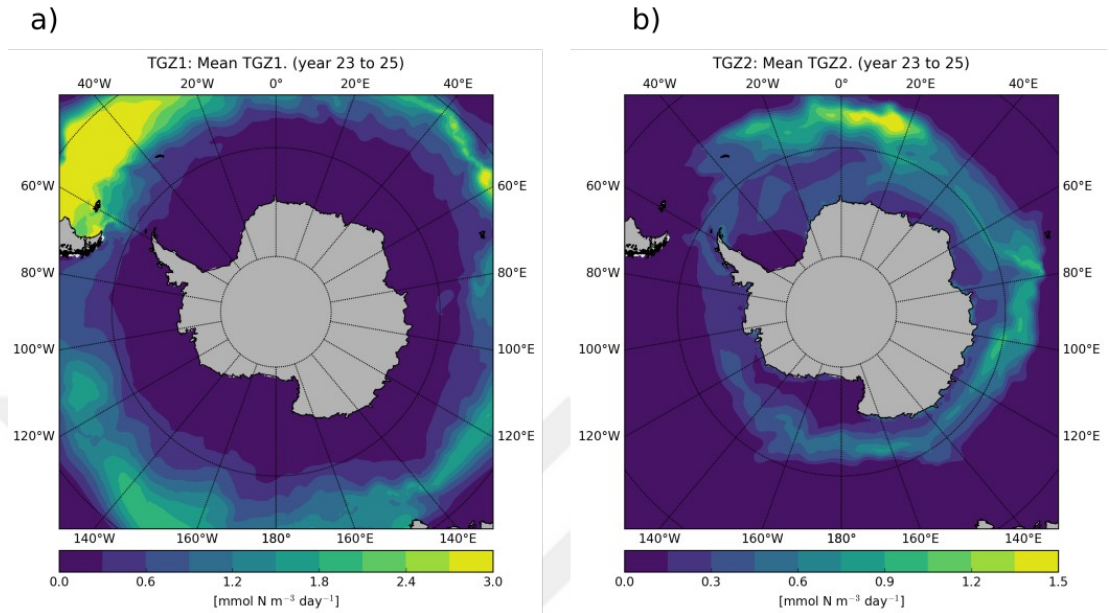


Figure 39. Three-year average total grazing patterns of each zooplankton group at surface a) Total grazing of first zooplankton b) Total grazing of second zooplankton group.

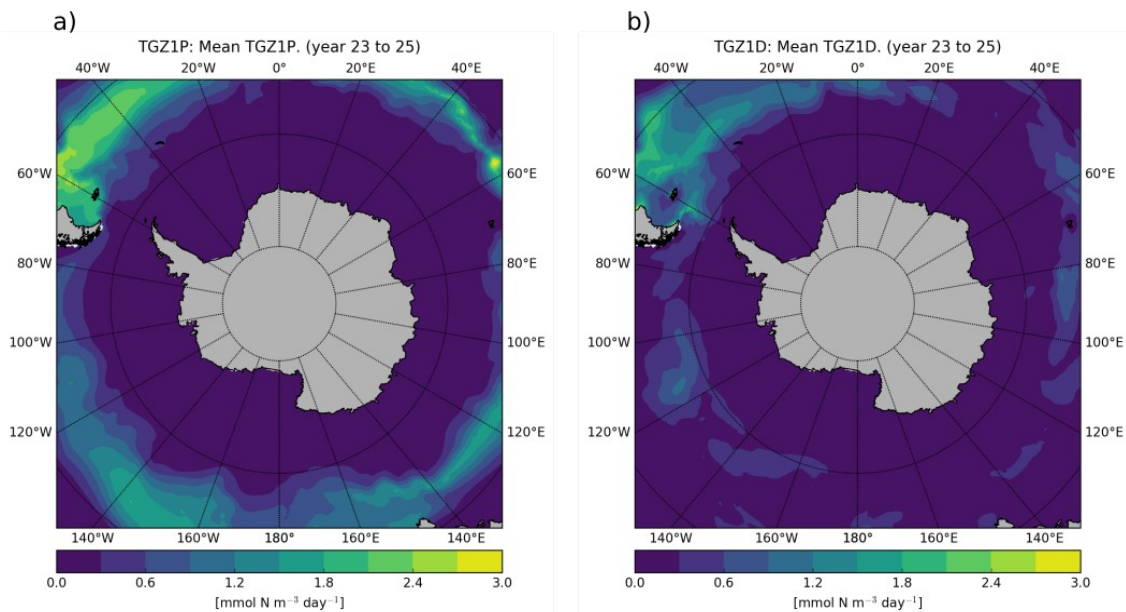


Figure 40. Three-year average grazing on different phytoplankton groups of first zooplankton group at surface a) Grazing on nano-phytoplankton b) Grazing on diatoms.

The first zooplankton group mainly grazes on the nano-phytoplankton group (54% of total grazing) and grazing on diatoms amounts to 46%. It grazes more on diatoms in the Atlantic sector rather than in the Pacific and Indian sectors (Figure 40 a,b).

The second zooplankton group grazes on the first zooplankton group additionally. The new group mainly grazes on diatoms rather than other food sources. Grazing on diatoms consists 76% while grazing on nanophytoplankton and the first zooplankton group are 21% and 3% of total grazing, respectively. Diatoms are mainly grazed in south of 50°S (Figure 41). Also, the amount of grazing on nanophytoplankton and on the first zooplankton group is lower. The highest grazing activity is in the Atlantic and Indian sectors of the Southern Ocean (Figure 42a, b). Since the abundance of the first zooplankton is low, the average grazing on this group is low. It reaches a maximum of 0.1 mmol N m⁻³ d⁻¹.

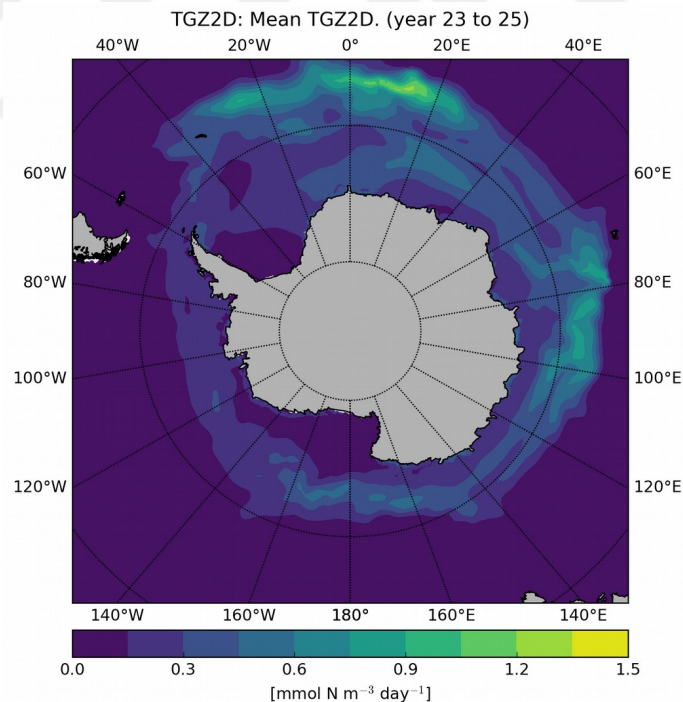


Figure 41. Three-year average grazing on diatoms of second zooplankton group at surface (krill)

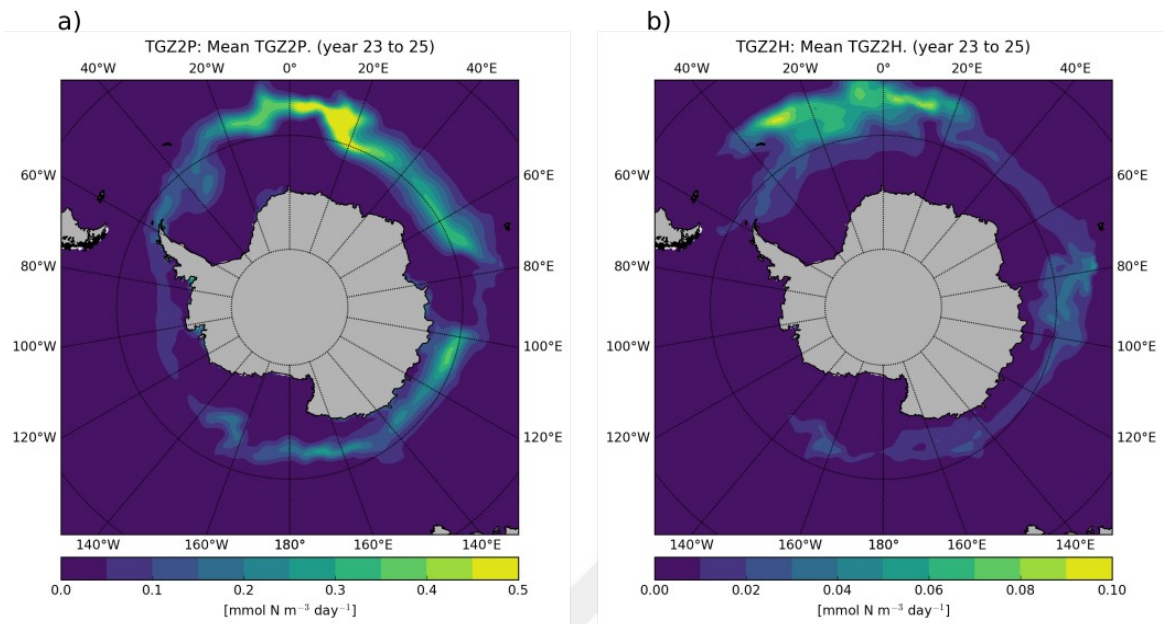


Figure 42. Three-year average grazing on different phytoplankton groups of second zooplankton group at surface a) Grazing on nano-phytoplankton b) Grazing on first zooplankton group.

3.2.3.2 Respiration and DOC Production by Zooplankton Groups

Respiration and DOC production by different zooplankton groups are between 0-2 mmol C m⁻³ and 0-0.6 mmol C m⁻³, respectively. Since the biomass distribution of the two groups are different, there is a difference in the spatial distribution of respiration

and DOC production rates. DOC production of the first zooplankton group is considerably higher than of the second zooplankton group (Figure 43a, b). First zooplankton group contributes 68.4% of total DOC production of zooplankton groups in the model. The other 31.6% is from the second zooplankton group. This difference stems from the different excretion rates of the zooplankton groups. The excretion rates were 0.15 and 0.02 for the first and second zooplankton groups, respectively (Table 1).

The respiration rates of the two zooplankton groups are in the same range. However, 11% of total respiration is from the first zooplankton group in the whole Southern Ocean. The other 89% is from the second zooplankton

group. As it is expected, the distribution of respiration follows the biomass distribution of each group (Figure 44 a, b).

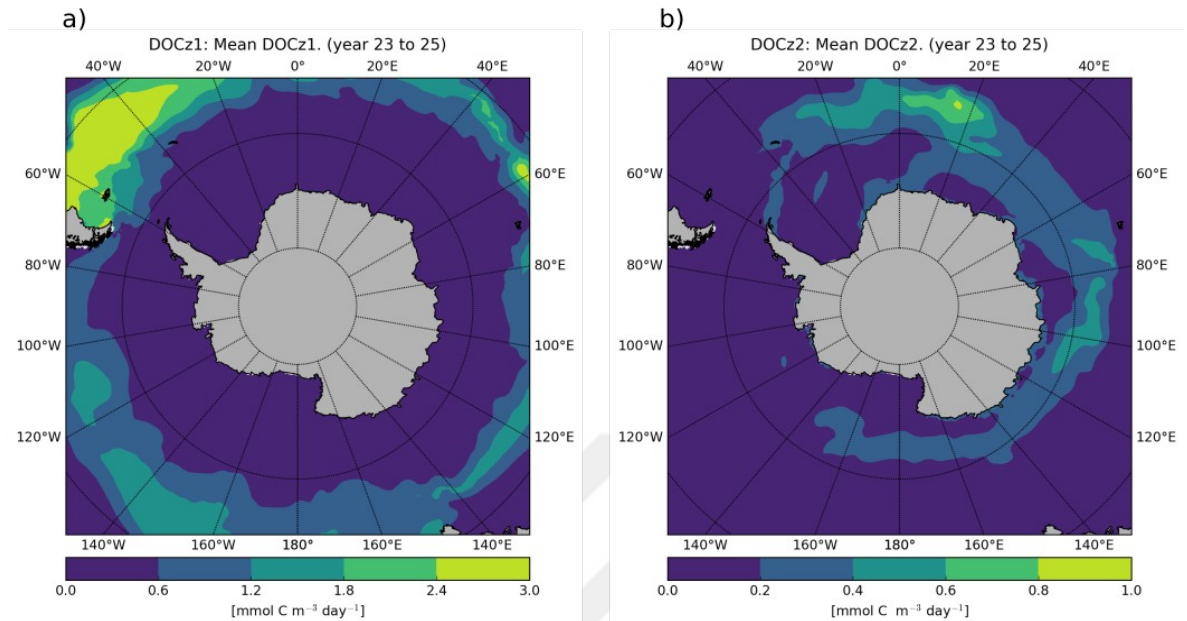


Figure 43. Three-year average DOC production of different zooplankton groups at surface a) DOC production of first zooplankton group b) DOC production of second zooplankton group.

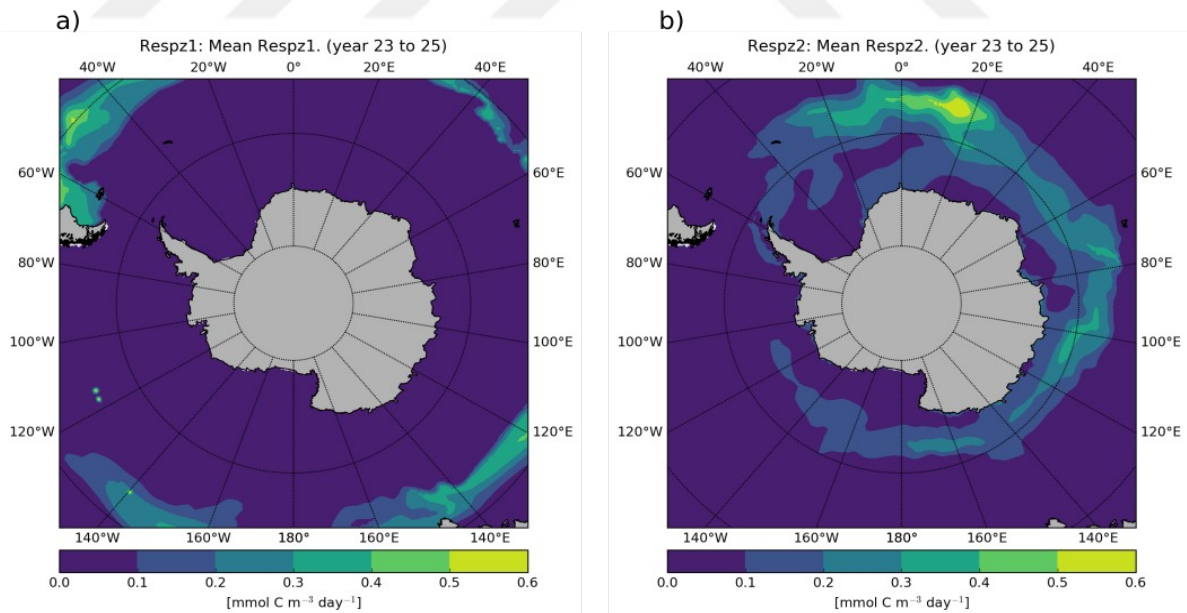


Figure 44. Three-year average respiration rates of different zooplankton groups at surface a) Respiration of first zooplankton group b) Respiration of second zooplankton group.

3.2.3.3 POC production by Zooplankton Groups

POC production of the two zooplankton groups was calculated using the rates of the mortality and sloppy feeding rate. The first zooplankton group's POC production is the sum of mortality of the group and sloppy feeding of krill on the first zooplankton group. In contrast, POC production of the second zooplankton group is just a result of mortality. As it is seen, the POC production of the first zooplankton group is higher than the second zooplankton group (Figure 45 a, b). The contribution of the first zooplankton group to total POC production is around 0.6%. The contribution of the second zooplankton group is 0.4%.

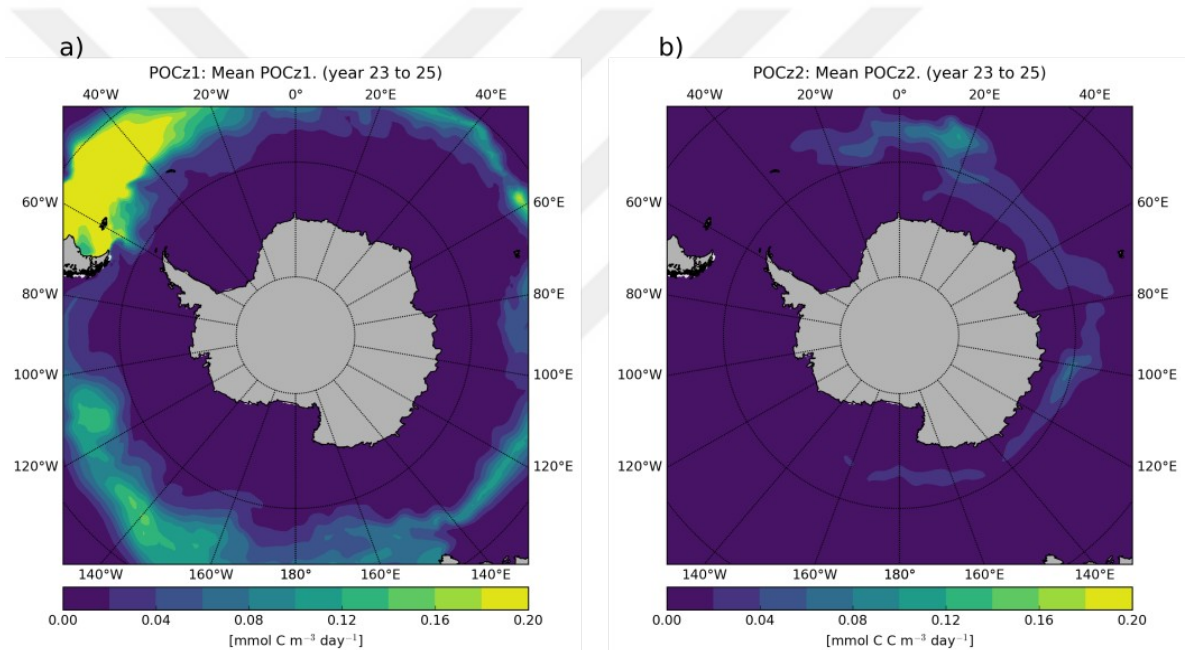


Figure 45. Three-year average POC production of different zooplankton groups at surface a) POC production of first zooplankton b) POC production of second zooplankton.

3.2.3.4 Seasonal Cycles of Zooplankton Groups

Nutrients and primary producers have strong seasonal cycles because of environmental conditions such as light and temperature. Since zooplankton groups graze on primary producers they display similar seasonal cycles. The first zooplankton group biomass starts to increase in October, austral spring.

In January, during austral summer, it reaches the highest concentrations of $0.14 \text{ mmol C m}^{-3}$. In austral winter concentrations of the first zooplankton carbon biomass are around $0.01 \text{ mmol C m}^{-3}$ (Figure 46).

The carbon concentration of the second zooplankton is higher than the first zooplankton group as expected. The biomass of the second zooplankton group decreases in winter. It reaches the highest values in April ($0.3 \text{ mmol C m}^{-3}$) and then declines until October. In contrast, the first zooplankton group reaches the peak concentrations in December and January. Concentrations in austral winter are really low, but slightly higher than the first zooplankton group (Figure 46). The minimum concentration of the second zooplankton group is around $0.05 \text{ mmol C m}^{-3}$ in September.

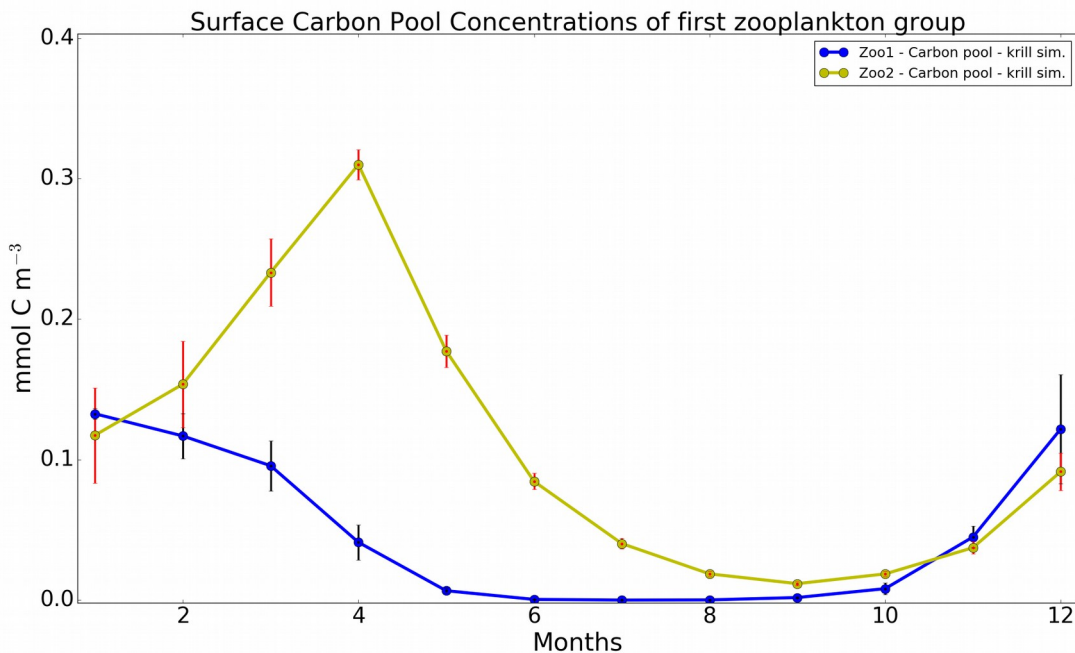


Figure 46. Three-year average seasonal cycle of zooplankton groups in the surface of the Southern Ocean. Error bars shows the standard deviation in last three years of model result.

3.3.3 Changes in NPP and Seasonal Cycles of Chl in Krill Simulation

The mean total NPP in the Southern Ocean for the last 3 years of the 25 years simulation with one zooplankton group is 3.3 Pg C per year. With the implementation of the new zooplankton group this value remains unchanged at ~3.4 Pg C per year. However, there are slight differences in the 25 years time series of the simulations (Figure 47).

In both model runs, diatoms contribute more to total NPP than nano-phytoplankton in the Southern Ocean. There is a minor increase of about 0.02 Pg C per year in the contribution of nano-phytoplankton to total NPP after the implementation of krill. Also, there is a proportional decrease in the contribution of diatoms to total NPP.

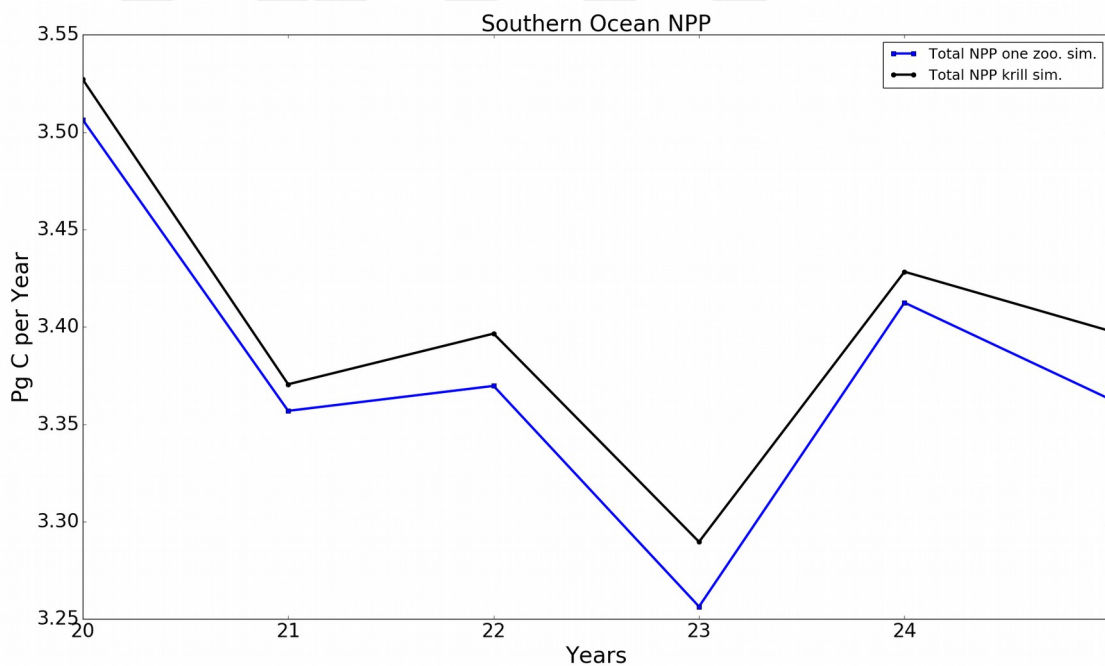


Figure 47. Time series of total NPP in the Southern Ocean during the last 5 years of the simulations (black line and dots - model run with two zooplankton groups, blue line and squares - model run with one zooplankton group).

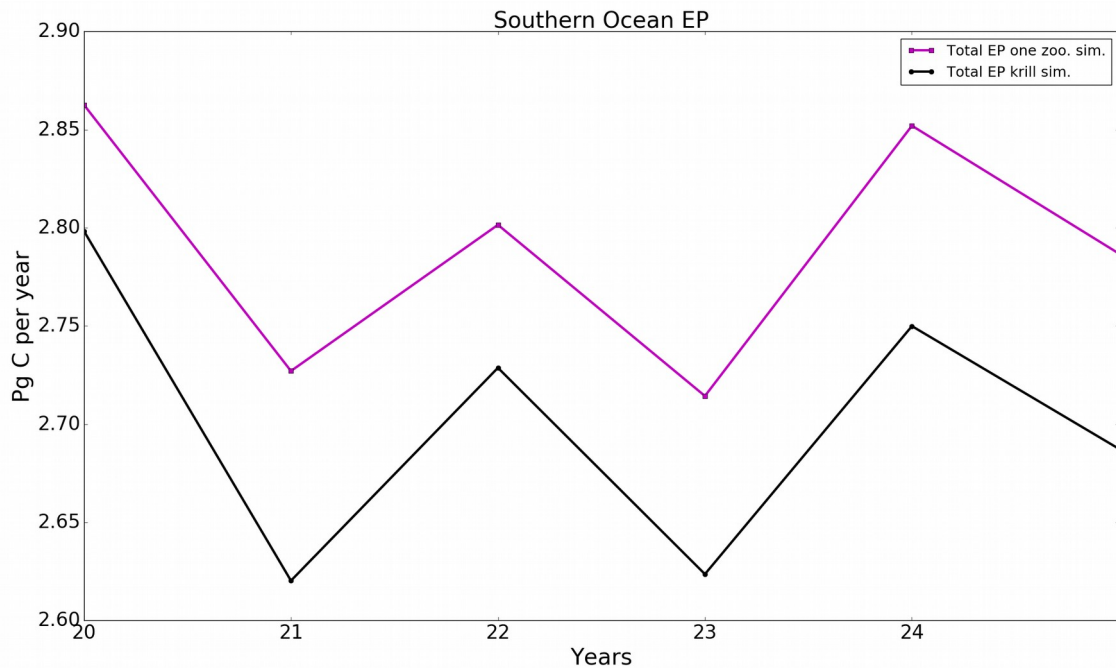


Figure 48. Time series of total EP in the Southern Ocean during the last 5 years of the simulations (black line and dots - model run with two zooplankton groups, magenta line and squares - model run with one zooplankton group).

Total EP decreases with the implementation of the new zooplankton group into the model. In the control run with one zooplankton, the mean EP over the last three years amounts to 2.8 Pg C per year. With the implementation of krill, EP decreases slightly to 2.7 Pg C per year (Figure 48).

The seasonal pattern of chl is similar to satellite data results (Figure 49). However, the simulated chl concentrations are lower compared to the satellite data from January to September. In contrast, especially in October and December, there is a good agreement between model results and satellite data (Figure 49). In November, the model markedly overestimates the chl concentration.

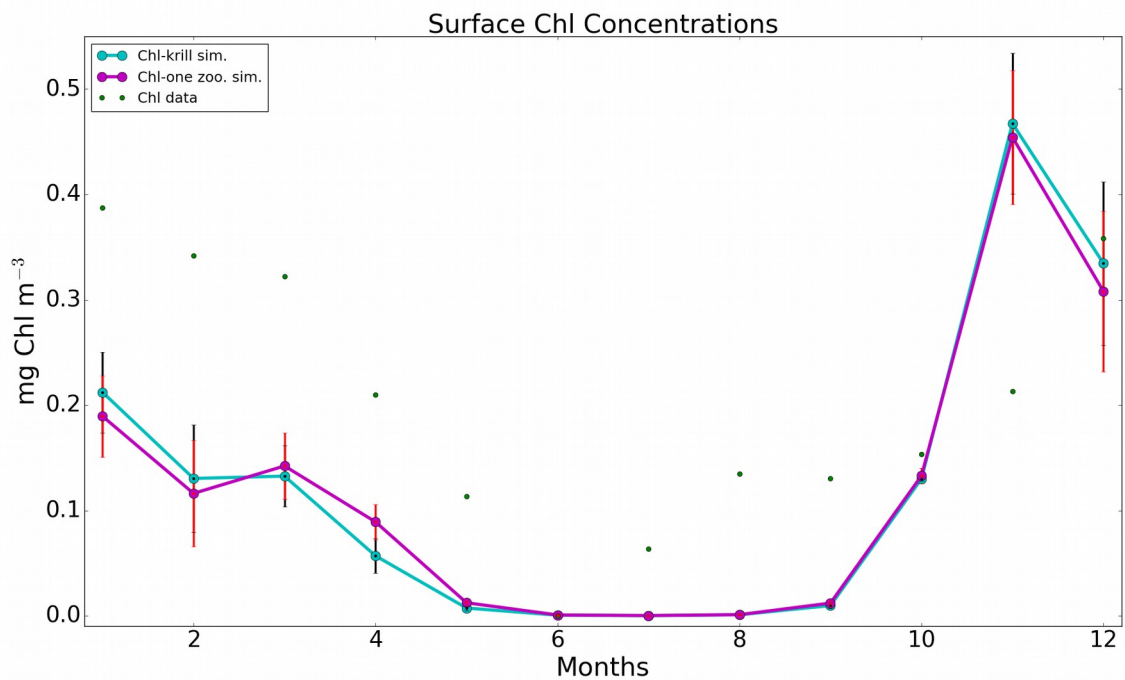


Figure 49. Three-year average seasonal cycle of chl concentration at the surface of the Southern Ocean (blue line and dots - model run with two zooplankton groups, purple line and dots - model run with one zooplankton group, green dots - Satellite data chl concentrations). Error bars shows the standard deviation in last three years of model result.

The chl concentrations of the nanophytoplankton group starts to increase in October and reaches the highest concentrations of 0.06 mg chl m⁻³ in February. Between June and September the chl concentration of this group approaches to 0. When the seasonal pattern of nano-phytoplankton is analysed, a less steep biomass increase during the spring bloom can be seen with the implementation of krill (Figure 50, month 11). This is an expected result because of the new grazing pressure. Surface chl concentration of the nano-phytoplankton group increases in spring and summer but decreases in autumn. The seasonal pattern of diatom chl concentration did change little with the implementation of krill. It reaches the peak concentration in October. In winter there is only little chl from both groups (Figures 50, and 51: months 6-8). In contrast, the presence of chl can be observed in summer and spring (Figures 50, and 51).

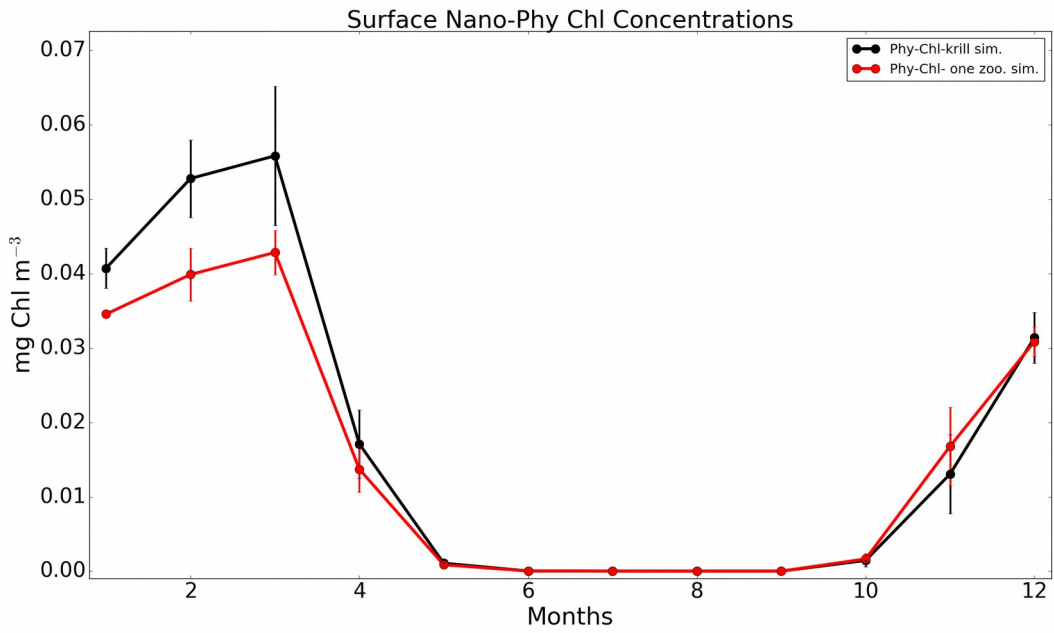


Figure 50. Three-year average seasonal cycle of nano-phytoplankton chl concentration at the surface of the Southern Ocean (black line and dots - model run with two zooplankton group, red line and dots - model run with one zooplankton group). Error bars shows the standard deviation in last three years of model result.

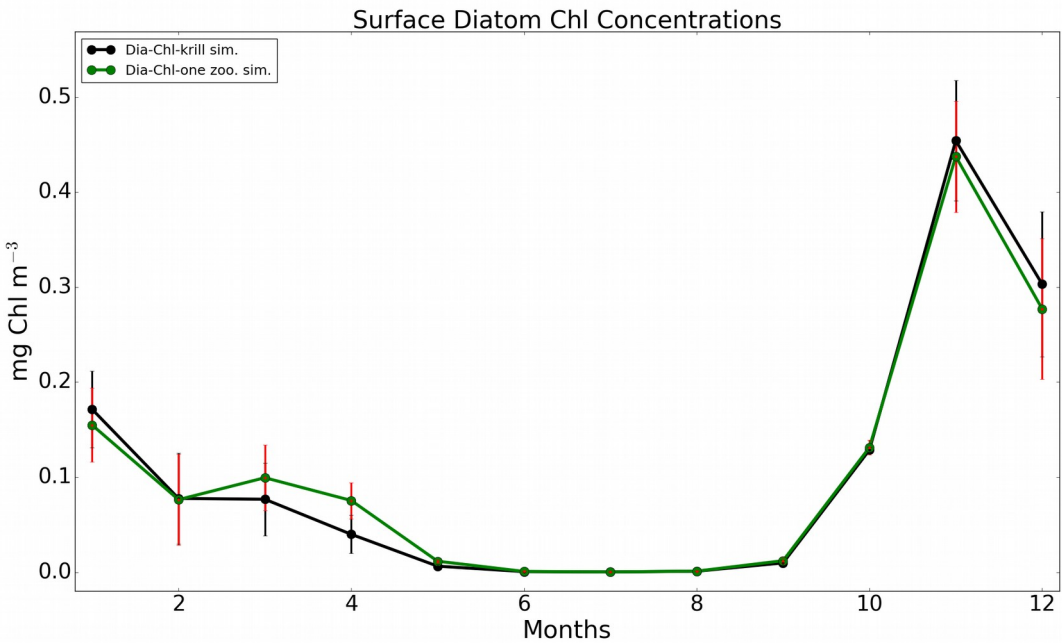


Figure 51. Three-year average seasonal cycle of diatom chl concentration at the surface of the Southern Ocean (black line and dots - model run with two zooplankton groups, red line and dots - model run with one zooplankton group). Error bars shows the standard deviation in last three years of model result.

The seasonal cycle of the first zooplankton changed when Antarctic krill is incorporated into the model. In summer and spring, the concentration of the first zooplankton group increased from 0.08 to 0.12 mmol C m⁻³. In winter and autumn, the concentrations are very low in both simulations and they are around 0.01 mmol C m⁻³ (Figure 52). The concentration of the first zooplankton group starts to increase in October and continues until January. The annual mean increased by 50%, from 0.04 to 0.06 mmol C m⁻³.

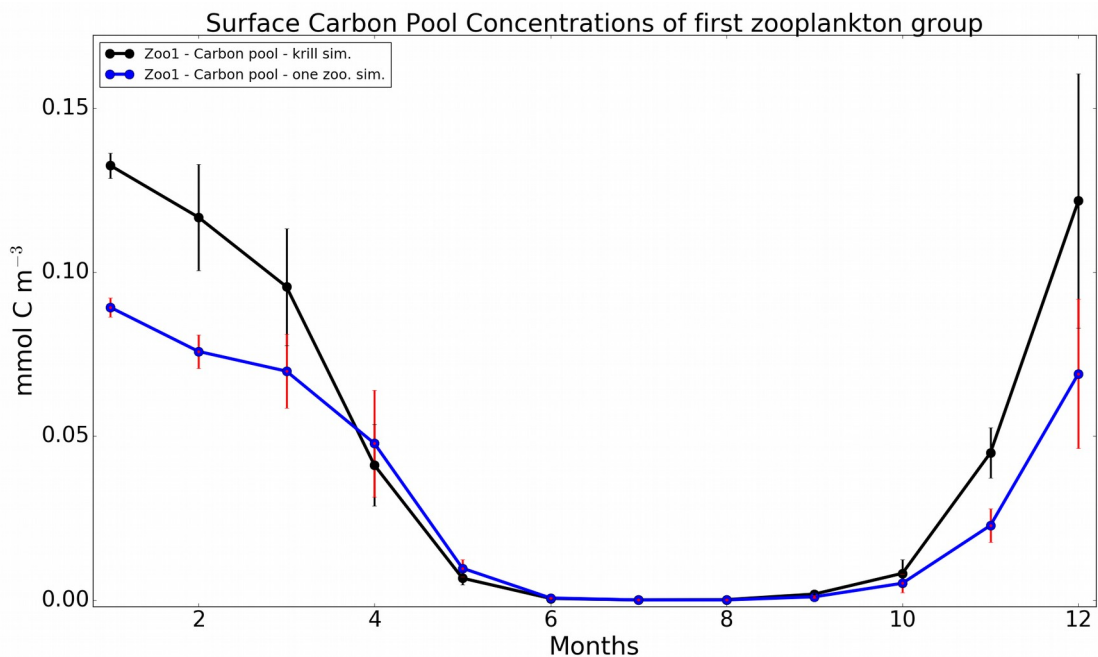


Figure 52. Three-year average seasonal cycle of the first zooplankton carbon pool at the surface of the Southern Ocean (black line and dots- model run with two zooplankton groups, blue line and dots - model run with one zooplankton group). Error bars shows the standard deviation in last three years of model result.

Besides the seasonal cycle of the first zooplankton group, the spatial distribution of this group was changed. North of 60°S the concentrations slightly increased by ~0.2 mmol C m⁻³. South of 60°S some small increases and decreases around 0.05 mmol C m⁻³, can be seen (Figure 53).

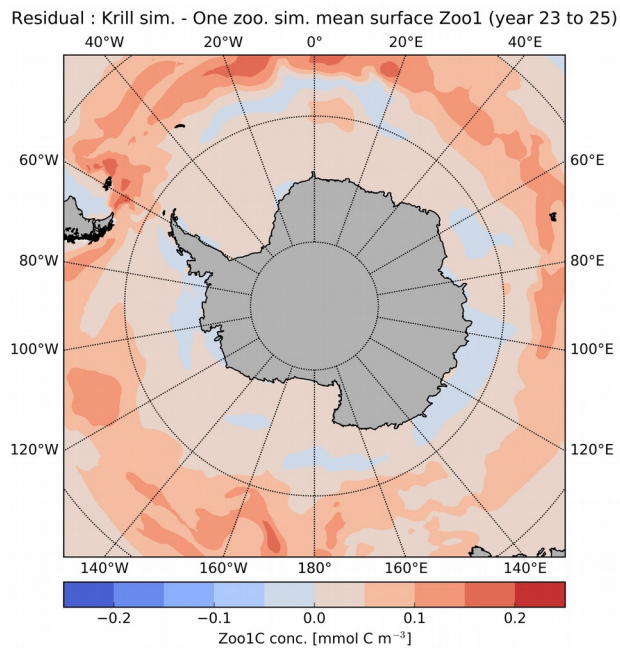


Figure 53. Three-year average residual plots (krill simulation - one zooplankton simulation) of first zooplankton group surface carbon pool concentration.

3.3 Model Simulations and Observation Comparisons

In an effort to assess the skill of the modeling system to reproduce observations apart from visual comparisons as were undertaken above, the correlation between observation and both simulations, as well as the root mean square error (RMSE) were calculated for DIN, DSi and chl. Also, the spatial standard deviation of the simulations and observation values were calculated and all of these parameters are shown together in the Taylor diagrams (Figure 54). Three-year averages were used for the comparisons. Correlations between the control simulation and observations for DIN, DSi and chl are 0.62, 0.59 and 0.59 in the Southern Ocean, respectively. RMSE, which shows the absolute differences between the model and observations, are 4.51 mmol DIN m⁻³, 20.11 mmol DSi m⁻³ and 0.35 mg chl m⁻³ for DIN, DSi and chl. When the krill simulation and observations were compared, correlations are 0.63, 0.59 and 0.58 for DIN, DSi and chl respectively. RMSEs are 4.52 mmol DIN m⁻³, 20.12 mmol DSi m⁻³, 0.37 mg chl m⁻³ for the

same fields. The standard deviations of the simulated DIN and chl are higher than in the observations, indicating that the model overestimates the gradient. In contrast, the standard deviation for the simulated DSi is lower than in the observations which means that the model underestimates the gradient. The RMSE is rather high for DSi and DIN compared to previous simulations with the same model in different configurations. This is consistent with the mismatch of nutrients in the residual plots (Figure 33, and 34) and the reported too strong stratification of this set-up (Downes et al., 2015; and 2018).

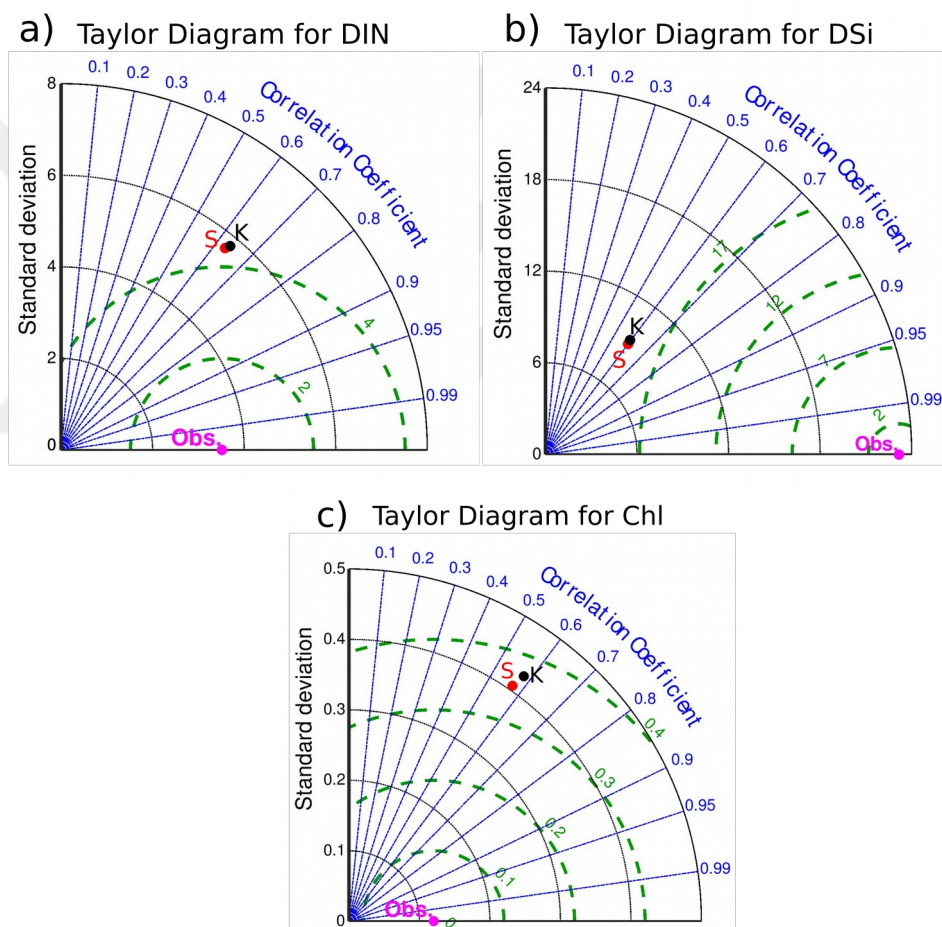


Figure 54. Taylor diagrams for three-year means of simulated DIN, DSi and chl. Black dot and K stands for krill simulation, red dot and S stands for control simulation and magenta dot and Obs. stands for observation. Black circle lines: standard deviation, green circle lines: RMSE, blue lines: correlation.

CHAPTER 4

DISCUSSION

This study describes the implementation of krill into the 3D global ocean ecosystem model FESOM-REcoM2 and the effects of this implementation on the simulated Southern Ocean ecosystem and nutrient dynamics. This goes beyond the study of LeQuéré et al. (2016) by parameterizing the macrozooplankton group specifically as Antarctic krill and implementing temperature and respiration functions accordingly. In the following discussion, current strengths and weaknesses of the model and potential further improvements are discussed.

4.1 Control FESOM-REcoM2 Simulation

The 25 years simulation of the control FESOM-REcoM2 set-up with one zooplankton group gives a generally reasonable spatial distribution of nutrients in the global oceans. However, the model has a negative bias for both macro nutrient fields (Figure 13b, 15b). Low concentrations of nutrients can be the result of too strong stratification and weak upwelling in the ocean circulation model FESOM on the CORE-II mesh (Downes et al., 2015; 2108). Simulated iron concentrations in the Southern Ocean are lower than observations as mentioned in the results section. Strong stratification, weak upwelling (Downes et al., 2015; 2018) and lack of a sedimentary source of iron in the biogeochemical model can be reasons for this underestimation. One of the effect of this underestimation of nutrient concentrations is lower simulated total chlorophyll than observed satellite-derived concentrations (Figure 49). The simulated 3.4 PgC yr^{-1} is in the range of estimates based on satellite observations ranging from $1.1 - 4.9 \text{ Pg C per year}$ (Carr et al, 2006) and similar to the value of 3.1 Pg C yr^{-1} that was obtained with a previous

version of the same model (Schroup-Kristensen, 2014). Results of the control run show a diatom dominated Southern Ocean ecosystem. The contribution of diatoms to chl and NPP is higher than the contribution of the nanophytoplankton group (Figure 26 a, b; Figure 29 a, b). This is consistent with previous simulations of the Southern Ocean ecosystem with other versions of the same biogeochemical model (Laufkötter et al., 2016; Schroup-Kristensen, 2014).

4.2 Effect of Antarctic Krill on the Simulated Ecosystem

The results of this study showed that the implementation of a new zooplankton group parameterized as Antarctic krill affects simulated nutrient and primary producer fields. The simulation including the second zooplankton gives results closer to observed nutrient concentrations (Figure 33; 34). In the whole Southern Ocean simulated DIN, DSi and DFe increased by 2.6%, 10.6% and 10.6%, respectively (Table 2). Also, these numbers are consistent across all three regions of the Southern Ocean (Table 2). These increases could be the effect of increased nutrient cycling in the surface ocean. Changes in the fields of DIN, DSi and chl are three year averages for the whole Southern Ocean and their subregions (Table 2). When these changes are interpreted with Taylor diagrams of the fields of DIN, DSi and chl (Figure 54), it can be seen that there are only minor differences between control and krill simulations.

The simulated NPP in the whole Southern Ocean and in the region between 0°W - 140°E increases by 0.84% and 3.72%, respectively. However, it decreases by 0.5% between 140°E - 60°W and by 1.07% between 0°W - 60°W. NPP from the diatom group decreases 2.5% in the whole Southern Ocean (Table 2). This decrease in diatom-NPP is a result of the increased grazing pressure in the model.

The simulated total NPP showed a change only +0.02 Pg C per year after the implementation of the second zooplankton group (Figure 47). In contrast, the

total EP of the Southern Ocean decreased by 0.1 Pg C yr⁻¹ in the krill simulation. The modelled total EP in the Southern Ocean in both simulations is higher than the simulated export production in the Southern Ocean (1-1.1 Pg C per year) in previous studies (Schlitzer, 2002; Schourup-Kristensen, 2014).

Table 2. Change in three year average nutrients and primary producer fields (control simulation vs krill simulation) after the implementation of the krill for the whole Southern Ocean, and for the regions between 0°W - 140°E, 140°E - 60°W and 0°W - 60°W. Red color is used for the increase and blue color is used for the decrease.

	Whole Southern Ocean	Between 0°W - 140°E	Between 140°E - 60°W	Between 0°W - 60°W
DIN mmol m ⁻³	16.7 to 17.1 +2.6%	19.5 to 20 +2.6%	13.4 to 13.7 +2.5%	19.6 to 20.1 +2.5%
DSi mmol m ⁻³	9 to 9.9 +10.6%	10.96to 12.68 +15.7%	5.37 to 5.75 +7.1%	14.3 to 15.3 +6.7%
DFe µmol m ⁻³	0.11 to 0.13 +10.6%	0.1 to 0.12 +22.4%	0.12 to 0.13 +9.3%	0.12 to 0.14 +14.76%
Total NPP mg C m ⁻²	194.4 to 201.1 +0.84%	192.8 to 199.9 +3.72%	205.2 to 204.3 -0.5%	197.4 to 195.3 -1.07%
NPP by diatom mg C m ⁻²	166.9 to 162.8 -2.5%	174.7to 172.5 -1.28%	159.5 to 156.6 -2.1%	169.9 to 160.2 -5.72%
NPP by nanophyto. mg C m ⁻²	32.5 to 38.3 +17.9%	18.1 to 27.5 +52%	45.2 to 47.6 +5.4%	27.5 to 35.1 +27.6%
Total Chl mg Chl m ⁻³	0.361to 0.366 +1.19%	0.34 to 0.36 +5.39%	0.362 to 0.36 -0.6%	0..40 to 0.39 -1.41%
Diatom Chl mmol m ⁻³	0.316 to 0.312 -1.2%	0.311 to 0.314 +1.18%	0.302 to 0.298 -1.37%	0.36 to 0.34 -4.75%
Nanophyto. Chl mmol m ⁻³	0.046 to 0.054 +17.7%	0.028 to 0.043 +51%	0.060 to 0.062 +3.3%	0.043 to 0.054 +26.6%

The other effect of the second zooplankton class is that through more nutrient availability a 17.7% increase in nanophytoplankton chl concentrations occurs. In contrast, diatom Chl concentrations decreased by 1.2% in the whole Southern Ocean (Table2) and total chl concentrations increased by 1.19% in the krill simulation. This is the result of the increase in nutrient concentrations by faster nutrient cycling in the upper ocean.

Since total NPP and EP are calculated by yearly summation of the Southern Ocean of these fields, the spatial changes (Figure 35) cannot be seen in the yearly total NPP and EP time series (Figure 49; 50).

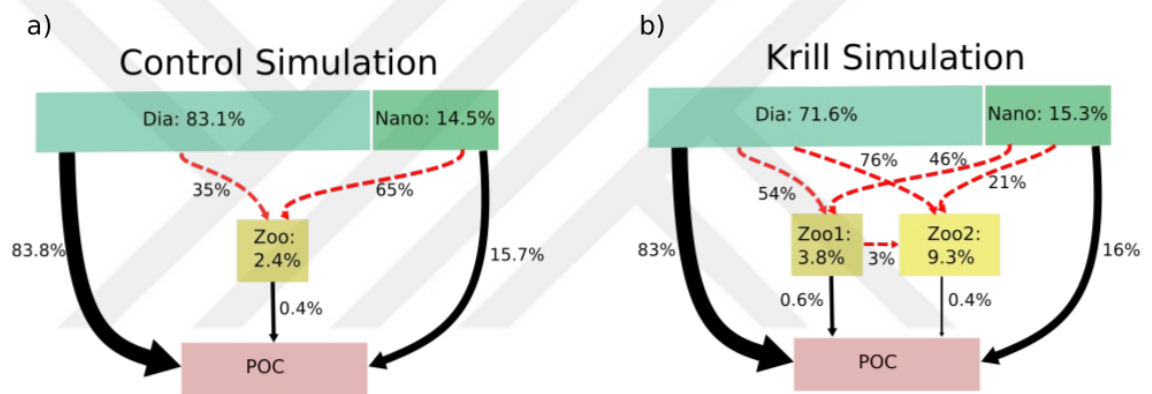


Figure 55. Diagrammatic representation of the ecosystem structure and the particle formation mechanisms in the Southern Ocean a) control simulation, b) krill simulation. The green boxes show diatom (Dia) and nanophytoplankton (Nano). Yellow boxes show the first zooplankton group (Zoo1) and the second zooplankton group (Zoo2). The numbers in the boxes are the percentage of the related compartment to all living compartments in the Southern Ocean. The pink box shows particulate organic carbon (POC). The black arrows show the contribution of each living compartment to the POC production (percentage of total POC production). The red arrows show the grazing of the zooplankton groups on diatom and nanophytoplankton groups (percentage of total grazing on all groups).

After the implementation of krill, the contributions of diatom, nanophytoplankton, the first and the second zooplankton groups to the total

biomass are 71.6%, 15.3%, 3.8% and 9.3%, respectively (Figure 55b). In the control run, the contributions of diatom, nanophytoplankton and zooplankton groups to the total biomass were 83.1%, 14.5% and 2.4%, respectively (Figure 55a). These changes in nutrient and primary producers fields cause an increase in the first zooplankton biomass by 42%. In the krill simulation, the second zooplankton group grazed mainly on the diatom group. Grazing on diatoms is 76% of total grazing of this group. In contrast, grazing on nanophytoplankton and on the first zooplankton group are 21% and 3% of the total grazing respectively. One of the differences between the control and krill simulations is the grazing pattern of the first zooplankton group. In the krill simulation 54% of total grazing of the first zooplankton group is on diatoms while in the control run it is 35% of total grazing. This may be the result of the increased first zooplankton biomass south of 60°S (Figure 53). Since the region south of 60°S is dominated by diatoms, the increase of the first zooplankton group in this region increased the portion of grazing on diatoms in the krill simulation.

The REcoM2 ocean ecosystem model was used in previous studies to do research on the Southern Ocean ecosystem. The MITgcm – RecoM2 version was used to understand ecosystem structure and export production (Laufkötter et al., 2016). The krill simulation produces more zooplankton in the Southern Ocean compared to a previous study which was carried out using REcoM2 in the Southern Ocean (Laufkötter et al., 2016), which is a considerable improvement. Diatoms were the dominant group for total biomass. One of the main differences between the model simulations with and without krill is the increase in the contribution of zooplankton groups to the total biomass. It is 13.1% and the second zooplankton group contributes 9.3%. In a previous study, the MITgcm-REcoM2 version was used and the contribution of the zooplankton group to the total biomass was only 0.2% and diatoms were responsible for 94% of the total biomass in the Southern Ocean (Laufkötter et al., 2016). These differences can be the result of different physical models, spatial resolution and length of runs.

4.3 Particulate Organic Carbon production

Aggregation of diatoms and sloppy feeding of the zooplankton groups on diatoms was calculated as POC production of the diatom group. 83% of POC is produced by diatoms in the krill simulation (Figure 55b). Similarly, aggregation of nanophytoplankton and sloppy feeding on this group was calculated as POC production from this group. 16% of POC is produced by nanophytoplankton (Figure 54b). The general pattern of the contribution by different groups to POC production are similar to the results of MITgcm-REcoM2 and BEC models (Laufkötter et al., 2016). Mortality and sloppy feeding of the second zooplankton group on the first zooplankton group is another source for POC. It amounts to 0.6% of total POC production of different groups. Mortality of the second zooplankton group contributes 0.4% to the total POC production. In total the contribution of zooplankton groups to POC is 1%. However, in the control simulation contribution of the zooplankton group was 0.4% (Figure 55a). Furthermore, the sloppy feeding which is counted here for POC production by diatoms and nanophytoplankton would not occur without zooplankton. These values are lower compared to the results of the BEC and PISCES models (Laufkötter et al., 2016). In these models, zooplankton groups form 30% and 40% of the total biomass in the Southern Ocean, respectively.

4.4 Simulated Antarctic krill biomass and distribution

The simulated carbon biomass of the second zooplankton group, Antarctic krill, is lower than the observed values (Figure 32). Biomass calculations by Atkinson et al. (2009) show that 70% of the entire circumpolar population is concentrated in the South West Atlantic. However the modelled biomass of krill does not show this distribution. The highest accumulation of simulated krill biomass is east of the Prime Meridian. The mismatch of the hotspots of krill biomass can be the result of a lack of sea ice algae in the model, an important component of krill diet in winter. The abundant sea ice simulated

around the Antarctic Peninsula is a suitable habitat for sea ice algae and inclusion of sea ice algae in the model could improve krill biomass representation in the Atlantic Sector. Moreover, the underestimation of iron input from sediments and from sea ice around the Antarctic Peninsula may cause the mismatch of high biomass of krill in the region since the iron cycle is closely related to sea ice dynamics in high latitudes (Wang et al., 2014).

Similarly, high krill abundance is observed in offshore waters in summer (Atkinson, 2009) and an increase of krill density in the shelf and coastal areas in winter (Siegel, 1988), which is not reproduced by the current model. In addition, a seasonal cycle of krill biomass can be observed because of a change in body composition of krill (Meyer, 2011). However, the model results show an 80% difference between winter and peak biomass concentration, which is much higher than the estimated seasonality of krill biomass.

These differences in biomass distribution and seasonal cycle may also be a result of uncertainties such as stratification and upwelling processes in the ocean circulation model. Low concentrations of nutrients due to too strong stratification and/or too weak upwelling (Downes et al., 2015; 2018) could be a reason for the shift in biomass distribution. In ocean ecosystem models, chlorophyll concentrations tend to approach zero in winter because of light limitation and low temperatures. This could be the reason for the strong seasonal cycle of krill biomass. Also, the currently implemented temperature function for krill could affect this distribution, as has been seen in other REcoM2 simulations that were undertaken during this study but are not shown here. However, the longitudinal distribution of Antarctic krill depends mostly on the available food for the second zooplankton group. In the current model set up, anywhere there is sea ice, there is no phytoplankton production and hence no food for Antarctic krill in this setting of the model. However, sea ice algae grow under the ice and have been found to be an important food source for krill along with small zooplankton that live under the

ice feeding on this algae (Meyer, 2011, Kohlbach et al., 2017). Therefore implementing sea ice algae can be a solution for the strong seasonal variation and generally low biomass of the new zooplankton group.

The increase in chlorophyll concentration of the nanophytoplankton group during the spring bloom is less steep in the krill run than in the reference run. However, still the biomass increase is rather steep. A similar decrease in the steepness of the diatom chlorophyll cannot be seen after the implementation of krill. When the seasonal cycle of the zooplankton groups (Figure 46) are examined, their biomass decreases close to zero. Since there is a lack of light as well as the occurrence of sea ice in winter in the Southern Ocean, food sources for the zooplankton groups are very low in the winter. This situation prevents high winter biomass of the second zooplankton group which could control the steep increase of the diatom chlorophyll. Therefore, the steep increase in the diatom chlorophyll still can be seen.

In the parameterization of krill respiration, the respiration activity factor was implemented as a function of Julian days. This parameterization was developed for the Southern Ocean based on a study of Hoffmann and Lascara (2000). If the second zooplankton group is parameterized as a general macrozooplankton group that occurs in the northern and southern high latitudes, it should be included as a function of light instead of Julian days in order to simulate the correct seasonal cycle in the Northern Hemisphere as well.

CHAPTER 5

CONCLUSION

This study provides an analysis of the Southern Ocean ecosystem with an ocean-ecosystem model. The implementation of a new zooplankton group into the REcoM2 ecosystem model enables us to see the effect of this new group on simulated nutrient distribution and primary production. Since the new zooplankton group was parameterized as Antarctic krill, one of the key species in the Southern Ocean was included into the model. The grazing pressure on phytoplankton was thereby increased in the model.

There were no significant changes in the primary producer fields of the model between simulations. Total NPP in the global and Southern Ocean were similar in both simulations. Chlorophyll concentrations changed with the implementation of the new group. The implementation of krill enhanced nutrient recycling in the upper ocean. Therefore, the nutrient distributions of DIN, DSi and DFe changed. The krill runs showed a smaller bias in surface spatial distributions of the simulated fields than the control run.

More importantly, the structure of the ecosystem model changed. Proportions of the different compartments in total biomass showed differences when compared with the control run of the model. The relative contributions of diatoms in the simulated ecosystem decreased because of the increased grazing activity in the model, while the relative contribution of the nanophytoplankton group increased. Furthermore, the inclusion of the second zooplankton group also led to an increase in the biomass of the first zooplankton group.

Ecosystem models provide a very good tool to assess the actual status in ecosystems and to make future projections. Because of this, it is important to continue to improve the capability of these models. Including sea ice algae in the model can improve the capability of the existing model to better resolve the trophic processes in the Southern Ocean



REFERENCES

Arrigo, K. R. (2003). A coupled ocean-ecosystem model of the Ross Sea: 2. Iron regulation of phytoplankton taxonomic variability and primary production. *Journal of Geophysical Research*, 108(C7), 3231. <https://doi.org/10.1029/2001JC000856>

Arrigo, K. R., van Dijken, G. L., and Bushinsky, S. (2008). Primary production in the Southern Ocean, 1997-2006. *Journal of Geophysical Research: Oceans*, 113(8), 1997–2006. <https://doi.org/10.1029/2007JC004551>

Atkinson, A., and Whitehouse, M. J. (2000). Ammonium excretion by Antarctic krill *Euphausia superba* at South Georgia. *Limnology and Oceanography*, 45(1), 55–63. <https://doi.org/10.4319/lo.2000.45.1.0055>

Atkinson, A., Shreeve, R. S., Hirst, A. G., Rothery, P., Tarling, G. A., Pond, D. W., ... Watkins, J. L. (2006). Natural growth rates in Antarctic krill (*Euphausia superba*): II. Predictive models based on food, temperature, body length, sex, and maturity stage. *Limnology and Oceanography*, 51(2), 973–987. Retrieved from <http://www.jstor.org/stable/3841104>

Atkinson, A., Siegel, V., Pakhomov, E., and Rothery, P. (2004). Long-term decline in krill stock and increase in salps within the Southern Ocean. *Nature*, 432(November), 100–103. <https://doi.org/10.1038/nature02950.1>.

Atkinson, A., Siegel, V., Pakhomov, E. A., Rothery, P., Loeb, V., Ross, R. M., ... Fleming, A. H. (2008). Oceanic circumpolar habitats of Antarctic krill. *Marine Ecology Progress Series*, 362, 1–23. <https://doi.org/10.3354/meps07498>

Atkinson, A., Siegel, V., Pakhomov, E. A., Jessopp, M. J., and Loeb, V. (2009). A re-appraisal of the total biomass and annual production of Antarctic krill. *Deep-Sea Research Part I: Oceanographic Research Papers*, 56(5), 727-740. <https://doi:10.1016/j.dsr.2008.12.007>

Atkinson, A. (2016). Chapter 5 Feeding and Food Processing in Antarctic Krill (*Euphausia superba* Dana). In: Siegel, V, (ed.) *Biology and Ecology of Antarctic krill*. Switzerland, Springer, 175-224, 441pp. (Advances in Polar Ecology).

Beaulieu, S. 2002. Accumulation and fate of phytodetritus on the sea floor. *Oceanogr. Mar. Biol. Annu. Rev.* 40: 171–232. doi:10.1201/9780203180594.ch4

Boyd, P.W., LaRoche, J., Gall, M., Frew, R., McKay, R.M.L., 1999. Role of iron, light, and silicate in controlling algal biomass in subantarctic waters SE of New Zealand. *J. Geophys. Res.* 104, 13395–13408.

Butzin, M. and Pörtner, H. O. (2016), Thermal growth potential of Atlantic cod by the end of the 21st century, *Global Change Biology*, 22 (12), pp. 4162-4168, doi:10.1111/gcb.13375

Carr, M. E., Friedrichs, M. A. M., Schmeltz, M., Noguchi Aita, M., Antoine, D., Arrigo, K. R., et al. (2006). A comparison of global estimates of marine primary production from ocean color. *Deep-Sea Research Part II: Topical Studies in Oceanography*, 53(5–7), 741–770. <https://doi.org/10.1016/j.dsr2.2006.01.028>

Clarke, A., Johnston, N., 2003. Antarctic marine benthic diversity. *Oceanography and Marine Biology*, 41, 47–104

Clarke A, Tyler PA (2008) Adult krill feeding at abyssal depths. *Curr Biol* 18:282–285

Cunningham, S. A., S. G. Alderson, B. A. King, and M. A. Brandon (2003). Transport and variability of the Antarctic Circumpolar Current in Drake Passage, *J. Geophys. Res.*, 108(C5), 8084. <https://doi:10.1029/2001JC001147>

Constable, A.J., Melbourne-Thomas, J., Trebilco, R., Press, A.J., Haward, M. (2017) ACE CRC Position Analysis: Managing change in Southern Ocean ecosystems. Antarctic Climate and Ecosystems Cooperative Research Centre, Hobart, Australia. 39 pp.

Daniel, B., and Hain, M. P. (2012). The Biological Productivity of the Ocean : Section 2 Aa on Long Time Scales ? *Nature Education*, 3(6), 1–16.

Downes, S. M., Spence, P., & Hogg, A. M. (2018). Understanding variability of the Southern Ocean overturning circulation in CORE-II models. *Ocean Modelling*, 123 (January), 98–109.

<https://doi.org/10.1016/j.ocemod.2018.01.005>

Downes, S. M., Farneti, R., Griffies, S. M., Marsland, S. J., Behrens, E., Bentsen, M., ... Yeager, S. G. (2015). An assessment of Antarctic Circumpolar Current and Southern Ocean meridional overturning circulation during 1958-2007 in a suite of interannual CORE-II simulations. *Ocean Modelling*, 93, 84–120. <https://doi.org/10.1016/j.ocemod.2015.07.009>

Everson I, (1977). The living resources of the Southern Ocean. Southern Ocean fisheries survey programme. FAO Report GLO/SO/77/1, 156 pp

Fach, B. A., Hofmann, E. E., and Murphy, E. J. (2002). Modeling studies of antarctic krill *Euphausia superba* survival during transport across the Scotia Sea. *Marine Ecology Progress Series*, 231, 187–203. <https://doi.org/10.3354/meps231187>

Falkowski, P.G., Barber, R.T. , Smetacek, V (1998). Biogeochemical controls and feedbacks on ocean primary production, *Science*, 281 , pp. 200-206

Frölicher, T.L., J.L. Sarmiento, D.J. Paynter, J.P. Dunne, J.P. Krasting, and M. Winton (2015). Dominance of the Southern Ocean in Anthropogenic Carbon and Heat Uptake in CMIP5 Models. *Journal of Climate*, 28, 862–886, doi: 10.1175/JCLI-D-14-00117.1

Garcia, H. E., R. A. Locarnini, T. P. Boyer, J. I. Antonov, O.K. Baranova, M.M. Zweng, J.R. Reagan, D.R. Johnson, 2014. *World Ocean Atlas 2013, Volume 4: Dissolved Inorganic Nutrients (phosphate, nitrate, silicate)*. S. Levitus, Ed., A. Mishonov Technical Ed.; NOAA Atlas NESDIS 76, 25 pp.

Gruber, N., Gloor, M., Mikaloff Fletcher, S. E., Doney, S. C., Dutkiewicz, S., Follows, M. J., Gerber, M., Jacobson, A. R., Joos, F., Lindsay, K., Menemenlis, D., Mouchet, A., Muller, S. A., Sarmiento, J. L., and Takahashi, T.: Oceanic sources, sinks, and transport of atmospheric CO₂, (2009), *Glob. Biogeochem. Cy.*, 23, GB1005, doi:10.1029/2008GB003349

Harris, R. P.; Wiebe, P. H.; Lenz, J.; Skoldal, H.R.; Huntley, M. (2000). ICES Zooplankton Methodology Manual. Academic press.
<https://doi.org/10.1016/B978-012327645-2/50007-4>

Hauck, J., Völker, C., Wang, T., Hoppema, M., Losch, M., and Wolf-Gladrow, D. (2013). Seasonally different carbon flux changes in the Southern Ocean in response to the Southern Annular Mode, *Global Biogeochem. Cy.*, 27, 1–10, doi:10.1002/2013GB004600.

Hauck, J., and Völker, C. (2015). A multi-model study on the Southern Ocean CO₂ uptake and the role of the biological carbon pump in the 21st century. *EGU General Assembly*, 17, 12225.
<https://doi.org/10.1002/2015GB005140.Received>

Hauck, J., and C. Völker (2015), Rising atmospheric CO₂ leads to large impact of biology on Southern Ocean CO₂ uptake via changes of the Revelle factor, *Geophys. Res. Lett.*, 42, 1459–1464,
<https://doi:10.1002/2015GL063070>.

Hauck, Judith; Köhler, Peter; Wolf-Gladrow, Dieter; Völker, Christoph (2016): Iron fertilisation and century-scale effects of open ocean dissolution of olivine in a simulated CO₂ removal experiment. In *Environ. Res. Lett.* 11 (2), p. 24007–24007. DOI 10.1088/1748-9326/11/2/024007.

Hense, I., Timmermann, R., Beckmann, A., and Bathmann, U. V. (2003). Regional ecosystem dynamics in the ACC: Simulations with a three-dimensional ocean-plankton model. *Journal of Marine Systems*, 42(1–2), 31–51. [https://doi.org/10.1016/S0924-7963\(03\)00063-0](https://doi.org/10.1016/S0924-7963(03)00063-0)

Hofmann, E.E., Klinck, J.M., Locarnini, R.O., Fach, B. and Murphy, E.J. (1998). Krill transport in the Scotia Sea and environs. *Antarctic Science*. 10, 406-415

Hofmann, E. E., and Lascara, C. M. (2000). Modeling the growth dynamics of Antarctic krill *Euphausia superba*. *Marine Ecology Progress Series*, 194, 219–231. <https://doi.org/10.3354/meps194219>

IHO (International Hydrographic Organization), (2000). Report of the International Hydrographic Organisation. Working Paper No. 57 (WP 57).

20th Session of the United Nations Group of Experts on Geographical Names, (New York), 17–28 January 2000.

IPCC, 2013: Climate Change 2013: The Physical Science Basis. Contribution of Working Group I to the Fifth Assessment Report of the Intergovernmental Panel on Climate Change [Stocker, T. F., D. Qin, G.-K. Plattner, M. Tignor, S. K. Allen, J. Boschung, A. Nauels, Y. Xia, V. Bex and P. M. Midgley (eds.)]. Cambridge University Press, Cambridge, United Kingdom and New York, NY, USA,

Joos, F., and Spahni, R. (2007). Rates of change in natural and anthropogenic radiative forcing over the past 20 , 000 years. Proceedings of the National Academy of Sciences of the United States of America, 105(5), 1425–1430. <https://doi.org/10.1073/pnas.0707386105>

Keeling, C. D., Piper, C. D., Bacastow, R. B., Wahlen, M., Whorf, T. P., Heimann, M. and Meijer, H. A., Exchanges of atmospheric CO₂ and ¹³CO₂ with the terrestrial biosphere and oceans from 1978 to 2000. I. Global aspects, SIO Reference Series, No. 01-06, Scripps Institution of Oceanography, San Diego, 88 pages, 2001. <http://escholarship.org/uc/item/09v319r9>

Key, R.M., A. Olsen, S. van Heuven, S. K. Lauvset, A. Velo, X. Lin, C. Schirnick, A. Kozyr, T. Tanhua, M. Hoppema, S. Jutterström, R. Steinfeldt, E. Jeansson, M. Ishi, F. F. Perez, and T. Suzuki. (2015). Global Ocean Data Analysis Project, Version 2 (GLODAPv2), ORNL/CDIAC-162, NDP-P093. Carbon Dioxide Information Analysis Center, Oak Ridge National Laboratory, US Department of Energy, Oak Ridge, Tennessee. doi: 10.3334/CDIAC/OTG.NDP093_GLODAPv2

Khatiwala, S., F. Primeau, and T. Hall (2009): Reconstruction of the history of anthropogenic CO₂ concentrations in the ocean, *Nature*, 462, 346–349, doi:10.1038/nature08526.

Kohlbach D, Lange BA, Schaafsma FL, David C, Vortkamp M, Graeve M, van Franeker JA, Krumpfen T and Flores H (2017) Ice Algae-Produced Carbon Is Critical for Overwintering of Antarctic Krill *Euphausia superba*. *Front. Mar. Sci.* 4:310. doi: 10.3389/fmars.2017.00310

Lancelot, C., Hannon, E., Becquevort, S., Veth, C., and De Baar, H. J. W. (2000). Modeling phytoplankton blooms and carbon export production in the Southern Ocean: Dominant controls by light and iron in the Atlantic sector in Austral spring 1992. *Deep-Sea Research Part I: Oceanographic Research Papers*, 47(9), 1621–1662. [https://doi.org/10.1016/S0967-0637\(00\)00005-4](https://doi.org/10.1016/S0967-0637(00)00005-4)

Laws R. M. (1985) The ecology of the southern ocean. *Am Sci* 26-40

Laufkötter, C. et al. (2016), Projected decreases in future marine export production: the role of the carbon flux through the upper ocean ecosystem, *Biogeosciences*, 13, 4023-4047, doi:10.5194/bg-13-4023-2016.

Lenton, A., and Matear, R. J. (2007). Role of the southern annular mode (SAM) in southern ocean CO₂ uptake. *Glob. Biogeochem. Cycles* 21:GB2016. doi: 10.1029/2006GB002714

Le Quéré, C., Moriarty, R., Andrew, R. M., Canadell, J. G., Sitch, S., Korsbakken, J. I., et al. (2015). Global Carbon Budget 2015. *Earth System Science Data*, 7(2), 349–396. <https://doi.org/10.5194/essd-7-349-2015>

Le Quéré, C., Rödenbeck, C., Buitenhuis, E. T., Conway, T. J., Langenfelds, R., Gomez, A., et al. (2007). Saturation of the Southern Ocean CO₂ sink due to recent climate change. *Science*, 316(May), 1735–1738. <https://doi.org/10.1126/science.1136188>

Leung, S., Cabré, A., and Marinov, I. (2015). A latitudinally banded phytoplankton response to 21st century climate change in the Southern Ocean across the CMIP5 model suite. *Biogeosciences* 12, 5715–5734. doi: 10.5194/bg-12-5715-2015.

Lovenduski, N. S., N. Gruber, S. C. Doney, and I. D. Lima (2007), Enhanced CO₂ outgassing in the Southern Ocean from a positive phase of the Southern Annular Mode, *Global Biogeochemical Cycles*, 21, GB2026, doi:10.1029/2006GB002900.

Marshall, J., and K. Speer. 2012. Closer of the meridional overturning circulation through Southern Ocean upwelling. *Nature Geoscience* 5: 171-180

Martin, J. H. (1990), Glacial-interglacial CO₂ change: The iron hypothesis, *Paleoceanography*, 5, 1–13, doi:[10.1029/PA005i001p00001](https://doi.org/10.1029/PA005i001p00001).

Meredith, M. P., and Brandon, M. A. (2016). Oceanography and sea ice in the Southern Ocean. *Sea Ice: Third Edition*, 216–238. <https://doi.org/10.1002/9781118778371.ch8>

Meyer, B., Fuentes, V., Guerra, C., Schmidt, K., Atkinson, A., Spahic, S., ... Bathmann, U. (2009). Physiology, growth, and development of larval krill *Euphausia superba* in autumn and winter in the Lazarev Sea, Antarctica. *Limnology and Oceanography*, 54(5), 1595–1614. <https://doi.org/10.4319/lo.2009.54.5.1595>

Meyer, B. (2011). The overwintering of Antarctic krill, 15–37. <https://doi.org/10.1007/s00300-011-1120-0>

Moriarty, Roisin (2009) *The role of macro-zooplankton in the global carbon cycle*. Doctoral thesis, University of East Anglia.

Morel, F. M. M., J. G. Rueter, and N. M. Price (1991), Iron nutrition of phytoplankton and its possible importance in the ecology of ocean regions with high nutrient and low biomass, *Oceanography*, 4, 56–61.

Murphy, E. J., Cavanagh, R. D., Hofmann, E. E., Hill, S. L., Constable, A. J., Costa, D. P., et al. (2012). Developing integrated models of Southern Ocean food webs: Including ecological complexity, accounting for uncertainty and the importance of scale. *Progress in Oceanography*, 102(November), 74–92. <https://doi.org/10.1016/j.pocean.2012.03.006>

Nevison, C. D., Keeling, R. F., Kahru, M., Manizza, M., Mitchell, B. G., and Cassar, N. (2012). Estimating net community production in the Southern Ocean based on atmospheric potential oxygen and satellite ocean color data. *Global Biogeochemical Cycles*, 26(1), 1–15. <https://doi.org/10.1029/2011GB004040>

Olsen, A., R. M. Key, S. van Heuven, S. K. Lauvset, A. Velo, X. Lin, C. Schirnick, A. Kozyr, T. Tanhua, M. Hoppema, S. Jutterström, R. Steinfeldt, E. Jeansson, M. Ishii, F. F. Pérez and T. Suzuki, (2016). The Global Ocean Data Analysis Project version 2 (GLODAPv2) - an internally consistent data product for the world ocean, *Earth System Science Data*, 8, 297-323, doi: 10.5194/essd-8-297-2016

Orsi, A. H., Whitworth, T., and Nowlin, W. D. (1995). On the meridional extent and fronts of the Antarctic Circumpolar Current. *Deep-Sea Research Part I*, 42(5), 641–673. [https://doi.org/10.1016/0967-0637\(95\)00021-W](https://doi.org/10.1016/0967-0637(95)00021-W)

Passow, U., and Carlson, C. (2012). The biological pump in a high CO₂ world. *Marine Ecology Progress Series*, 470(2), 249–271. <https://doi.org/10.3354/meps09985>

Pollard, R. T., et al. (2009), Southern Ocean deep-water carbon export enhanced by natural iron fertilization, *Nature*, 457, 577–580, <https://doi:10.1038/nature07716>.

Pollard R, Treguer P, Read J. Quantifying nutrient supply to the Southern Ocean. *J Geophys Res*. 2006;111(C5):C05011.

Sarmiento, J. L., Gruber, N., Brzezinski, M. A., and Dunne, J. P. (2004). High-latitude controls of thermocline nutrients and low latitude biological productivity, *Nature*, 427, 56–60.

Schlitzer, R. (2002): Carbon export fluxes in the Southern Ocean: results from inverse modeling and comparison with satellite based estimates *Deep-sea research ii*, 49 pp. 1623-1644

Schourup-Kristensen, V, Sidorenko, D., Wolf-Gladrow, D., Völker, C. (2014). A skill assessment of the biogeochemical model REcoM2 coupled to the Finite Element Sea Ice–Ocean Model (FESOM 1.3), 2769–2802. <https://doi.org/10.5194/gmd-7-2769-2014>.

Sieburth J M, Smetacek V, Lenz J (1987) Pelagic ecosystem structure: heterotrophic compartments of the plankton and their relationship to plankton size fraction. *Limnology and Oceanography* 23:1256 -1263

Siegel, V., Loeb, V., and Gröger, J. (1998). Krill (*Euphausia superba*) density, proportional and absolute recruitment and biomass in the Elephant Island region (Antarctic Peninsula) during the period 1977 to 1997. *Polar Biology*, 19(6), 393–398. <https://doi.org/10.1007/s003000050264>

Siegel, V. (2016). Biology and ecology of the Antarctic krill. *Advances in Polar Ecology* (Vol. 1). <https://doi.org/10.1007/978-3-319-29279-3>

Smetacek, V., Klaas, C., Strass, V. H., Assmy, P., Montresor, M., Cisewski, B., ... Wolf-Gladrow, D. (2012). Deep carbon export from a Southern Ocean iron-fertilized diatom bloom. *Nature*, 487(7407), 313–319. <https://doi.org/10.1038/nature11229>

Smetacek, V. S. (1985). Role of sinking in diatom life-history: ecological, evolutionary and geological significance. *Marine Biology*, 84, 239–251. <https://doi.org/10.1007/BF00392493>

Smith, W. O., and D. M. Nelson. 1985. Phyto-plankton bloom produced by a receding ice edge in the Ross Sea: spatial coherence with the density field. *Science* 227: 163-166

Steinberg, D. K., Landry, M. R. (2017). Zooplankton and the Ocean Carbon Cycle. *Annual Review of Marine Science*, 9(1), 413–444. <https://doi.org/10.1146/annurev-marine-010814-015924>

Tagliabue, A., Mtshali, T., Aumont, O., Bowie, A. R., Klunder, M. B., Roychoudhury, A. N., and Swart, S. (2012). A global compilation of dissolved iron measurements: focus on distributions and processes in the Southern Ocean, *Biogeosciences*, 9, 2333–2349, doi:10.5194/bg-9-2333-2012.

Tagliabue, A., R. G. Williams, N. Rogan, E. P. Achterberg, and P. W. Boyd (2014), A ventilation-based framework to explain the regeneration-scavenging balance of iron in the ocean, *Geophys. Res. Lett.*, 41, 7227–7236, doi:10.1002/2014GL061066.

Takahashi, T., Sutherland, S. C., Sweeney, C., Poisson, A., Metz, N., Tilbrook, B., et al. (2002). Global sea-air CO₂ flux based on climatological surface ocean pCO₂, and seasonal biological and temperature effects. *Deep-Sea Research Part II: Topical Studies in Oceanography*, 49(9–10), 1601–1622. [https://doi.org/10.1016/S0967-0645\(02\)00003-6](https://doi.org/10.1016/S0967-0645(02)00003-6)

Trenberth, K. E., Large, W. G., and Olson, J. G. (1990). The Mean Annual Cycle in Global Ocean Wind Stress. *Journal of Physical Oceanography*. [https://doi.org/10.1175/1520-0485\(1990\)020](https://doi.org/10.1175/1520-0485(1990)020)

Tomczak, Matthias and J Stuart Godfrey: *Regional Oceanography: an Introduction* 2nd edn (2001)

Turner JT. Zooplankton fecal pellets, marine snow and sinking phytoplankton blooms. *Aquat Microb Ecol.* 2002;27:57–102. doi: 10.3354/ame027057

Volk, T., and M. I. Hoffert (1985), Ocean carbon pumps: Analysis of relative strengths and efficiencies in ocean driven atmospheric CO₂ changes, in the carbon cycle and atmospheric CO₂ : natural variations, Archean to present, edited by E. T. Sundquist and W. S. Broecker, pp. 99–110, Geophysical Monograph 32, American Geophysical Union.

Wang, Q., Danilov, S., and Schröter, J. (2008). Finite element ocean circulation model based on triangular prismatic elements, with application in studying the effect of topography representation. *Journal of Geophysical Research: Oceans*, 113(C5). DOI: 10.1029/2007JC004482

Wang, S., Bailey, D., Lindsay, K., Moore, J. K., & Holland, M. (2014). Impact of sea ice on the marine iron cycle and phytoplankton productivity. *Biogeosciences*, 11(17), 4713–4731. <https://doi.org/10.5194/bg-11-4713-2014>

Webb, D. J., Kilworth, P. D., Coward, A. C. and Thompson, S. R. (1991). The FRAM Atlas of the Southern Ocean. NERC, Swindon, UK.

Zeebe, R. E., and D. A. Wolf-Gladrow (2001), CO₂ in seawater: equilibrium, kinetics, isotopes, Elsevier Oceanography Series, vol. 65, p. 346, Elsevier.